



University of Kentucky
UKnowledge

Theses and Dissertations--Electrical and
Computer Engineering

Electrical and Computer Engineering

2011

CONTROL OF METAL TRANSFER AT GIVEN ARC VARIABLES

Yi Huang

University of Kentucky, hithuangyi@hotmail.com

[Right click to open a feedback form in a new tab to let us know how this document benefits you.](#)

Recommended Citation

Huang, Yi, "CONTROL OF METAL TRANSFER AT GIVEN ARC VARIABLES" (2011). *Theses and Dissertations--Electrical and Computer Engineering*. 4.
https://uknowledge.uky.edu/ece_etds/4

This Doctoral Dissertation is brought to you for free and open access by the Electrical and Computer Engineering at UKnowledge. It has been accepted for inclusion in Theses and Dissertations--Electrical and Computer Engineering by an authorized administrator of UKnowledge. For more information, please contact UKnowledge@lsv.uky.edu.

STUDENT AGREEMENT:

I represent that my thesis or dissertation and abstract are my original work. Proper attribution has been given to all outside sources. I understand that I am solely responsible for obtaining any needed copyright permissions. I have obtained and attached hereto needed written permission statements(s) from the owner(s) of each third-party copyrighted matter to be included in my work, allowing electronic distribution (if such use is not permitted by the fair use doctrine).

I hereby grant to The University of Kentucky and its agents the non-exclusive license to archive and make accessible my work in whole or in part in all forms of media, now or hereafter known. I agree that the document mentioned above may be made available immediately for worldwide access unless a preapproved embargo applies.

I retain all other ownership rights to the copyright of my work. I also retain the right to use in future works (such as articles or books) all or part of my work. I understand that I am free to register the copyright to my work.

REVIEW, APPROVAL AND ACCEPTANCE

The document mentioned above has been reviewed and accepted by the student's advisor, on behalf of the advisory committee, and by the Director of Graduate Studies (DGS), on behalf of the program; we verify that this is the final, approved version of the student's dissertation including all changes required by the advisory committee. The undersigned agree to abide by the statements above.

Yi Huang, Student

Dr. YuMing Zhang, Major Professor

Dr. Zhi Chen, Director of Graduate Studies

CONTROL OF METAL TRANSFER AT GIVEN ARC VARIABLES

DISSERTATION

A dissertation submitted in partial fulfillment of the
requirements for the degree of Doctor of Philosophy in the
College of Engineering
at the University of Kentucky

By

Yi Huang

Lexington, Kentucky

Director: Dr. YuMing Zhang, Professor of Electrical Engineering

Lexington, Kentucky

2011

Copyright © Yi Huang 2011

ABSTRACT OF DISSERTATION

CONTROL OF METAL TRANSFER AT GIVEN ARC VARIABLES

Gas Metal Arc Welding (GMAW) is one of the most important welding processes in industrial application. To control metal transfer at given variables is a focus in the field of research and development in welding community.

In this dissertation, laser enhanced GMAW is proposed and developed by adding a lower power laser onto the droplet to generate an auxiliary detaching force. The electromagnetic force needed to detach droplets, thus the current that determines this force, is reduced. Wire feed speed, arc voltage, and laser intensity were identified as three major parameters that affect the laser enhanced metal transfer process and a systematic series of experiments were designed and conducted to test these parameters. The behaviors of the laser enhanced metal transfer process observed from high speed images were analyzed using the established physics of metal transfer. In all experiments, the laser was found to affect the metal transfer process as an additional detaching force that tended to change a short-circuiting transfer to drop globular or drop spray, reduce the diameter of the droplet detached in drop globular transfer, or decrease the diameter of the droplet such that the transfer changed from drop globular to drop spray. The enhancement of the laser was found to increase as the laser intensity increased. The larger laser intensity tended to help reduce the size of the droplet detached. The arc voltage affected the metal transfer process through changing the current and changing the gap and

possible time interval of the droplet development. A larger arc voltage helped reduce the size of the droplet detached through an increased electromagnetic force. Desired heat input and current/arc pressure waveforms may thus be both delivered and controlled by GMAW through laser enhancement. Laser recoil pressure force was estimated based on the difference of gravitational force with and without laser pulse, and the result was with an acceptable accuracy. Good formation of welds and full penetration of thin plate could be obtained using laser enhanced GMAW. A nonlinear model was established to simulate the dynamic metal transfer in laser enhanced GMAW, and the results agree with the experimental one.

KEYWORDS: GMAW, Laser, Metal Transfer, Laser Recoil Pressure, Nonlinear Model

Yi Huang

11/08/2011

CONTROL OF METAL TRANSFER AT GIVEN ARC VARIABLES

By

Yi Huang

YuMing Zhang

Director of Dissertation

Zhi Chen

Director of Graduate Studies

11/08/2011

ACKNOWLEDGEMENTS

This work is funded by the National Science Foundation under grant CMMI-0825956 entitled “Control of Metal Transfer at Given Arc Variables”.

First of all, I would give sincere thanks and appreciations to my advisor Dr. YuMing Zhang for his profound knowledge, patient guidance, continuous encouragement and support. I am also grateful to Dr. Larry Holloway, Dr. Alan T. Male, Dr. Yuan Liao, Dr. Jingshan Li, and Dr. Paul Xu for their helpful instructions and advices. It has been a great honor for me to have the opportunity learning from all these professors. I would like to express my appreciation to Dr. Chuansong Wu from Shandong University, China, Dr. Yu Shi from Lanzhou University of Technology, China, Dr. Yusheng Liu from Sichuan University, China, and Dr. Xuewu Wang from East China University of Science and Technology, China. Moreover, I would like to thank my colleagues in Welding Research Laboratory: Dr. Hongsheng Song, Dr. Xiaopei Liu, Dr. Kehai Li, Dr. Kun Qian, Dr. Xiaodong Na, Dr. Zhijiang Wang, Mrs. Jinsong Chen, Yan Shao, Xiaoji Ma, Weijie Zhang, and Xiang Zhang.

Additionally, I thank my parents for their love and support. I want to thank my wife Xiaoqian Li and my daughter Elaine Huang for their encouragement and support.

TABLE OF CONTENTS

Acknowledgments.....	iii
List of Tables.....	vii
List of Figures.....	viii
CHAPTER 1 INTRODUCTION AND BACKGROUND.....	1
1.1 Background and Motivation	1
1.2 Objective and Focus.....	3
1.3 Dissertation structure	5
CHAPTER 2 LITERATURE REVIEW.....	7
2.1 Review of GMAW	7
2.1.1 Basic variables of GMAW.....	9
2.2 Metal Transfer in GMAW	11
2.2.1 Short-circuit metal transfer	13
2.2.2 Globular transfer.....	15
2.2.3 Spray transfer.....	16
2.2.4 Factors Affecting Metal Transfer Types.....	17
2.3 Previous Research of Novel Welding Process on Metal Transfer.....	18
2.3.1 Laser-MIG hybrid welding.....	18
2.3.2 Surface Tension Transfer.....	20
2.3.3 Cold Metal Transfer.....	25
2.3.4 Double Electrodes GMAW.....	27
2.3.5 Double Bypass GMAW	30
2.3.6 Other Metal Transfer Control Methods of GMAW	31
CHAPTER 3 PRINCIPLES OF LASER ENHANCED GMAW AND EXPERIMENT SYSTEM.....	33
3.1 Principle and System Construction.....	33

3.1.1 Principle of Laser Enhanced GMAW.....	33
3.1.2 System Construction.....	34
3.2 Sensing system.....	38
3.2.1 Hardware to build sensing and control system.....	38
3.2.2 Software System.....	39
3.3 Experimental Materials and Conditions	40
3.4 Summary.....	40
CHAPTER 4 METAL TRANSFER PHENOMENON IN LASER ENHANCED GMAW	41
4.1 Theories of Metal Transfer.....	41
4.1.1 Force Balance Theory.....	42
4.1.2 Pinch Instability Theory	45
4.2 Preliminary Results of Metal Transfer in Laser Enhanced GMAW.....	45
4.2.1 Experimental Conditions	45
4.2.2 Metal Transfer	46
4.2.3 Current Waveforms	53
4.2.4 Process Parameters	58
4.2.5 Analysis of Laser Effect	59
4.3 Conclusions.....	62
CHAPTER 5 METAL TRANSFER INFLUENCE FACTORS IN LASER ENHANCED GMAW	63
5.1 Basic Analysis of Metal Transfer in Laser Enhanced GMAW	63
5.2 Experiment Conditions to Study Metal Transfer in Laser Enhanced GMAW	65
5.3 Observation and Analysis in Laser Enhanced GMAW	68
5.3.1 Observations	68
5.3.2 Analysis	79
5.4 Laser Intensity.....	81
5.5 Arc Length	88

5.6 Laser Recoil Pressure Force Estimation	92
5.7 Conclusions.....	98
CHAPTER 6 PULSED LASER ENHANCED GMAW	100
6.1 Laser Enhanced GMAW with Pulsed Laser Power.....	100
6.2 Laser Enhanced GMAW with Pulsed Laser Power and Welding Current	101
6.3 Conclusions.....	104
CHAPTER 7 CONTROLLED DROPLET TRANSFER AND FULL PENETRATION USING LASER ENHANCED GMAW	105
7.1 Controlled Droplet Transfer in Laser Enhanced GMAW.....	105
7.1.1 Surface Quality	105
7.1.2 Controlled Drop Globular Transfer	107
7.2 Full Penetration.....	113
7.2.1 Bead on Plate Welds.....	115
7.2.2 Butt joint.....	Error! Bookmark not defined.
7.3 Conclusions.....	126
CHAPTER 8 NONLINEAR CONTROL MODELING OF DYNAMIC METAL TRANSFER IN LASER ENHANCED GMAW.....	127
8.1 Nonlinear Modeling of Dynamic Metal Transfer	127
8.1.1 Nonlinear Model Setup.....	128
8.1.2 Simulation Results	132
8.2 Neural Network Model to Predict the Metal Transfer	140
8.2.1 Least Squares Regression	142
8.2.2 BPNN Model Establishment.....	147
8.2.3 PSO Based BPNN Model	150
8.2.4 TSCPSO-BPNN Model	153
8.2.5 Comparison with LS Model.....	155
8.2.6 Dimensions Reduction and Discussion	157
8.3 Conclusions.....	159

CHAPTER 9 CONCLUSIONS AND FUTURE WORK	160
9.1 Conclusions.....	160
9.2 Future Work.....	163
REFERENCES	164
VITA.....	178

LIST OF TABLES

Table 2-1 Classification of Metal Transfer in GMAW.....	12
Table 2-2 Comparison of GMAW to STT	23
Table 4-1 Experimental conditions and welding currents	46
Table 5-1 Constants used for laser recoil pressure force estimation	95
Table 8-1 Constants used for nonlinear model	132
Table 8-2 Auxiliary and estimation variables.....	144
Table 8-3 Simulation errors of LS regression with 9 parameters	144
Table 8-4 Simulation errors of LS regression with 19 parameters	147
Table 8-5 Simulation errors of BPNN Model.....	148
Table 8-6 Simulation errors of PSO-BPNN Model	151
Table 8-7 Simulation errors of TSCPSO -BPNN model	155
Table 8-8 Simulation errors of dimensions reduction model for DD	157
Table 8-9 Corresponding variables of the models for DD.....	157
Table 8-10 Parameters for Model 6	158

LIST OF FIGURES

Fig. 1-1 Principle of Laser Enhanced GMAW	4
Fig. 2-1 Illustration of GMAW process	9
Fig. 2-2 Electrode extension	11
Fig. 2-3 Short-circuiting transfer	14
Fig. 2-4 Bead contour and penetration patterns for various shielding gases	18
Fig. 2-5 Laser-MIG/MAG welding process.....	19
Fig. 2-6 Torch installation of laser-MIG: (a) Instruction diagram (b) Real torch	20
Fig. 2-7 Surface tension transfer (STT) process	21
Fig. 2-8 Cold Metal Transfer Process	25
Fig. 2-9 Voltage versus current diagram with addition of the region for the pure CMT- process.....	27
Fig. 2-10 Non-consumable DE-GMAW system diagram.....	28
Fig. 2-11 System diagram of consumable DE-GMAW	29
Fig. 2-12 Arc forces act on the droplet in DB-GMAW	30
Fig. 2-13 Illustration of DB-GMAW	31
Fig. 3-1 System installation	35
Fig. 3-2 Olympus i-speed high speed camera.....	36

Fig. 3-3 Installation of GMAW and Laser (the shielding board is not shown in the picture)	37
Fig. 4-1 Major forces acting on the droplet in Laser Enhance GMAW	42
Fig. 4-2 Metal transfer process during conventional GMAW under experimental condition #2 (without laser). Consecutive images in the figure were acquired at 3000 frames per second.	47
Fig. 4-3 Metal transfer in Laser Enhanced GMAW at experimental condition #1. Consecutive images in the figure were acquired at 3000 frames per second	48
Fig. 4-4 Metal transfer in Laser Enhanced GMAW at experimental condition #2. Consecutive images in the figure were acquired at 3000 frames per second	49
Fig. 4-5 Metal transfer in Laser Enhanced GMAW at experimental condition #3. Consecutive images in the figure were acquired at 3000 frames per second	50
Fig. 4-6 Metal transfer in Laser Enhanced GMAW at experimental condition #4. Consecutive images in the figure were acquired at 3000 frames per second	51
Fig. 4-7 Metal transfer in Laser Enhanced GMAW at experimental condition #5. Consecutive images in the figure were acquired at 3000 frames per second	52
Fig.4-8 Current waveforms in Laser Enhanced GMAW experiments: a) Experiment #1, b) Experiment #2, c) Experiment #3, d) Experiment #4, and e) Experiment #5.....	54
Fig. 4-9 Comparative conventional and Laser Enhanced GMAW using condition #4. The average current does not change significantly. This implies that the heat applied by the laser to the wire is insignificant for wire melting	57
Fig. 4-10 Effect of wire feed speed on current and droplet transfer time in Laser Enhanced GMAW	59
Fig. 4-11 Pinch effect in the Laser Enhance GMAW process	60

Fig. 5-1 Welding current under different wire feed speeds and different laser powers: a) W.F.S. 250, b) W.F.S. 300, c) W.F.S. 350, and d) W.F.S. 400	66
Fig. 5-2 Illustration of metal transfer image	68
Fig. 5-3 Typical metal transfer in comparative experiments with and without laser under (300 in./min, 30 V, 0) and (300 in./min, 30 V, 62 W/mm ²).....	70
Fig. 5-4 Current waveforms for (300 in./min, 30 V, 0 W/mm ²) and (300 in./min, 30 V, 62 W/mm ²)	71
Fig. 5-5 Typical metal transfer in comparative experiments with and without laser under (250 in./min, 30 V, 0) and (250 in./min, 30 V, 62 W/mm ²).....	72
Fig. 5-6 Typical metal transfer in comparative experiments with and without laser under (350 in./min, 30 V, 0) and (350 in./min, 30 V, 62 W/mm ²).....	73
Fig. 5-7 Typical metal transfer in comparative experiments with and without laser under (400 in./min, 30 V, 0) and (400 in./min, 30 V, 62 W/mm ²).....	74
Fig. 5-8 Current waveforms for (250 in./min, 30 V, 0 W/mm ²) and (250 in./min, 30 V, 62 W/mm ²)	76
Fig. 5-9 Current waveforms for (350 in./min, 30 V, 0 W/mm ²) and (350 in./min, 30 V, 62 W/mm ²)	77
Fig. 5-10 Current waveforms for (400 in./min, 30 V, 0 W/mm ²) and (400 in./min, 30 V, 62 W/mm ²).....	78
Fig. 5-11 Droplet sizes with welding voltage 30 V under different wire feed speeds	79
Fig. 5-12 Typical metal transfer in comparative experiments with and without laser under (300 in./min, 30 V, 46 W/mm ²) and (300 in./min, 30 V, 54 W/mm ²)	82

Fig. 5-13 Droplet diameter with 30 V and 300 in./min under different laser power levels. The droplet diameter is the mean of the diameter of the droplet that is detached or touches the weld pool.....	83
Fig. 5-14 Typical metal transfer in comparative experiments with and without laser under (250 in./min, 30 V, 46 W/mm ²), and (250 in./min, 30 V, 54 W/mm ²)	84
Fig. 5-15 Typical metal transfer in comparative experiments with and without laser under (350 in./min, 30 V, 46 W/mm ²), and (350 in./min, 30 V, 54 W/mm ²)	85
Fig. 5-16 Typical metal transfer in comparative experiments with and without laser under (350 in./min, 30 V, 46 W/mm ²) and (350 in./min, 30 V, 54 W/mm ²)	86
Fig. 5-17 Droplet diameter with 30 V under different wire feed speed laser power levels. The droplet diameter is the mean of the diameter of the droplet that is detached or touches the weld pool.....	87
Fig. 5-18 Typical metal transfer in comparative experiments with laser under (350 in./min, 26 V, 62 W/mm ²), (350 in./min, 28 V, 62 W/mm ²) and (350 in./min, 32 V, 62 W/mm ²)	90
Fig. 5-19 Droplet sizes with welding feed speed 350 in./min under different voltages ...	92
Fig. 5-20 Typical metal transfer in comparative experiments with laser under (400 in./min, 26 V, 62 W/mm ²), (400 in./min, 28 V, 62 W/mm ²) and (400 in./min, 32 V, 62 W/mm ²)	93
Fig. 5-21 Variation of f2 as the function of half-angle θ	96
Fig. 5-22 Gravitational forces in conventional GMAW and laser enhanced GMAW	97
Fig. 6-1 Typical metal transfer in pulsed laser enhanced GMAW	101
Fig. 6-2 Welding current waveform in pulsed laser enhanced GMAW.	102

Fig. 6-3 Welding current waveform and laser power intensity waveform in pulsed laser enhanced GMAW	103
Fig. 7-1 Surface appearance of the weld beads with 250 in./min under different voltages and different laser power levels	106
Fig. 7-2 Surface appearance of the weld beads with 300 in./min under different voltages and different laser power levels	108
Fig. 7-3 Surface appearance of the weld beads with 350 in./min under different voltages and different laser power levels	109
Fig. 7-4 Surface appearance of the weld beads with 400 in./min under different voltages and different laser power levels	110
Fig. 7-5 Images of Uncontrolled drop globular process	111
Fig. 7-6 Images of controlled drop globular process	112
Fig. 7-7 Typical surface appearance in comparative experiments with and without laser under (400 in./min, 30 V, 0) and (400 in./min, 30 V, 62 W/mm ²)	113
Fig. 7-8 Different full penetration levels	114
Fig. 7-9 Full penetration with travel speed at 4.0 mm/s and welding current 125A: a) front image, b) back image	116
Fig. 7-10 Full penetration with travel speed at 4.1 mm/s and welding current 125A: a) front image, b) back image	117
Fig. 7-11 Full penetration with travel speed at 4.2 mm/s and welding current 125A: a) front image, b) back image	117
Fig. 7-12 Full penetration with travel speed at 4.3 mm/s and welding current 125A: a) front image, b) back image	118

Fig. 7-13 Full penetration with travel speed at 4.4 mm/s and welding current 125A: a) front image, b) back image	119
Fig. 7-14 Full penetration with travel speed at 4.2 mm/s and welding current 130A: a) front image, b) back image	120
Fig. 7-15 Full penetration with travel speed at 4.35 mm/s and welding current 130A: a) front image, b) back image	120
Fig. 7-16 Full penetration with travel speed at 4.5 mm/s and welding current 130A: a) front image, b) back image	121
Fig. 7-17 Full penetration with travel speed at 4.2 mm/s and welding current 135A: a) front image, b) back image	122
Fig. 7-18 Full penetration with travel speed at 4.35 mm/s and welding current 135A: a) front image, b) back image	123
Fig. 7-19 Full penetration with travel speed at 4.45 mm/s and welding current 135A: a) front image, b) back image	123
Fig. 7-20 Full penetration with travel speed at 4.05 mm/s and welding current 125A: a) front image, b) back image	124
Fig. 7-21 Full penetration with travel speed at 4.15 mm/s and welding current 125A: a) front image, b) back image	125
Fig. 7-22 Full penetration with travel speed at 4.27 mm/s and welding current 125A: a) front image, b) back image	125
Fig. 8-1 Schematic image of GMAW process	130
Fig. 8-2 Welding current waveform simulation result	133
Fig. 8-3 Wire extension simulation result	133

Fig. 8-4 Droplet radius simulation result	134
Fig. 8-5 Droplet mass simulation result.....	134
Fig. 8-6 Aerodynamic drag force simulation result	135
Fig. 8-7 Momentum force simulation result	135
Fig. 8-8 Electromagnetic force simulation result.....	136
Fig. 8-9 Gravitational force simulation result.....	136
Fig. 8-10 Laser recoil pressure force simulation result.....	136
Fig. 8-11 The total detaching force simulation result	137
Fig. 8-12 The droplet displacement simulation result	137
Fig. 8-13 The droplet velocity simulation result.....	138
Fig. 8-14 Droplet radius simulation result with pulsed laser	138
Fig. 8-15 Wire extension simulation result with pulsed laser	139
Fig. 8-16 Laser recoil pressure force simulation result with pulsed laser	139
Fig. 8-17 The total detaching force simulation result with pulsed laser	140
Fig. 8-18 System inputs and outputs.....	143
Fig. 8-20 Simulation results based on LS regression with 19 parameters: a) <i>DD</i> , b) <i>DTR</i>	146
Fig. 8-21 Simulation results based on BPNN model: a) <i>DD</i> , b) <i>DTR</i>	149
Fig. 8-22 Simulation results based on PSO-BPNN model: a) <i>DD</i> , b) <i>DTR</i>	152

Fig. 8-23 Simulation results based on TSCPSO-BPNN model: a) *DD*, b) *DTR* 156

CHAPTER 1 INTRODUCTION AND BACKGROUND

1.1 Background and Motivation

Welding process, which joins materials, usually metals or thermoplastics, by causing coalescence, is one of the most important manufacturing processes in industry, such as automotive, aerospace, shipbuilding, and boiler. Fusion welding is the most important process compared to brazing and soldering as it was adopted in the most metal joining processes [1-2].

Among all the fusion welding methods, gas metal arc welding (GMAW) is the most common method adopted in the industry. It is operated as a semi-automatic or automatic arc process for metals joining. It is the most widely used process for robot welding, in which a robot carries a welding torch to travel along the weld seam or apply electrodes on the sheets being joined [3-4].

Metal and energy transfer from the GMAW process is not gap dependent and is set independently. The American Welding Society classifies the metal transfer into three major types: short-circuiting transfer, globular transfer, and spray transfer [1]. When a continuous waveform current is used and the current is small, the droplet may not be detached until the droplet contacts the weld pool. In this case, the droplet is transferred into the weld pool by the surface tension at a short-circuiting condition and the transfer mode is short-circuiting. As a result of the low current, the heat input is relatively small and relatively thin materials can be welded with relatively low heat input, distortion and residual stress. However, the process needs to be appropriately controlled to minimize the spatters that otherwise may be severe. If the current increases, but not large enough to

generate a sufficiently large electromagnetic force [5] to detach the formed droplet, then the droplet may surpass the diameter of the electrode wire and be detached mainly by gravity. This transfer mode is globular metal transfer. If the current further increases such that the detaching electromagnetic force becomes sufficiently large, the transfer mode may change to projected spray transfer in which discrete droplets detached at diameters similar with that of the wire; or even streaming or rotating spray transfer resulting in a stream of small continuous droplets. With spray transfers, high productivity is obtained due to the high current but may be at the expenses of high heat input, distortion and residual stress.

While the pulsed GMAW has been widely adopted in industry, it does have certain limitations. The fundamental cause of these limitations is that a peak current higher than the transition current [1] must be used in order to detach the droplet to complete the metal transfer. Vaporization occurs under high amperage and results in fumes. More critically, the arc pressure is proportional to the square of the amperage [6-7]. The high arc pressure may blow liquid metal away from the weld pool. For full penetration application where the work-piece has to be fully penetrated through the entire thickness, the high arc pressure may easily cause burn-through. This is the major reason why the less productive GTAW process, whose amperage can be set at whatever level needed, has to be used for the root pass in full penetration applications.

It is apparent that the major role of the high peak current in pulsed GMAW is to generate the electromagnetic force to detach the droplets. However, the high peak current produces undesirable side-effects that affect the GMAW's capability to be used in full penetration applications and to be a "clean" process to compete with the less productive GTAW. In this case, an alternative way was proposed to apply a needed force to detach the droplets without producing undesirable side-effects. The ultimate goal is to apply a pulsed laser of low power to the droplet to detach it whenever needed such that the droplet be detached at whatever amperage that best suits for the control of the weld pool. The resultant process is referred to as Laser Enhanced GMAW. In the novel laser enhanced GMAW, a low power laser was projected onto the droplet to generate an auxiliary detaching force. In this case, free flight metal transfer would be obtained with welding current below

transition one. By controlling laser intensity, droplet could be detached at desired arc variables and desired size.

1.2 Objective and Focus

As aforementioned, in conventional GMAW, when the welding current is lower than the transition one, the metal transfer type will be short-circuiting or repelling globular transfer mode. Both the two transfer modes will be along with some shortcomings. Projected spray metal transfer is a preferred metal transfer type, but relatively high welding current through work-piece will take distortion and internal stress to the welds. In this case, to obtain free flight transfer with welding current under transition one becomes a main concern in the research and application field. To fully control the GMAW process, droplet size should be monitored and controlled. If droplet could be detached at desired arc variables, forces affected on the droplet and welding parameters will be combined to control the metal transfer process.

There are many methods which are “neat” using smart approaches to resolve different issues and difficulties but being “neat” also restricts their applications in wider ranges. Toward the development of a more general method, the laser enhanced GMAW as shown in Fig. 1 has been proposed/developed. It adds a relatively low power laser to a conventional GMAW and the objective is to provide an auxiliary force to help detach the droplet at a desired diameter with any desired current that most suits for the application including future adaptive control applications where the current needs to be adjusted freely as determined by the control algorithm. It is apparent that the laser enhanced GMAW is fundamentally different from the laser hybrid GMAW [8-15] where a laser beam of substantially high power aims at the base metal rather than the droplet. In laser enhanced GMAW, the laser recoil pressure force was to be the additional force to help detach the droplet. To fully control this novel process, control algorithm should be set up to build closed-loop control system to get a stable and full controlled process. As the metal transfer process will be controlled at a desired level, the formation of welds will be improved. Full penetration could be obtained in such a controlled metal transfer process.

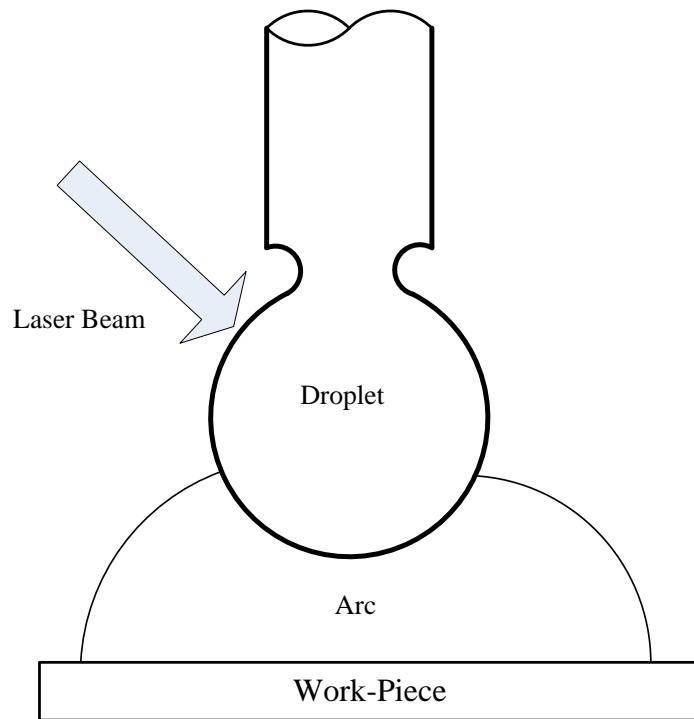


Fig. 1-1 Principle of Laser Enhanced GMAW

To this end, the main approach to reach objectives in this dissertation including following steps:

- (1) Construct a laser enhanced GMAW experimental system with sensors monitoring the current, voltage, wire feed speed, travel speed and laser power information to help evaluating whether the system satisfies experimental requirements.
- (2) Analyze the metal transfer process and identify the main parameters to effect stability of this process.
- (3) Propose an estimating method to calculate the laser recoil pressure force which is the main effect on the droplet from the laser.
- (4) Obtain full penetration using laser enhanced GMAW.
- (5) Design control algorithm based on nonlinear modeling and neural network modeling to full control this novel process.

1.3 Dissertation structure

Respecting the approach above, this dissertation has an organizational structure which is listed below.

Chapter 1: Introduction and Background

The background and motivation of this dissertation will be illustrated, and the objectives of this research are also introduced.

Chapter 2: Literature Review

In this section, the Gas Metal Arc Welding process will be introduced. Other improved GMAW related with this dissertation will be reviewed. The metal transfer process will be fully discussed.

Chapter 3: Principles of Laser Enhanced GMAW and Experiment System

The proposed experiment system will be introduced, and experiment materials and equipments used in this dissertation will be also illustrated. Important configuration and parameters relation of laser enhanced GMAW will be introduced.

Chapter 4: Metal Transfer Phenomenon in Laser Enhanced GMAW

The proposed laser enhanced GMAW is developed and realized. The metal transfer type is changed due to the auxiliary detaching force. The novel process will be analyzed, and the main reason to cause this change will be discussed.

Chapter 5: Metal Transfer Influence Factors in Laser Enhanced GMAW

Metal transfer process in laser enhanced GMAW will be sufficiently discussed. The influence factors will be identified. A method will be proposed to estimate the laser recoil pressure force.

Chapter 6: Pulsed Laser Enhanced GMAW and Related Wire Melting Phenomenon

Laser enhanced GMAW with pulses welding current and pulsed laser power will be developed. It could further enhance metal transfer.

Chapter 7: Controlled Droplet Transfer and Full Penetration Using Laser Enhanced GMAW

The surface quality of welds will be introduced, and good formation of welds will be obtained with controlled metal transfer. Full penetration of mild steel will be obtained using laser enhanced GMAW. Good formation of welds both front and back sides will be achieved.

Chapter 8: Predictive and Nonlinear Control of Laser Enhanced GMAW

Two control models based on neural network and nonlinear analysis will be proposed, and results will be shown to demonstrate that they satisfy the requirements of laser enhanced GMAW control.

Chapter 9: Conclusion and Future Work

This part concludes the whole project in every academic aspect. The future research objective of this research is also discussed.

Copyright © Yi Huang 2011

CHAPTER 2 LITERATURE REVIEW

2.1 Review of GMAW

Gas metal arc welding (GMAW) is a semi-automatic or automatic arc welding process in which a continuous and consumable wire electrode and a shielding gas are fed through a welding gun. The principles of gas metal arc welding began to be understood in the early 1800s, after Humphry Davy's discovery of the electric arc in 1800. Initially, carbon electrodes were used, but by the late 1800s, metal electrodes had been invented by N.G. Slavianoff and C. L. Coffin. In 1920, an early predecessor of GMAW was invented by P. O. Nobel of General Electric. It used a bare electrode wire and direct current, and used arc voltage to regulate the feed rate. It did not use a shielding gas to protect the weld, as developments in welding atmospheres did not take place until later that decade. In 1926 another forerunner of GMAW was released, but it was not suitable for practical use [1-2, 17].

It was not until 1948 that GMAW was finally developed by the Battelle Memorial Institute. It used a smaller diameter electrode and a constant voltage power source, which had been developed by H. E. Kennedy. It offered a high deposition rate, but the high cost of inert gases limited its use to non-ferrous materials and cost savings were not obtained. In 1953, the use of carbon dioxide as a welding atmosphere was developed, and it quickly gained popularity in GMAW, since it made welding steel more economical. In 1958 and 1959, the short-arc variation of GMAW was released, which increased welding versatility and made the welding of thin materials possible while relying on smaller electrode wires and more advanced power supplies. It quickly became the most popular GMAW variation. The spray-arc transfer variation was developed in the early 1960s, when experimenters added small amounts of oxygen to inert gases. More recently, pulsed

current has been applied, giving rise to a new method called the pulsed spray-arc variation [2, 16-18].

GMAW is currently one of the most popular welding methods, especially in industrial environments. It is adopted extensively by the sheet metal industry and, by extension, the automobile industry. There, the method is often used to do arc spot welding, thereby replacing riveting or resistance spot welding. It is also popular in robot welding, in which robots handle the work-pieces and the welding gun to quicken the manufacturing process [1, 3, 16-18].

Generally, it is unsuitable for welding outdoors, because the movement of the surrounding atmosphere can dissipate the shielding gas and thus make welding more difficult, while also decreasing the quality of the weld [1-3, 16-18]. This problem can be alleviated to some extent by increasing the shielding gas output, but this can be expensive and may also affect the quality of the weld. In general, processes such as shielded metal arc welding and flux cored arc welding are preferred for welding outdoors, making the use of GMAW in the construction industry rather limited. Furthermore, the use of a shielding gas makes GMAW an unpopular underwater welding process, and for the same reason it is rarely adopted in space applications.

In GMAW process as illustrated in Fig. 2-1 [1], a mandatory wire is fed to the contact tube which is typically connected to the positive terminal of the power supply. When the wire touches the negatively charged work piece, the tip of the wire is rapidly burnt forming a gap between the wire and the work piece and an arc is ignited across this gap. The arc melts the wire and melted metal forms a droplet at the tip of the wire; after the droplet is detached, a new droplet starts to form and a new cycle starts. This metal transfer process is subject to periodic change in the arcing conditions and plays the most critical role in determining/controlling the weld quality in GMAW. To produce high quality welds similarly as the gas tungsten arc welding (GTAW) where the arcing conditions are stationary, the metal transfer needs to be appropriately controlled.

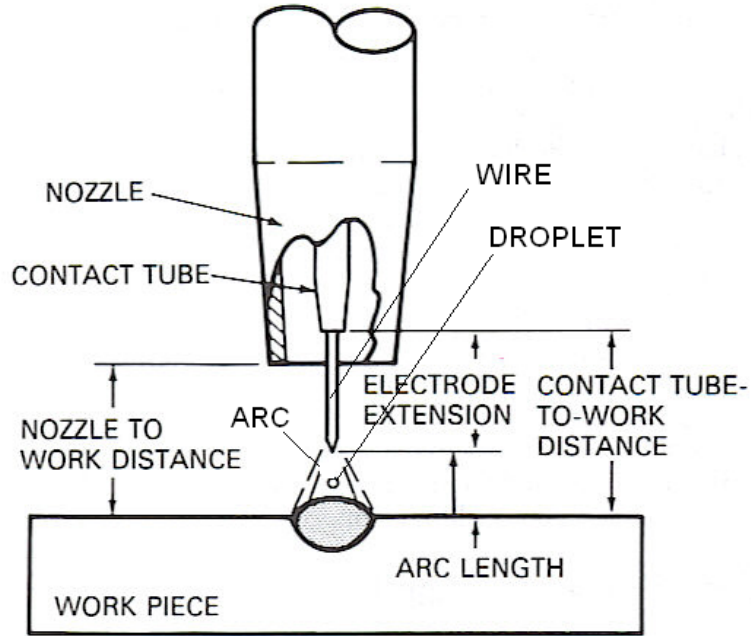


Fig. 2-1 Illustration of GMAW process

As GMAW is a focus topic in welding research and application, there are many aspects which need special work. Hereby, basic variables will be introduced for the later analysis.

2.1.1 Basic variables of GMAW

There are some basic variables of GMAW which will affect metal transfer, weld penetration, bead geometry and overall weld quality. The basic variables of GMAW usually have strong coupling relationship which means that they influence each other significantly [1-3, 16-18].

Current Density: Current density is defined as the current employed with a particular electrode diameter divided by its current carrying cross-sectional area. If the wire feed speed is low with other parameter the same, then the current density will be low, and vice versa. Lower current density applied to a given electrode is associated with the short-circuit mode of metal transfer. At the same time, higher current density is associated with the higher energy modes of metal transfer: globular, axial spray transfer or the more advanced pulsed spray metal transfer.

Welding Current: When all other variables are held constant, the welding current varies with the electrode feeding speed or melting rate in a nonlinear relation. Generally speaking, for a chosen filler wire, welding current increases itself along with the increment of wire feeding speed. The upper limit of welding current is often regulated by the material and geometry of base metal in order to prevent burn through.

Electrode Efficiencies: Electrode efficiency refers to the percentage of electrode that actually ends up in the weld deposit. Spatter levels, smoke, and slag formers affect the electrode efficiency in GMAW. The electrode efficiency is a numeric value that is assigned to the particular mode of metal transfer.

Polarity: Polarity is used to describe the electrical connection of the welding gun with relation to the terminals of a direct current power source. When the gun power lead is connected to the positive terminal, the polarity is designated as direct current electrode positive (DCEP), arbitrarily called reverse polarity. When the gun is connected to the negative terminal, the polarity is designated as direct current electrode negative (DCEN), originally called straight polarity [18].

Arc Voltage: Arc voltage and arc length are terms that are often used interchangeably. With GMAW, arc length is a critical variable that must be fully controlled [1].

Travel speed: Travel speed is the linear rate at which the arc is moved along the weld joint. With all other conditions held constant, weld penetration is a maximum at an intermediate travel speed [1-3, 16-19].

Deposition Rate: The melt-off rate for a particular electrode does not include consideration for the efficiency of the mode of metal transfer or the process. Its interest is in how much electrode is being melted. Deposition rate is applied to the amount of electrode, measured in wire feed speed per unit of time, that is fed into the molten puddle. Importantly, its value reflects the use of the factor for electrode efficiency.

Electrode Extension: The electrode extended from the end of the contact tip to the arc is properly known as electrode extension. The popular non-standard term is electrical stick-

out (ESO). In GMAW, this is the amount of electrode that is visible to the welder. The electrode extension includes only the length of the electrode, not the extension plus the length of the arc. The use of the term electrode extension is more commonly applied for semiautomatic welding than it is for robotic or mechanized welding operations. Fig. 2-2 shows the scheme image of electrode extension in GMAW.

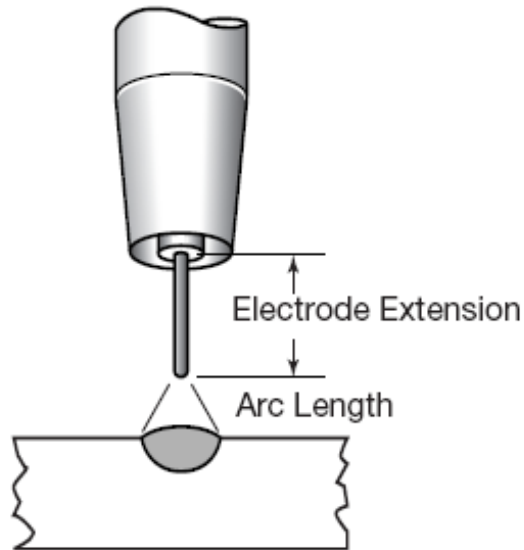


Fig. 2-2 Electrode extension

Besides, other parameters such as electrode orientation and shielding gas are also important which influence the process significantly.

2.2 Metal Transfer in GMAW

In GMAW, the electrode wire melts forming a droplet at its end and the droplet eventually transfers into the base metal. This periodical metal melting and droplet forming, growing, detaching, and traveling process is traditionally referred to as the metal transfer process.

As previously mentioned [1], the American Welding Society classifies the metal transfer into three major types/modes: short-circuiting, globular, and spray. Metal transfer modes

are affected by several operational factors, such as welding current, composition of shielding gas, wire extension, the ambient pressure, active elements in the electrode, polarity, and welding material [20-23]. Of all of these, welding current is the most important factor to determine the metal transfer mode. When a continuous waveform current is used and the current is small, the droplet may not be detached until the droplet contacts the weld pool. This transfer mode is referred as short-circuiting transfer. If the welding current increases or the arc length increases, the droplet will gradually grow until the gravitational force could balance the surface tension, and then the droplet will detach. This transfer mode is globular transfer. When the current further increases, the electromagnetic force may become a sufficiently large enough detaching force to detach the droplets whose diameter is similar (drop spray) to or much smaller (streaming spray) than that of the electrode wire. The metal transfer modes were widely studied in the literatures [23-25]. Metal transfer control was also a focus in the research community [26-29]. The International Institute of Welding (IIW) further classifies globular transfer into Drop Globular and Spelled Globular [25, 30]. The IIW classification of metal transfer is shown in Table 2-1 [25, 31].

Table 2-1 Classification of Metal Transfer in GMAW



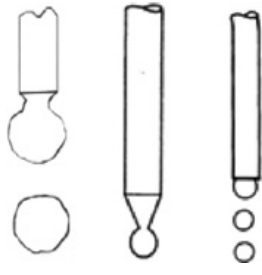

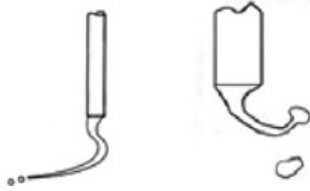
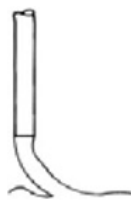
Metal Transfer Mode		Sketch	Examples
1. Free Flight Transfer	1.1 Globular 1.1.1 Drop		Low Current GMAW
	1.1.2 Repelled		CO ₂ Shield GMAW

Table 2-1 Classification of Metal Transfer in GMAW (Continued)

Metal Transfer Mode		Sketch	Examples
	1.2 Spray 1.2.1 Projected		Intermediate Current GMAW
	1.2.2 Streaming		Medium-Current GMAW
	1.2.3 Rotating		High-Current GMAW
	1.3 Explosive		SMA (Coated Electrode)
	2 Bridging Transfer	2.1 Short-Circuiting	
	2.2 Bridging without interruptions		Welding with Filler Wire Addition
3 Slag Protected Transfer	3.1 Flux Wall Guided		SAW
	3.2 Other Modes		SMA, Cored Wire, Electroslag

2.2.1 Short-circuit metal transfer

Different modes of metal transfer are generated by different levels of current. When the current is small, the droplet may not be detached until the droplet contacts the weld pool. In this case, the transfer mode is short-circuiting [1-3, 16-18, 32-35].

The transfer of a single molten droplet of electrode occurs during the shorting phase of the transfer cycle (See Fig. 2-3). Physical contact of the electrode occurs with the molten weld pool, and the number of short-circuiting events can occur up to 200 times per second. The current delivered by the welding power supply rises, and the rise in current accompanies an increase in the magnetic force applied to the end of the electrode. The electromagnetic field, which surrounds the electrode, provides the force, which squeezes (more commonly known as pinch) the molten droplet from the end of the electrode.

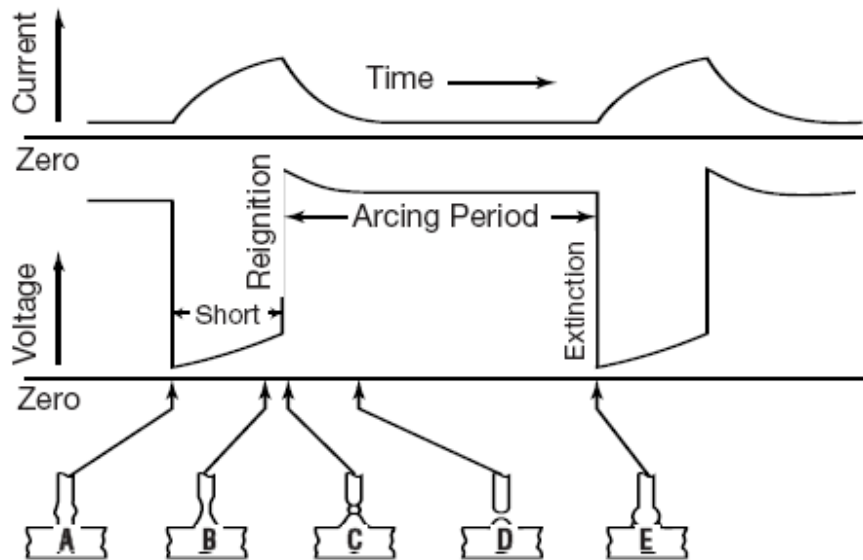


Fig. 2-3 Short-circuiting transfer

A The solid or metal-cored electrode makes physical contact with the molten puddle. The arc voltage approaches zero, and the current level increases. The rate of rise to the peak current is affected by the amount of applied inductance.

B This point demonstrates the effect of electromagnetic forces that are applied uniformly around the electrode. The application of this force necks or pinches the electrode. The voltage very slowly begins to climb through the period before detachment, and the current continues to climb to a peak value.

C This is the point where the molten droplet is forced from the tip of the electrode. The current reaches its maximum peak at this point. Jet forces are applied to the molten puddle and their action prevents the molten puddle from rebounding and reattaching itself to the electrode.

D This is the tail-out region of the short-circuit waveform, and it is during this downward excursion toward the background current when the molten droplet reforms.

E The electrode at this point is, once again, making contact with the molten puddle, preparing for the transfer of another droplet. The frequency of this varies between 20 and 200 times per second. The frequency of the short-circuit events is influenced by the amount of inductance and the type of shielding gas. Additions of argon increase the frequency of short-circuit and it reduces the size of the molten droplet.

Because of the low-heat input associated with short-circuiting transfer, it is more commonly applied to sheet metal thickness material. However, it has frequently found use for welding the root pass in thicker sections of material in open groove joints. The short-circuiting mode lends itself to root pass applications on heavier plate groove welds or pipe.

2.2.2 Globular transfer

If the current increases, but not large enough to generate a sufficiently large electromagnetic force [1] to detach the formed droplet, then the droplet may surpass the diameter of the electrode wire and be detached mainly by gravity. This transfer mode is globular [1-3, 16-18, 32-35].

Globular metal transfer is one of GMAW metal transfer modes, whereby a continuously fed solid or metal-cored wire electrode is deposited in a combination of short-circuits and gravity-assisted large drops. The larger droplets are irregularly shaped.

During the use of all metal-cored or solid wire electrodes for GMAW, there is a transition where short-circuiting transfer ends and globular transfer begins. Globular transfer characteristically gives the appearance of large irregularly shaped molten droplets that are larger than the diameter of the electrode. The irregularly shaped molten droplets do not follow an axial detachment from the electrode, instead they can fall out of the path of the weld or move towards the contact tip. Cathode jet forces, which move upwards from the work-piece, are responsible for the irregular shape and the upward spinning motion of the molten droplets.

The process at this current level is difficult to control, and spatter is severe. Gravity is instrumental in the transfer of the large molten droplets, with occasional short-circuits.

2.2.3 Spray transfer

If the current further increases, then the transfer mode may become the projected spray if the detaching electromagnetic force becomes sufficiently large. In this case, the streaming or rotating spray transfer may occur [1-3, 16-18, 25, 32-35].

Spray metal transfer is the highest energy mode of metal transfer, whereby a continuously fed solid or metal-cored wire electrode is deposited at a higher energy level, resulting in a stream of small molten droplets. The droplets are propelled axially across the arc. It is the highest energy form of GMAW metal transfer.

There are many advantages of spray metal transfer.

- High deposition rates.
- High electrode efficiency of 98% or more.
- Employing a wide range of filler metal types in an equally wide range of electrode diameters.

- Excellent weld bead appearance.
- High operator appeal and ease of use.
- Little post weld cleanup required.
- Absence of weld spatter.
- Excellent weld fusion.
- Widely applications in semiautomatic, robotic, and hard automation fields.

But there are still some limitations of axial spray transfer. For example, welding fume generation is higher. The higher-radiated heat and the generation of a very bright arc require extra welder and bystander protection. The higher heat input may cause welder distortion.

2.2.4 Factors Affecting Metal Transfer Types

Metal transfer modes are affected by several operational factors, such as welding current, composition of shielding gas, wire extension, the ambient pressure, active elements in the electrode, polarity, and welding material [1-3, 20-25, 32-35] Of all of these, welding current is the most important factor to determine the metal transfer mode and it has been discussed before.

Different shielding gases can produce totally different metal transfer types. Argon and helium are the two inert shielding gases used for protecting the molten weld pool. These two inert shielding gases do not react with the molten metal so that they will not influence the components of welds. In the GMAW process, the shielding gas will be ionized to become a conductive gas. The thermal conductivity is the most important consideration for selecting a shielding gas. High thermal conductivity levels result in more conduction of the thermal energy into the work-piece. The thermal conductivity also affects the shape of the arc and the temperature distribution within the region. As argon has a lower thermal conductivity rate which is about 10% of level for helium, it is suitable for the full penetration research. CO₂ is a reactive shielding gas used in GMAW. When CO₂ is adopted, it is very difficult to obtain free flight metal transfer as the

electromagnetic force will become retaining force. Fig. 2-4 shows the different bead contour and penetration patterns for various shielding gas [3].

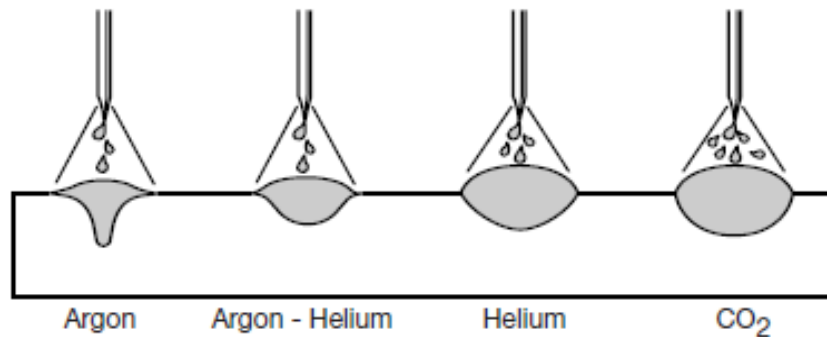


Fig. 2-4 Bead contour and penetration patterns for various shielding gases

Wire extension is also important to influence the metal transfer types. With a longer electrode extension, the transition current from globular to spray will decrease. Other influence factors play important roles in metal transfer, and it will be not discussed in this dissertation as they are not as important as the ones discussed before.

2.3 Previous Research of Novel Welding Process on Metal Transfer

As the distortion and internal stress in the welds is related to the square of welding through work-pieces, the best way to reduce them is to reduce the welding current. However, when the welding current is lower than the transition current, short-circuiting or globular transfer will be generated. In this case, researchers did much work to propose and develop novel modified GMAW to lower welding current and eliminate the spatters.

2.3.1 Laser-MIG hybrid welding

The laser-MIG hybrid welding process is a coupling of a traditional MIG welding process and a laser welding process [8-15, 36-40]. In laser-MIG hybrid welding process, the laser beam aims at the welding pool to increase the welding penetration. The laser preheats the work piece to make the droplet transfer easier which also results in a deeper penetration. The MIG torch provides the molten metal for the joining process. The metal transfer type

is mainly determined by the GMAW process. To ensure a stable metal transfer process, the welding current is usually higher than the transition current. Fig. 2-5 shows the working process of laser-MIG hybrid welding [40]. Laser –MIG hybrid welding leads to significant improvements in welding speed and weld quality [15]. Figure 2-6 shows torch installation of laser-MIG [39].

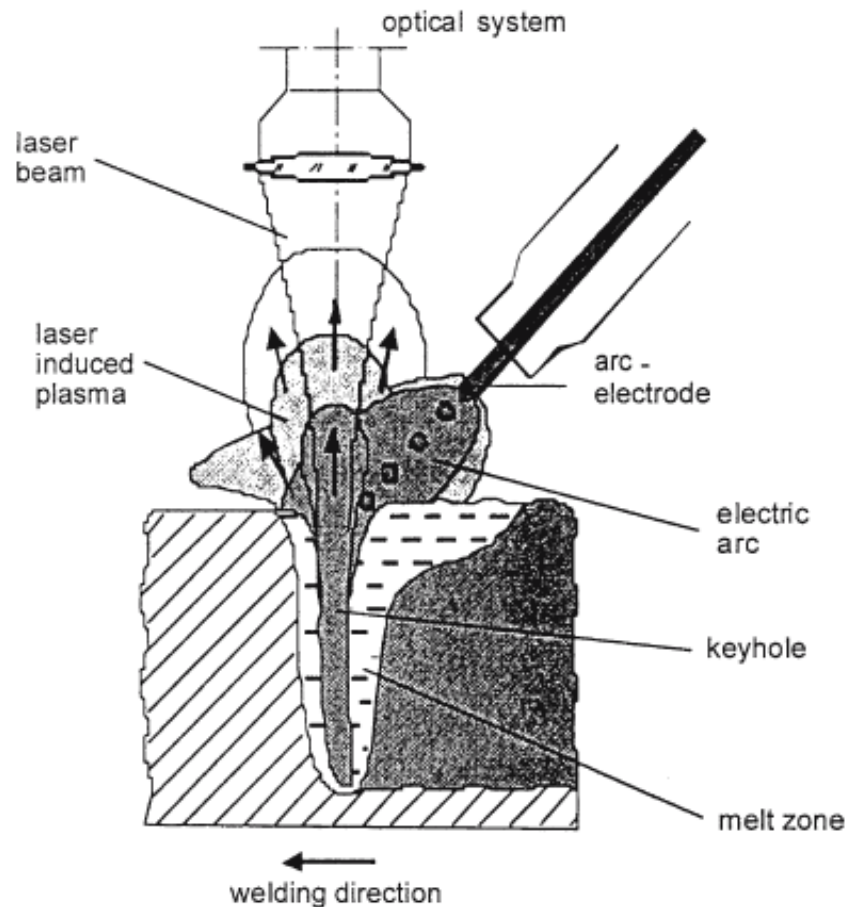


Fig. 2-5 Laser-MIG/MAG welding process

The hybrid welding process is involved in a growing number of industrial applications due to its technical advantages. It will increase the welding speed thus high productivity. In hybrid process, the cost of power source will be reduced and the electrical efficiency will increase. A good weld quality is obtained with low and predictable distortion, which implies a reduction in the need for rework.

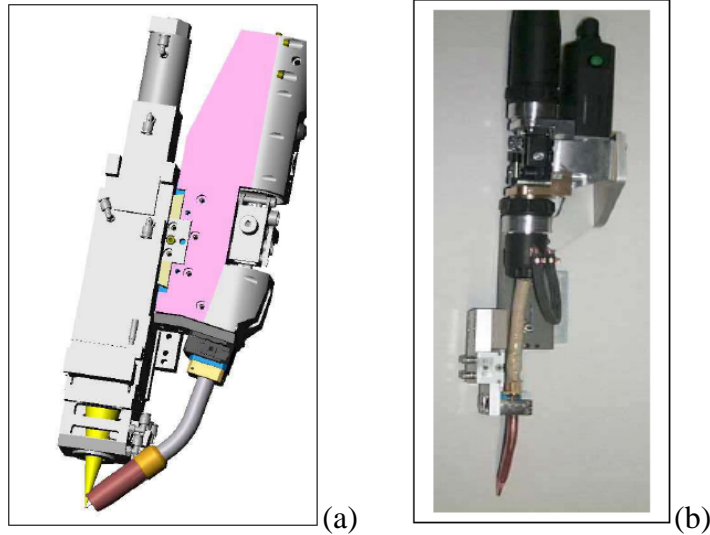


Fig. 2-6 Torch installation of laser-MIG: (a) Instruction diagram (b) Real torch

The disadvantage of laser-MIG welding firstly limits its application. First it is a little expensive to employ a high power laser in the industry process. Second the laser-MIG hybrid welding process has large numbers of parameters to be set up. The set up of the processing parameters requires a high degree of skill and accuracy, and these imperatives added to an incomplete knowledge of the process are limiting factors for the industrial application. Moreover, laser-MIG hybrid welding can't reduce base metal heat input because laser is a great heat source and metal transfer was determined by the GMAW itself.

2.3.2 Surface Tension Transfer

Surface Tension Transfer (STT) welding is a GMAW, controlled short circuit transfer process developed and patented by The Lincoln Electric Company [41-42]. Unlike standard CV GMAW machines, the STT machine has no voltage control knob. STT uses current controls to adjust the heat independent of wire feed speed, so changes in electrode extension do not affect heat.

A Background Current between 50 and 100 A maintains the arc and contributes to base metal heating. After the electrode initially shorts to the weld pool, the current is quickly reduced to ensure a solid short. Pinch Current is then applied to squeeze molten metal

down into the pool while monitoring the necking of the liquid bridge from electrical signals. When the liquid bridge is about to break, the power source reacts by reducing the current to about 45-50 A. Immediately following the arc re-establishment, a Peak Current is applied to produce plasma force pushing down the weld pool to prevent accidental short and to heat the puddle and the joint. Finally, exponential Tail-out is adjusted to regulate overall heat input. Background Current serves as a fine heat control [43-44].

The basic principle of STT control technology can be explained below with reference to Fig. 2-7 in [45-51]:

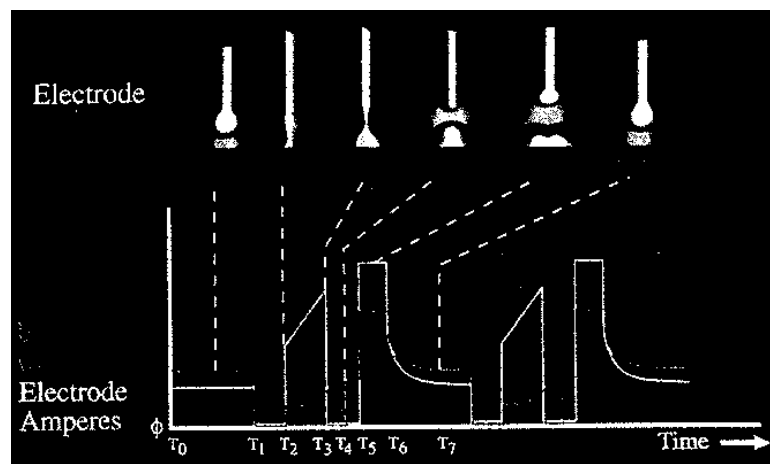


Fig. 2-7 Surface tension transfer (STT) process

(1) Background current period $T_0 - T_1$: In this period, the current is at the level of the arc prior to shorting to the weld pool. It is a steady-state current level, between 50 and 100 A.

(2) Ball time $T_1 - T_2$: When the electrode initially shorts (at the background current), the “arc voltage” detector provides a signal that the “arc” is shorted. The background current is further reduced from the background level to 10 A for approximately 0.75 ms. This time interval is referred to as the ball time.

(3) Pinch mode $T_2 - T_3$: Following the ball time, a high current is applied to the shorted electrode in the form of an increasing, dual-slope rA. This accelerates the transfer of the

molten metal from the electrode to the weld pool by applying electric pinching forces. (Note that the electrode-to-work voltage is non zero during this period due to the high resistivity of iron at its melting point of 1550 °C)

(4) The dv/dt calculation $T_3 - T_4$: This calculation is included within the pinch mode. It is the calculation of the rate of change of the shorted electrode voltage vs. time. When this calculation indicates that a specific dv/dt value has been attained, indicating that fuse separation is about to occur, the current is reduced to 50 A in milliseconds. (Note, this event occurs before the shorted electrode separates. T_4 indicates the separation has occurred, but at a low current.)

(5) Plasma boost $T_5 - T_6$: This mode follows immediately the separation of the electrode from the weld pool. It is the period of high arc current where the electrode is quickly “melted back.”

(6) Plasma $T_6 - T_7$: During this period, the arc is reduced from plasma boost to the background current level.

STT welding has many advantages. First, good penetration and low heat input control could be obtained, so that it is ideal for welding on joints with open root, gaps, or on thin material with no burn-through. The ability to concentrate the arc also aids in the elimination of cold lapping on open root joints for pipe and pressure vessels. The lower heat input provides the advantage of less material distortion and burn-through by providing only the required amount of heat to produce the weld, even in sensitive material like stainless steel. This precise control of heat means that even thin gauge galvanized sheet metal can be welded without burning off the galvanized plating on the back side of the metal. Second, as current is controlled to achieve optimum metal transfer, spatters and fumes will be reduced. As STT has the ability to use 100% CO₂ or argon shielding gas blends with larger diameter wires, costs will be reduced. Good bead control and faster travel speeds will be achieved [41-51].

The detail comparison of GMAW to STT is shown in Table. 2-2 [43].

Table 2-2 Comparison of GMAW to STT

	Gas Metal Arc Welding	Surface Tension Transfer
Metal Transfer Process	Short Circuiting Transfer	Modified Short Arc with the Aerage and Voltage changed based upon the needs of the Arc
Voltages	16V To 22V	16V To 22V
Aerages	Low Aerages: (30A to 200A)	Two Aerage Levels: <ul style="list-style-type: none"> • Peak Current (0A to 450A) • Background Current (0A to 125A)
Wire Electrode Size	Typically Smaller Diameters (0.025 in to 0.045 in) (0.60 mm to 1.10 mm)	Typically Larger Diameters (0.035 and 0.045)
Shielding Gases	<ul style="list-style-type: none"> • 100% CO2 (Lowest Cost) • 75% Ar/25% CO2 Gas Mix 	<ul style="list-style-type: none"> • 100% CO2 (Lowest Cost) • Custom blended to meet the optimum arc physics
Advantages	<ul style="list-style-type: none"> • All Position Welding • Low Cost 	<ul style="list-style-type: none"> • Low Heat Input • Controlled Heat Input • All Position Welding • Handles Poor Fit Up • Minimal Spatter • Can Use a Larger Wire Size • Minimal Smoke • Low Cost Gas • Good Fusion
Limitations	<ul style="list-style-type: none"> • Spatter • Potential Lack of Fusion • Limited to a Modified Short-Circuit 	<ul style="list-style-type: none"> • More Expensive Equipment • Limited to Thin Material Mode
Costs	\$3,000	\$6,000

Table 2-2 Comparison of GMAW to STT (Continued)

	Gas Metal Arc Welding	Surface Tension Transfer
Training/Skill	Similar	Similar
Materials	<ul style="list-style-type: none"> • Carbon and Low Alloy Steels • Galvanized/Zinc Coated • Stainless and Nickel Alloys • Silicon Bronze and Copper Alloys 	<ul style="list-style-type: none"> • Carbon and Low Alloy Steels • Galvanized/Zinc Coated (plating unaffected on backside) • Stainless and Nickel Alloys (with greatly reduced spatter) • Silicon Bronze and Copper Alloys
Industries	<ul style="list-style-type: none"> • Automotive • Food and chemical processing • Consumer products 	<ul style="list-style-type: none"> • Automotive • Pipe and Pressure Vessel • Power Generation • Food and chemical processing • Thin gauge consumer products

Like other welding processes, STT also has some limitations. By the use of a patent protected technology [41-51] and the cost savings that are realized through its benefits, the STT power source is initially more expensive than a constant voltage power source. The deposition rates are lower than globular, spray arc and pulse spray, but are equal to that of short circuit welding. As in pulsed spray welding, setting the welding parameters for STT are quite different than settings normally used and may require additional training. Finally, the STT process differs from the conventional short circuiting process through its inability to perform aluminum welding at this time. The key aspect of STT technology appears to be the application of a high current to impose an electric pinching force to speed the transfer and the application of a rapid current reduction when the liquid metal bridge is about to break to reduce the explosion and spatters. In order to eliminate the spatters, the current should be reduced to zero. However, reduction to zero will extinguish the arc and re-strike of the arc will cause larger amount of spatters.

Alternatively, if the current is too small, the arc may also be extinguished. Hence, 50 A has been selected based on a trade-off between the spatter reduction and arc maintenance.

2.3.3 Cold Metal Transfer

Developed by Fronius International GmbH, Wels, Austria, the CMT process is based on short circuiting transfer, or rather, on a deliberate, systematic discontinuing of the arc [52-55]. The result is a sort of alternating "hot-cold-hot-cold" sequence. This "hot-cold" process greatly reduces the arc pressure.

The CMT process is a dip arc process with a completely new method of the droplet detachment from the wire. In the conventional dip arc process the wire is advanced until a short circuit occurs. At that moment the welding current rises and this high current is responsible for the short circuit to open so that the arc can ignite again. On the one hand the high short circuit current corresponds to a high heat input. On the other hand the short circuit opens rather uncontrolled which results in lots of spatters in the conventional dip arc process.

In the CMT process the wire is not only pushed towards but also drawn back from the work-piece, an oscillating wire feeding with an average oscillation frequency up to 70 Hz is performed as it is shown in Fig. 2-8 [53].

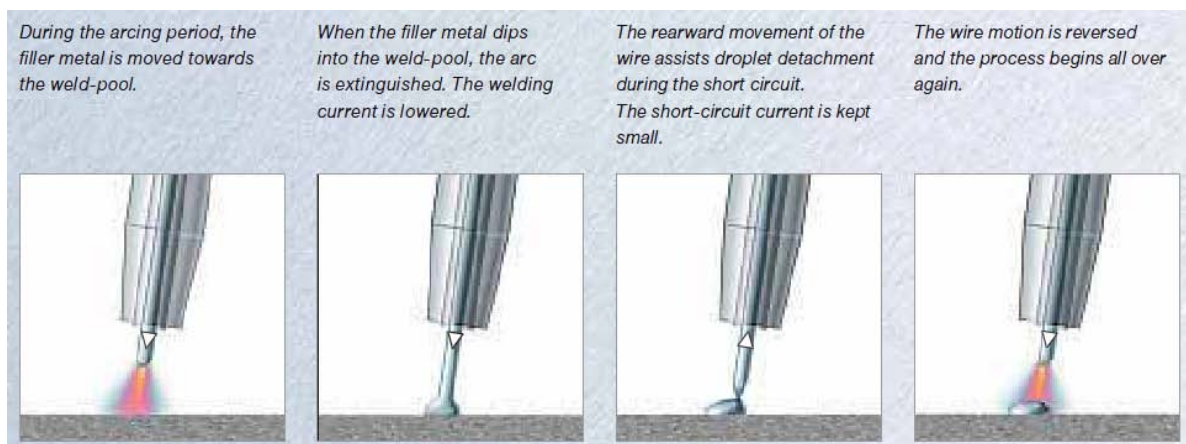


Fig. 2-8 Cold Metal Transfer Process

In the CMT-process the wire is moved towards the work-piece until a short circuit occurs. At that moment the wire speed is reversed and the wire pulled back. When the short circuit opens again, the wire speed is again reversed, the wire moves towards the work-piece again and the process begins again. Here there is no predetermined time schedule for the wire movement, but the occurrence and the opening of a short circuit determine the wire speed and direction. Therefore the wire movement determines what is happening in the weld pool, and the things happening in the weld pool determine the wire movement.

The CMT-process has many advantages.

- Assists droplet detachment by means of the wire-motions incorporated in the digital process-control
- Reduces the thermal input by achieving almost current-free metal transfer
- Ensures spatter-free metal transfer by controlling the short circuiting
- Permits spatter-free MIG/MAG robot welding and brazing of ultra-light gauge sheets from 0.3 mm (0.012"), and joining of steel to aluminum

Compared to conventional GMAW, the CMT process reduces heat input to the work-piece, and it is a spatter-free process as wire motions are incorporated into process control. Another important advantage of the CMT-process is the extremely perfect arc length control. In conventional GMA welding, the surface of the work-piece and the welding speed can both have a very marked effect on the stability of the arc. In CMT, the arc length is acquired and adjusted mechanically. This means that the arc remains stable, no matter what the surface of your work-piece is like or how fast you want to weld. Further the CMT-process is the extremely high gap bridgability. The problem for thin sheets and large gaps with conventional GMAW processes is the relatively high heat input. In CMT-process, as low heat input to the work-piece, thin sheet welding and brazing could be obtained with less distortion. The concentrations of pollutants investigated in CMT brazing are far below those encountered in MIG brazing – nearly 90 % less copper fumes, and as much as 63 % less zinc than with conventional dip-transfer arc-technology. The CMT-process could join different metal, such as aluminum and steel, aluminum and magnesium [56-59].

As with every other welding process, the CMT-process has also its limits. Fig. 2-9 shows the region of the pure CMT-process (with no addition of the pulsed arc) in the diagram of welding voltage versus welding current [52].

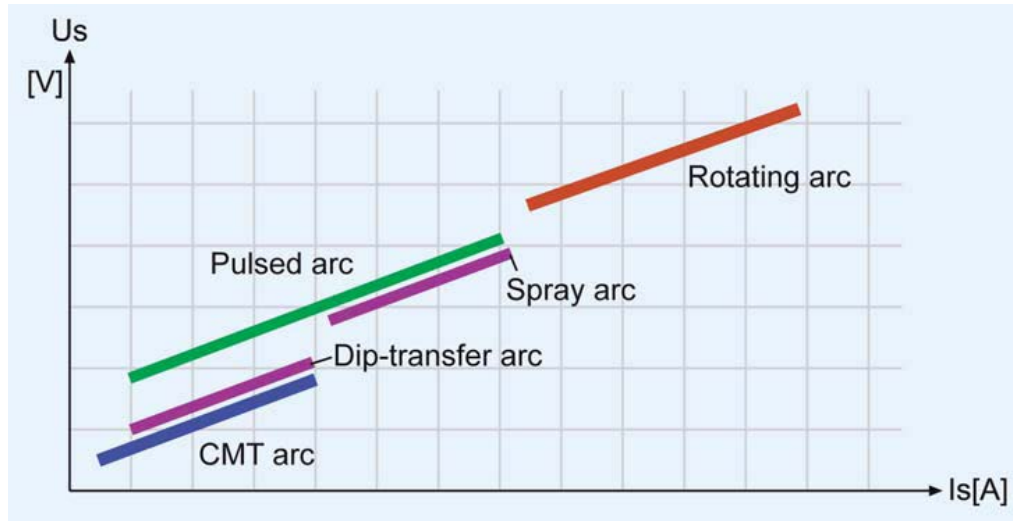


Fig. 2-9 Voltage versus current diagram with addition of the region for the pure CMT-process

The CMT-process has its upper limit at the point where the transition arc starts to appear. For higher currents a short circuit does not occur any more and therefore the CMT process cannot be performed any more. The lower limit for the CMT-process is lower compared to the standard dip arc process. Therefore the range of welding becomes larger. The diagram also clearly shows that the power and therefore the heat input of the CMT process is lower compared to the conventional dip arc process.

As heat input is low in CMT-process, the height-to-width-ratio of weld seam is relatively high, so the penetration is not good. So the CMT-process could be combined with other GMAW process to produce good weld penetration, such as with pulsed GMAW [52, 60].

2.3.4 Double Electrodes GMAW

Double Electrodes GMAW (DE-GMAW) was proposed and developed in Center of Manufacturing at University of Kentucky [61-67]. The aims are to seek a method to

double the welding productivity meanwhile reducing heat input to welds and monitoring the metal transfer. High welding productivity requires faster wire feeding speed. To melt more metal, a larger melting current is an essential condition. In conventional GMAW, all melting current flows through base metal which means that melting current equals base metal current. Thus, it is impossible to increase base metal current freely because base metal current is always restricted by the application and material. Excessive heat input to work-piece will take distortion and internal stress to welds which will increase the cost of after treatment.

DE-GMAW is oriented to solve this dilemma by adding a bypass torch to conventional GMAW so the melting current does not have to all pass through the base metal, as shown in Fig. 2-10 [61]. In the system shown in Fig. 2-10, a GTAW torch was added to bypass the total current through the GMAT torch.

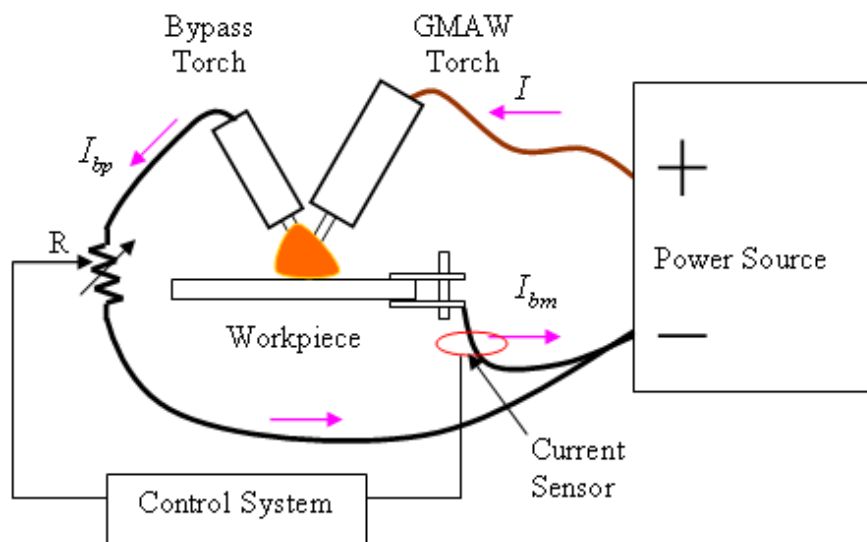


Fig. 2-10 Non-consumable DE-GMAW system diagram

In DE-GMAW, the current relationship is represented by

$$I_{total} = I_{melting} = I_{base\ metal} + I_{Bypass} \quad (2-1)$$

From Eq. (2-1), the total welding current is divided into base metal current and bypass current. The total current of DE-GMAW is determined by the wire feed speed and

welding current (Constant voltage mode) or the welding power current (Constant welding mode). In this case, the base current could be adjusted by changing the bypass current. The melting current could be significantly increased without changing the base current. The metal transfer type could be also controlled by controlling the bypass current such that free flight metal transfer could be obtained with welding current a little below the transition current.

To better utilize the bypass current, DE-GMAW is further developed and the bypass GTAW torch is replaced by another GMAW torch. In this case, the bypass current will be used to melt welding wire and productivity will be further increased. The system schematic figure is shown in Fig. 2-11 [64].

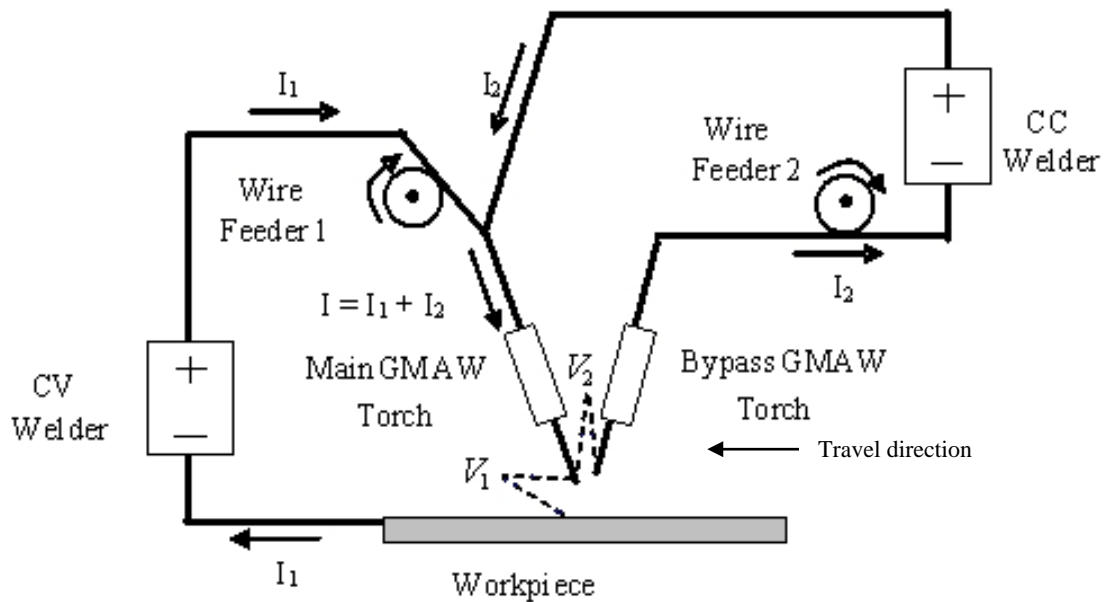


Fig. 2-11 System diagram of consumable DE-GMAW

The DE-GMAW provides an effective way to increase welding productivity and minimize the heat input to work-piece. However, the total current is higher than the transition current. The capability to control metal transfer is not obvious. As bypass torch is adopted, it will reduce the arc stability and cause magnetic blow.

2.3.5 Double Bypass GMAW

To increase arc stability and eliminate magnetic below, Double Bypass GMAW (DB-GMAW) is developed in Center of Manufacturing at University of Kentucky [68-70]. Two GTAW torches are adopted as the two bypass one. As shown in Fig. 2-12, the force acting on the droplet will be balanced by the bypass forces themselves. The left bypass current will be the same as the right one, and they could be monitored and controlled. In this case, magnetic below will be avoided.

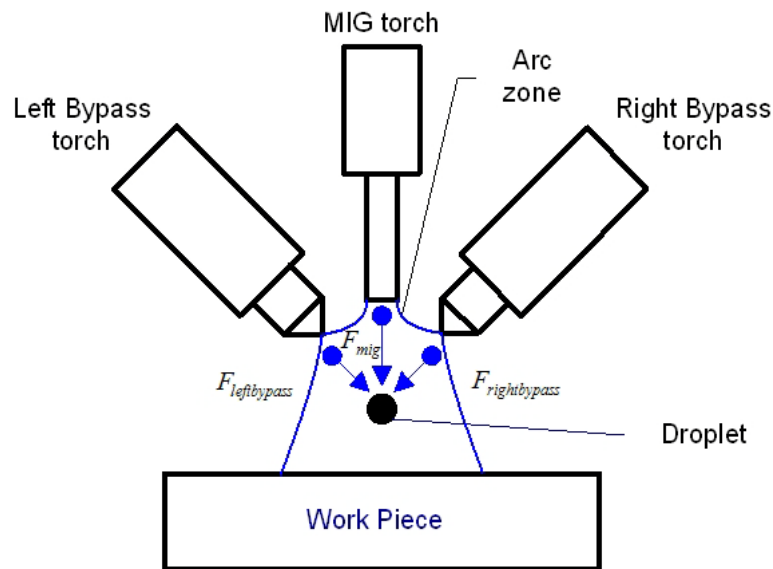


Fig. 2-12 Arc forces act on the droplet in DB-GMAW

The schematic image of DB-GMAW is shown in Fig. 2-13. As the bypass welding currents could be controlled, the current through the base metal is also well controlled. Heat input to work-piece is also reduced to a desired level.

Similar as the DE-GMAW, the metal transfer type in DB-GMAW is changed. Free flight metal transfer could be obtained with total welding current a little below transition current. Much electric energy is used on the bypass torches which take little benefits to the metal transfer process.

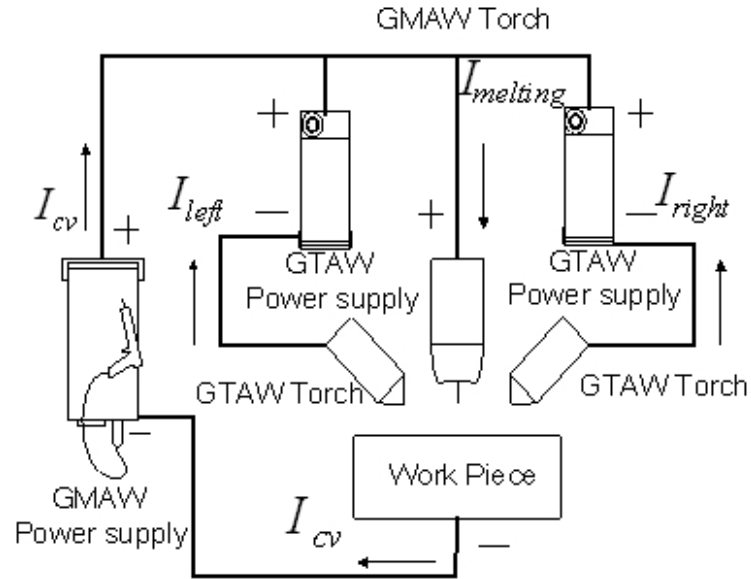


Fig. 2-13 Illustration of DB-GMAW

2.3.6 Other Metal Transfer Control Methods of GMAW

Pulsed spray metal transfer (GMAW-P) is a highly controlled variant of axial spray transfer, in which the welding current is cycled between a high peak current level to a low background current level. In GMAW-P, the base current is used to keep the arc on while the peak current is adopted to melt the electrode and detach droplet. The heat input and average current will be lowered to an acceptable level. While the pulsed GMAW has been widely adopted in industry, it does have certain limitations. The fundamental cause of these limitations is that a peak current higher than the transition current [1] must be used in order to detach the droplet to complete the metal transfer. Vaporization occurs under high Aerge and results in fumes. More critically, the arc pressure is proportional to the square of the Aerge [4]. The high arc pressure may blow liquid metal away from the weld pool. For full penetration application where the work-piece has to be fully penetrated through the entire thickness, the high arc pressure may easily cause burn-through. This is the major reason why the less productive GTAW process, whose Aerge can be set at whatever level needed, has to be used for the root pass in full penetration applications.

An improved method of gas metal arc welding (GMAW) is developed in Center of Manufacturing at University of Kentucky [27-28, 71]. The method includes utilizing a pulsed current having a variable waveform to ensure the detachment of one-droplet-per-pulse of current. During the welding process, the current is sufficient to produce a droplet at the end of a consumable electrode wire. After the droplet reaches a desired size, the current is lowered to induce an oscillation in the droplet. The current is then increased which, in combination with the momentum created by the oscillation, effects droplet detachment. The oscillation may be monitored by observing the arc voltage to determine a preferred detachment instant. A computer implemented method allows for the adaptive control of the current waveform to accommodate for anticipatable variations in the welding conditions, while maintaining ODPP transfer and a constant pulse period.

Methods based on mechanically assisted droplet transfer have also been proposed/developed to produce the spray transfer below the transition current [72-73] but the torch size and weight are greatly increased resulting in a special and costly equipment that is not suitable for other applications. Ultrasonic GMAW is recently developed to control metal transfer. However, a high ultrasonic power will be used and the process stability should be further developed.

To sum up, aforementioned methods are “neat” using smart approaches to resolve different issues and difficulties but being “neat” also restricts their applications in wider ranges. Toward the development of a more general method, the laser enhanced GMAW has been proposed and developed in this dissertation. It adds a relatively low power laser to a conventional GMAW and the objective is to provide an auxiliary force to help detach the droplet at a desired diameter with any desired current that most suits for the application including future adaptive control applications where the current needs to be adjusted freely as determined by the control algorithm.

CHAPTER 3 PRINCIPLES OF LASER

ENHANCED GMAW AND EXPERIMENT

SYSTEM

Laser enhanced GMAW is proposed and developed by adding a low power laser to generate an auxiliary detaching force. To obtain a stable process, experiment system should be constructed properly, and welding parameters should be selected in a reasonable range.

3.1 Principle and System Construction

3.1.1 Principle of Laser Enhanced GMAW

Fig. 1-1 shows the principle of the Laser Enhanced GMAW proposed. A laser beam aims to the droplet. The intention is to detach the droplet using the laser recoil pressure as an auxiliary detaching force to compensate for the lack of the electromagnetic force associated with relatively small amperage that is needed for a particular application, rather than to provide an additional heat to speed the melting of the wire. The associated additional heat from the laser should be insignificant in comparison with that of the arc used.

It should be mentioned, although the Laser Enhanced GMAW also applies a laser beam into GMAW process, it is different from the Laser-GMAW hybrid process [8-15, 36-40] where a laser of significant power enhances the results of the arc in the weld pool. To this end, the laser in the hybrid process interacts with the GMAW process and is applied either at the arc or in the weld pool as shown in Fig. 2-6. Hence, the proposed Laser

Enhanced GMAW is different from the hybrid laser-GMAW process in both operation principle and objective.

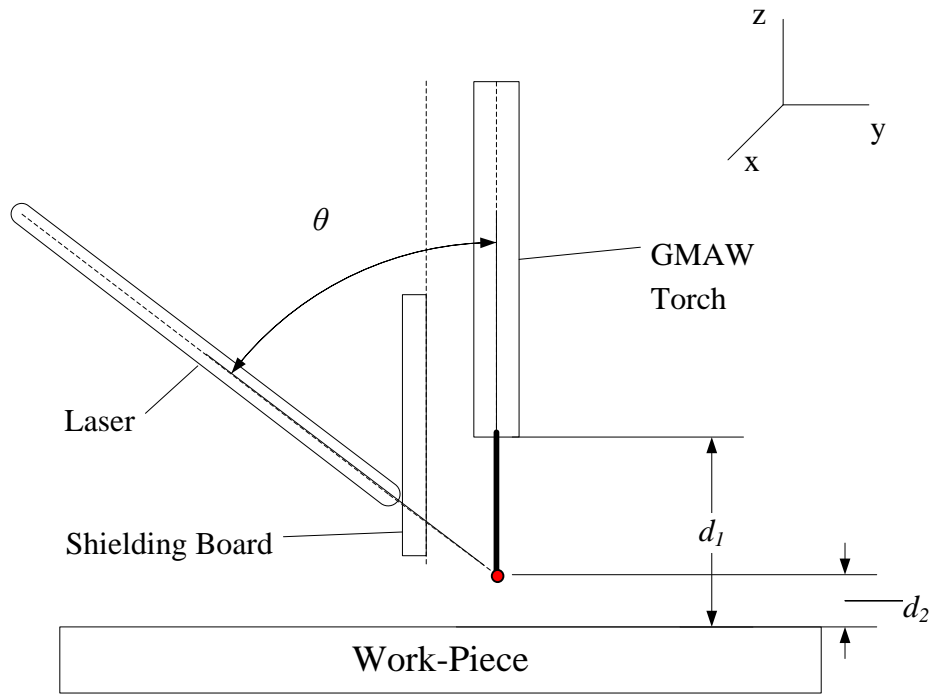
3.1.2 System Construction

Fig. 3-1 shows important parameters that specify a realization of Laser Enhanced GMAW system developed to prove the concept. To conduct the Laser Enhanced GMAW process in an expected way, parameters need to be set appropriately. In this dissertation, the GMAW torch and the laser head do not move. The work-piece moves at a constant speed. The direction of this movement will be perpendicular to plane shown in the Fig. 3-1 (a). The camera was also placed in this direction with a distance about 1.2 m from torch.

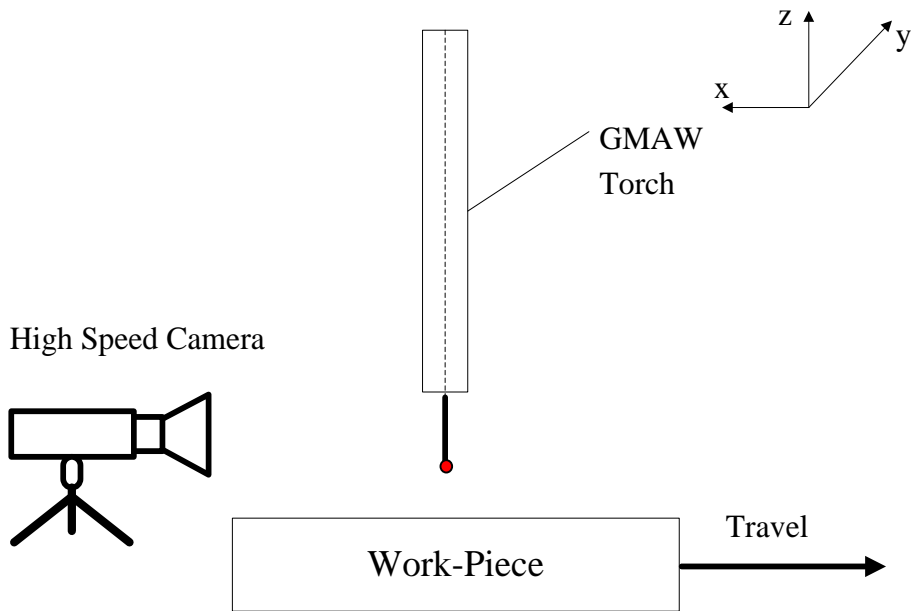
Contact tube-to-work-piece distance: In conventional GMAW, it plays a role in determining the stability of the process. In Laser Enhanced GMAW, a too small d_1 would make it difficult to install other components. Experimental results suggest that d_1 be set around 20 mm.

Angle between Laser Beam to GMAW torch: θ determines the orientation of the laser recoil force as a vector in relation to other forces and its component/projection as the effective detaching force. It also affects the compactness and realizability of possible future system for industry use. While a large angle would reduce the effective detaching force along the wire axis and affect the compactness of the system, a small angle would require the gas nozzle to be modified such that the laser can reach the droplet. In this feasibility study, the nozzle is not modified and the angle is selected to be around 60 degree for easy installation at the expenses of reducing system compactness.

Another important parameter is the distance from the point where the laser intersects the wire axis and is denoted as (d_2) in Fig. 3-1. As the laser beam must be applied onto the droplet to detach, a high speed camera was first used to record conventional GMAW process and then the recorded video was analyzed.



a) Installation parameters



b) Camera installation

Fig. 3-1 System installation

The Thermal Arc® EXCEL-ARC® 8065 CC/CV weld power supply is used in this research as the welding power. It is a combination stick and wire machine in one case. The digital meter is standard for preset welding conditions. A locking switch keeps the machine locked into the CC or CV mode, preventing any chance of slipping into a different mode while welding. The welder power supply could provide 600A/44V (CC mode) at 60% duty cycle or 650A/44V (CV mode) at 100% duty cycle. There is a remote connector for remote control, and the welding voltage/current waveform could be monitored and controlled by PC computer.

A high speed camera was used to capture the video of the welding process for off-line analysis. Fig. 3-2 shows the high speed camera used that is capable of recording the metal transfer at 33,000 frames per second. A band-pass filter centered at 810 ± 2 nm with full width at half maximum 10 ± 2 nm was used to observe the process and record the images. All images presented in this study were recorded using the high speed camera shown in Fig. 3-2 with this band-pass filter.



Fig. 3-2 Olympus i-speed high speed camera

Choice of Laser: As the laser is supposed to point to the droplet rather than the weld pool, the focal zone of the laser should be not much larger than the diameter of the wire. In this

study, the diameter of the wire is 0.8 mm and the diameter of droplet may be just slightly greater. The laser should thus be selected accordingly. For the research purpose in this dissertation, the efficiency of the laser is not a primary concern and the use of a laser of larger power and larger focal zone should not affect the effectiveness of the experimental results. The University of Kentucky Welding Research Laboratory possesses a Nuvonyx Diode laser ISL-1000L whose focal beam dimension is 1 mm × 14 mm and wavelength is 808 nm. When this laser is used, only less than 1/14 of the laser beam can be applied onto the droplet to generate the recoil force to detach the droplet.

Fig. 3-3 shows the arrangement of the laser in relation with the torch. In this experimental setup, the laser beam is aligned with the wire. In order to protect the end of laser from contamination of possible fumes, a shielding board (not shown in Fig. 3-3) is added between the laser and torch and the laser is projected through a hole on the shielding board to the wire.



Fig. 3-3 Installation of GMAW and Laser (the shielding board is not shown in the picture)

3.2 Sensing system

Experimental data is collected through sensing system via several sensors to data acquisition board, meanwhile the control signals should be sent to experiment system to conduct the welding process. The sensing and control system includes the hardware and software system.

3.2.1 Hardware to build sensing and control system

(1) Welding current:

The metal transfer and wire melting are mainly determined by the welding current, and it should be monitored. In this research, a CLN-500 closed loop Hall Effect current sensors are used to monitored the current value. CLN-500 current sensor has a nominal current of 500A rms with a measuring range of 0 to $\pm 1200A$. The accuracy at 25°C is $\pm 0.5\%$ of the nominal current and response time is less than $1\mu s$. The welding current is also measured from the 19-pin connector at the back of the welder power supply. Experiment results show that the welding currents from these two methods are almost the same.

(2) Welding Voltage:

Welding voltage influences the arc length, wire extension, etc. To monitor and control welding voltage is very important to obtain stable welding process. The self-made divider circuit is used to monitor the welding voltage. Similar as the welding current, the welding voltage can also be measured from the output of 19-pin connector at the back of the welder power supply. The two results are almost the same.

(3) Isolation Module

There are some noises when monitoring the welding voltage and current. Considering the fluctuation of electric network, isolation module should be adopted in the experiment system. The SCM5B41-02 input isolation module from Dataforth Company is used in the research. SCM5B41 wide bandwidth voltage input module provides a single channel of

analog input which is amplified, isolated, and converted to a high level analog voltage output. This voltage output is logic-switch controlled, allowing these modules to share a common analog bus without the requirement of external multiplexers. The SCM5B49 output isolation module from Dataforth Company is used in the research. Each SCM5B49 voltage output module provides a single channel of analog output. The track-and-hold circuit in the input stage can be operated in a hold mode where one DAC can supply many output modules, or a track mode where one DAC is dedicated to each module. In addition to the track-and-hold circuit, each module provides signal buffering, isolation, filtering, and conversion to a high-level voltage output.

(4) Data Acquisition Board

In this research, the experiment data should be collected at 1k Hz (at least). The output signals should be at least at 1k Hz. In this research, the PCI-DAS 1602/12 from Measurement Computing Company is adopted. The PCI-DAS 1602/12 multifunction analog and digital I/O board sets a new standard for high performance data acquisition on the PCI bus. It has 8 differential inputs or 16 single-ended 12-bit analog inputs, and the sample rates could be up to 330 kHz. It has 24 bits of digital I/O. The two FIFO-buffered 12-bit analog outputs have the update rate up to 250 kHz.

(5) Travel Stage

To better record the metal transfer process using high speed camera, the GMAW torch and laser do not move in this experiment. In this case, a motorized circular guide linear stage is adopted. It has travel distance about 300 mm, and the travel speed could be up to 25mm/s. The minimum resolution of travel speed could be up to 0.02mm/s.

3.2.2 Software System

Labview 2009 is adopted as the main software to monitor and control the welding parameters in this research. Labview is a graphical programming environment used to develop sophisticated measurement, test, and control systems using intuitive graphical icons and wires that resemble a flowchart. It offers unrivaled integration with thousands

of hardware devices and provides hundreds of built-in libraries for advanced analysis and data visualization. Combined with the software from Measurement Computing Company, the experiment software system is established.

3.3 Experimental Materials and Conditions

The mild steel is adopted as the welding materials in this research. The wire used was ER70S-6 of 0.8 mm (0.03 inch) diameter. Pure argon was used as the shield gas and the flow rate was 12L/min (25.4 ft³/h). The travel speed is determined by the objectives of practical research. For the metal transfer research, experiments were done as bead-on-plate at a travel speed 6.6 mm/s (15.6 in./min). For the full penetration research, as the Constant Current (CC) power supply was adopted, the travel speed was an important parameter to be controlled to achieve the penetration. In this case, the travel speed was not fixed, and it should be determined by the experiments.

3.4 Summary

The experiment system for the proposed laser enhanced GMAW was realized. Sensing system was established for the data acquisition and signal outputs. High speed camera was used to record metal transfer process for the later analysis. This platform satisfies the requirements of this research.

CHAPTER 4 METAL TRANSFER PHENOMENON IN LASER ENHANCED GMAW

Laser enhanced GMAW is a recent modification of conventional GMAW by applying a relatively low power laser to the droplet. An auxiliary detaching force was generated, and the electromagnetic force needed to detach droplets, thus the current that determines this force, is reduced. In this case, metal transfer type would be changed.

4.1 Theories of Metal Transfer

In GMAW, the electrode wire melts forming a droplet at its end and the droplet eventually transfers into the base metal. This periodical metal melting and droplet forming, growing, detaching, and traveling process is traditionally referred to as the metal transfer process. A good understanding of this metal transfer process and its mechanism plays a fundamental role in effectively using/improving this welding process for production of better welds at higher productivity and has thus been an active area of research and development in welding community [5, 7, 20-32, 41-75].

There are two main well quoted theories of metal transfer, and they are force balance theory and the pinch instability theory. To better understand the metal transfer phenomenon in laser enhanced GMAW, both the two theories will be illustrated.

4.1.1 Force Balance Theory

In force balance theory, the droplet detaches when the detaching forces on the droplet exceed the static retaining force. In conventional GMAW, the major forces acting on the droplet include the gravitational force, electromagnetic force (Lorentz force), aerodynamic drag force, surface tension, and momentum force [20-25, 76]. In Laser Enhanced GMAW, a laser is applied and an additional force is introduced as shown in Fig. 4-1. Considering the momentum of the droplet, the dynamic-force balance theory (DFBM) [77] is proposed to conduct preliminary analysis of the forces for the laser enhanced GMAW.

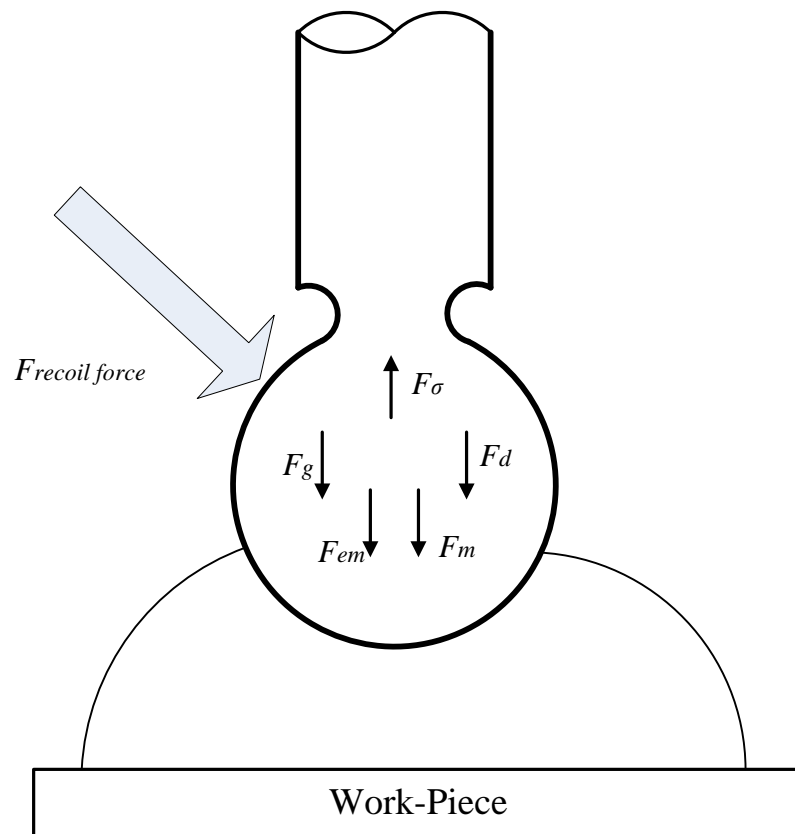


Fig. 4-1 Major forces acting on the droplet in Laser Enhance GMAW

The surface tension force, which acts to retain the droplet on the electrode, can be expressed by

$$F_{\sigma} = 2\pi r_w \sigma \quad (4-1)$$

where r_w is the electrode radius, while σ is the surface tension coefficient.

The gravitational force due to mass of droplet, which will be a detaching force, can be expressed as

$$F_g = m_d g = \frac{4}{3} \pi r_d^3 \rho g \quad (4-2)$$

where m_d is the mass of the droplet, r_d is the droplet radius, ρ is the droplet density, and g is the acceleration of the gravity.

The shielding gas covers the arc region and protects the arc and the work-piece from contamination. In GMAW, the shielding gas passes around the drop and exerts a detaching force on the droplet, and it is referred as aerodynamic drag force. In GMAW, the contribution from aerodynamic drag on the drop can be approximated by a force acting on a spherical object immersed in a uniform velocity fluid stream. The aerodynamic drag force can be expressed as

$$F_d = \frac{1}{2} C_d A_d \rho_p v_p^2 \quad (4-3)$$

where C_d is the aerodynamic drag coefficient, A_d is the area of the drop seen from above, ρ_p and v_p are the density and fluid velocity of the plasma.

In GMAW, the mass of the drop changes continuously with the molten metal melted from the solid welding wire. To consider the change of mass and the speed of metals added to the droplet and wire feed speed, the momentum is introduced. The momentum force can be expressed as

$$F_m = v_e \dot{m}_d \quad (4-4)$$

where v_e is the wire feed speed, \dot{m}_d is the change of the droplet mass.

As the welding current flows through the electrode and droplet, electromagnetic force will be generated and acted on the droplet. The direction of electromagnetic force is determined by the current pass. A diverging current pass will generate a detaching force, while a converging current will generate a detaining force. In laser enhanced GMAW, experiment results show that the arc will climb to the root of the droplet. It indicates that the electromagnetic force will be a detaching force. The electromagnetic force, F_{em} , is given by

$$F_{em} = \frac{\mu_0 I^2}{4\pi} \left(\ln \frac{r_d}{r_w} \sin \theta - \frac{1}{4} - \frac{1}{1-\cos \theta} + \frac{2}{(1-\cos \theta)^2} \ln \frac{2}{1+\cos \theta} \right) \quad (4-5)$$

where μ_0 is the magnetic permittivity, I is the welding current, θ is the half-angle subtended by the arc root at the centre of the droplet.

In conventional GMAW process, the droplet is not detached when the retaining force F_σ is still sufficient to balance the detaching force F_t

$$F_t = F_g + F_d + F_m + F_{em} \quad (4-6)$$

In laser enhanced GMAW, the total detaching force F_T will be expressed by

$$F_t = F_g + F_d + F_m + F_{em} + F_{laser\ recoil\ force} \quad (4-7)$$

When the total detaching force F_T could balance the surface tension, the droplet will be detached. However, the laser recoil pressure force $F_{laser\ recoil\ force}$ is unknown because there is less accurate calculation theory to achieve this value. In this case, the author proposes a calculating method to estimate this force which will be discussed in the later section.

During metal transfer process, the major variables that change or can be changed to affect the detaching force are the droplet mass and the current as can be seen from Eq. (4-1)-(4-5). Because the surface tension is the major retaining force and it is fixed for the given wire, the droplet can only be detached either (1) by waiting for the droplet to grow into a larger size such that the gravitational force is sufficient to break the balance; (2) by

waiting for the droplet to touch the weld pool such that an additional detaching force – surface tension between the droplet and weld pool- be added or (3) by increasing the current to increase the electromagnetic force. Since neither of these is ideal, a laser is introduced in this paper to increase the detaching force to a sufficient level. Because this laser force is controllable through laser intensity/power, droplets may be detached at a desired diameter at desired amperage.

4.1.2 Pinch Instability Theory

The pinch instability theory was developed from the Rayleigh instability model of a liquid cylindrical column. It postulates that the pinch force on the liquid column due to the self-induced electromagnetic force enhances the break-up of the liquid column into droplets, and the pressure generated in the cylinder by the electromagnetic force should be balanced by the pressure gradient in the field. This theory is not adopted in this research, so it will be discussed in detail.

4.2 Preliminary Results of Metal Transfer in Laser Enhanced GMAW

In proposed laser enhanced GMAW, a low power laser was added to generate an auxiliary detaching force. This novel process is different from the conventional GMAW.

4.2.1 Experimental Conditions

A CV (constant voltage) continuous waveform power supply was used to conduct experiments. The wire used was ER70S-6 of 0.8 mm (0.03 inch) diameter. Pure argon was used as the shield gas and the flow rate was 12 L/min (25.42 ft³/h). The work-piece was mild steel and experiments were done as bead-on-plates at a travel speed 10 mm/s (24 in./min). In the experiments, the power of the laser was set at 864 W and applied to the wire continuously. For the wire diameter and material, the transition current for the spray transfer is approximately 150 A (see table 4.1 in Ref. 1). Table 1 shows a number of experimental conditions designed to conduct Laser Enhanced GMAW and comparative conventional GMAW whenever needed. The current shown in the table is

the actual measurements from the conventional GMAW experiments. It is apparent that in all experiments, the currents were lower than the transition current that is approximately 150 A [1] and a short-circuit should be expected in conventional GMAW.

Table 4-1 Experimental conditions and welding currents

Experimental Condition Number	Voltage (V)	Wire Feeding Speed (inches/min)	Welding current Measured in Conventional GMAW (A)
1	29	200	82.6±21.0
2	30	250	98.8±13.0
3	30	300	115.0±8.1
4	30	350	125.0±11.1
5	30.5	400	131.6±9.6

4.2.2 Metal Transfer

In the designed experiments shown in the Table 4-1, the voltage was set approximately at the same and the wire feed speed was altered. When conventional GMAW experiments were conducted without the application of the laser, short-circuiting transfer and spatters were observed for all conditions in Table 4-1.

A band-pass filter centered at the laser waveform 808 nm was used to observe the process and record the images. All images presented in this study were recorded using the high speed camera shown in Fig. 3-2 with this band-pass filter. Fig. 4-2 is an image series, at 3000 frames per second, that demonstrates the metal transfer process under experimental condition #2 without the laser. In this series, Fig. 4-2 (c) clearly shows that the droplet does touch the weld pool. From Fig. 4-2 (d), spatters are seen clearly. Hence, the metal transfer is at the short-circuiting mode. This was because F_T is smaller than the maximum

retaining force that can be provided by F_{σ} in the whole process before the droplet torches the weld pool. It is apparent that the current smaller than the transition current is the cause.

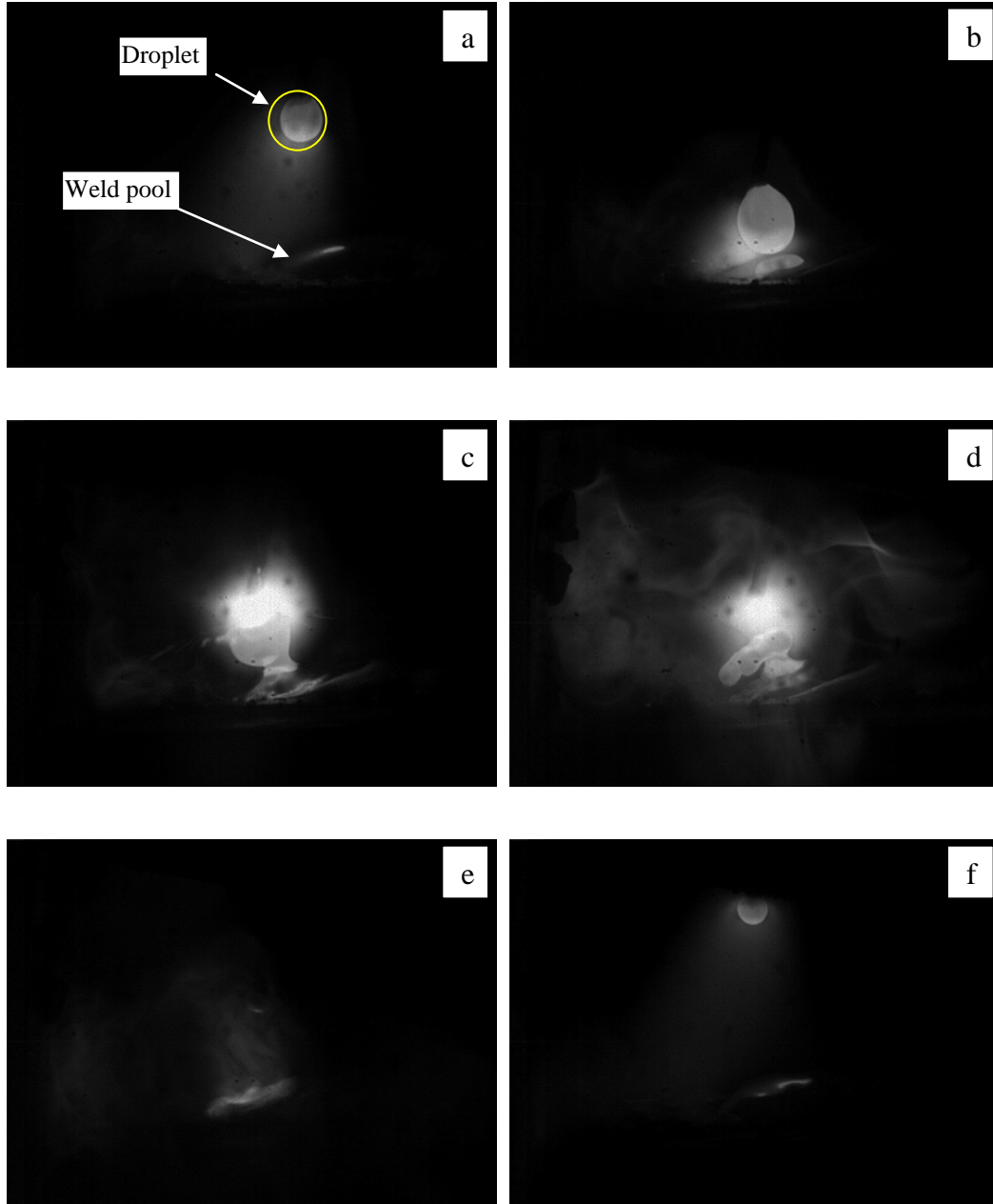


Fig. 4-2 Metal transfer process during conventional GMAW under experimental condition #2 (without laser). Consecutive images in the figure were acquired at 3000 frames per second.

Fig. 4-3, Fig. 4-4, Fig. 4-5, Fig. 4-6, Fig. 4-7 show the metal transfer processes when the Laser Enhanced GMAW process was performed using the experimental conditions given in Table 4-1.

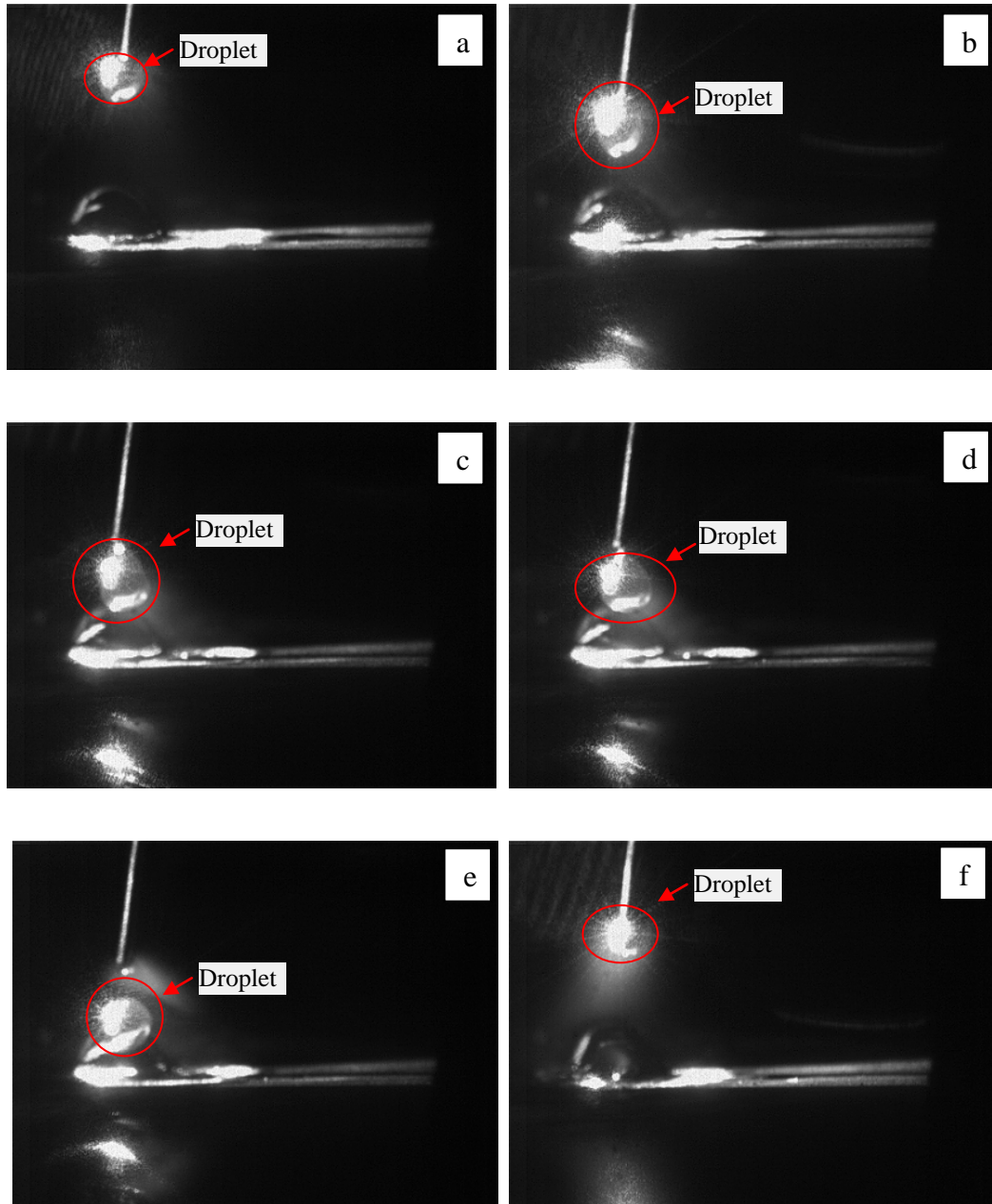


Fig. 4-3 Metal transfer in Laser Enhanced GMAW at experimental condition #1.
Consecutive images in the figure were acquired at 3000 frames per second

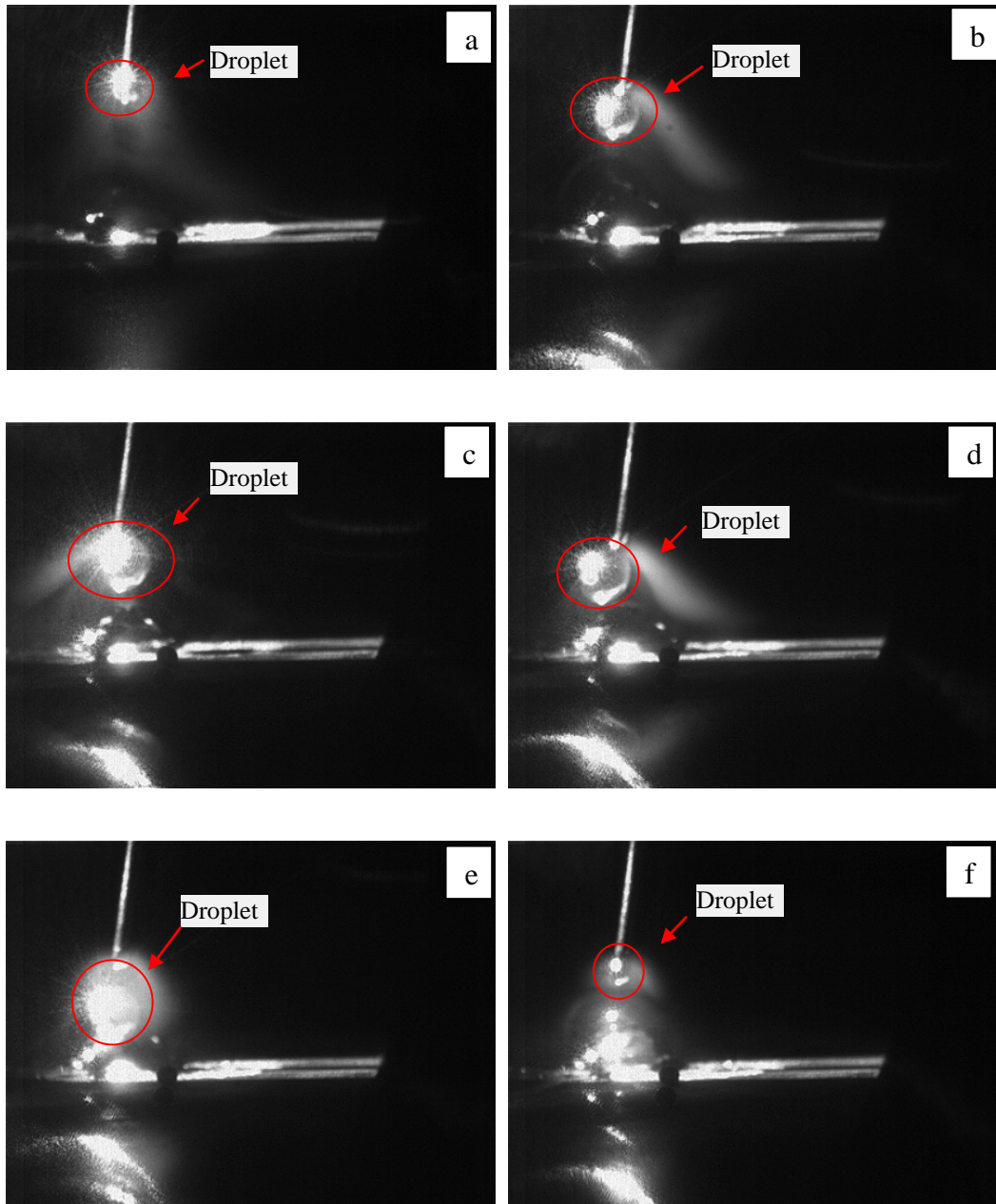


Fig. 4-4 Metal transfer in Laser Enhanced GMAW at experimental condition #2.
Consecutive images in the figure were acquired at 3000 frames per second

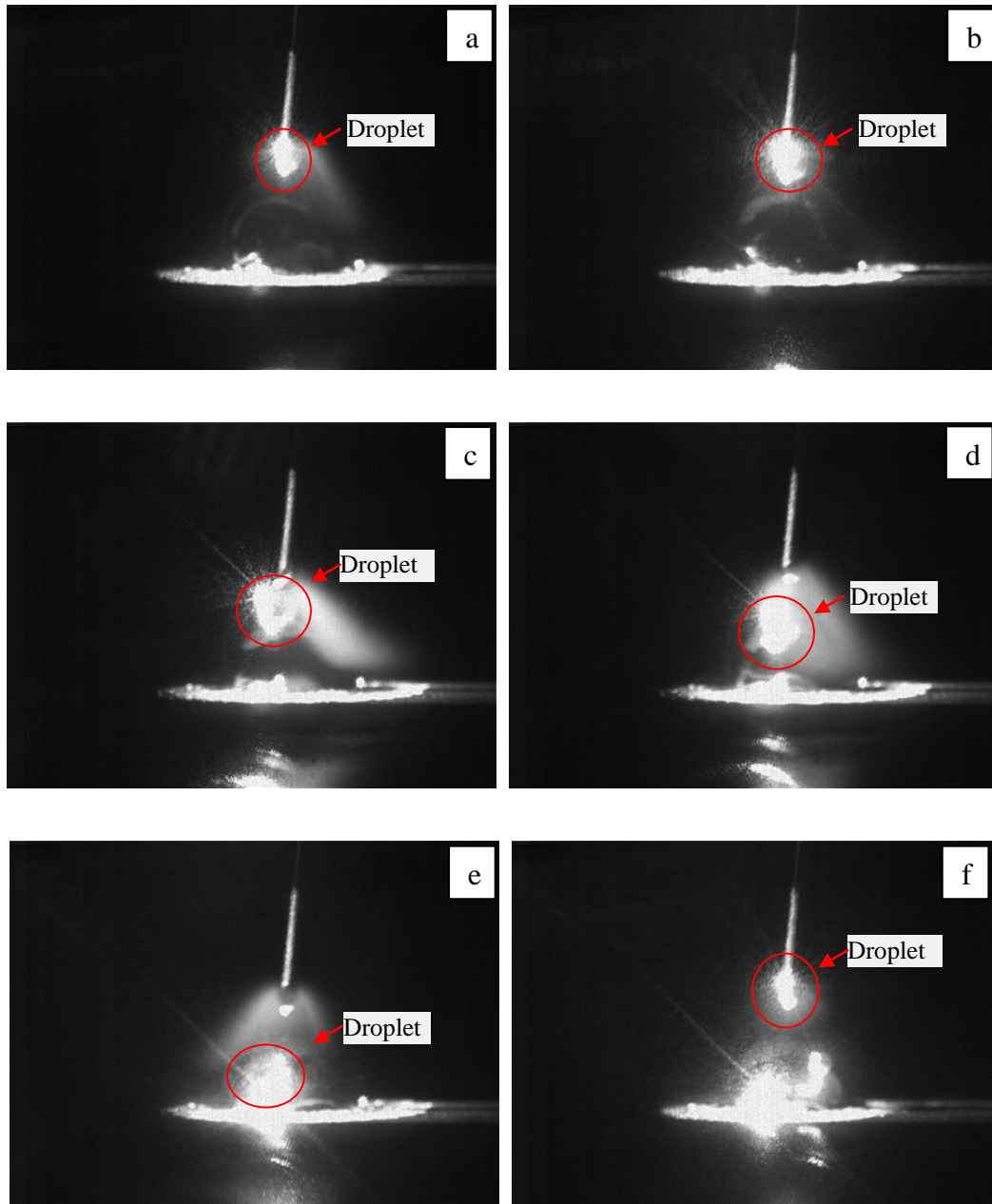


Fig. 4-5 Metal transfer in Laser Enhanced GMAW at experimental condition #3.
Consecutive images in the figure were acquired at 3000 frames per second

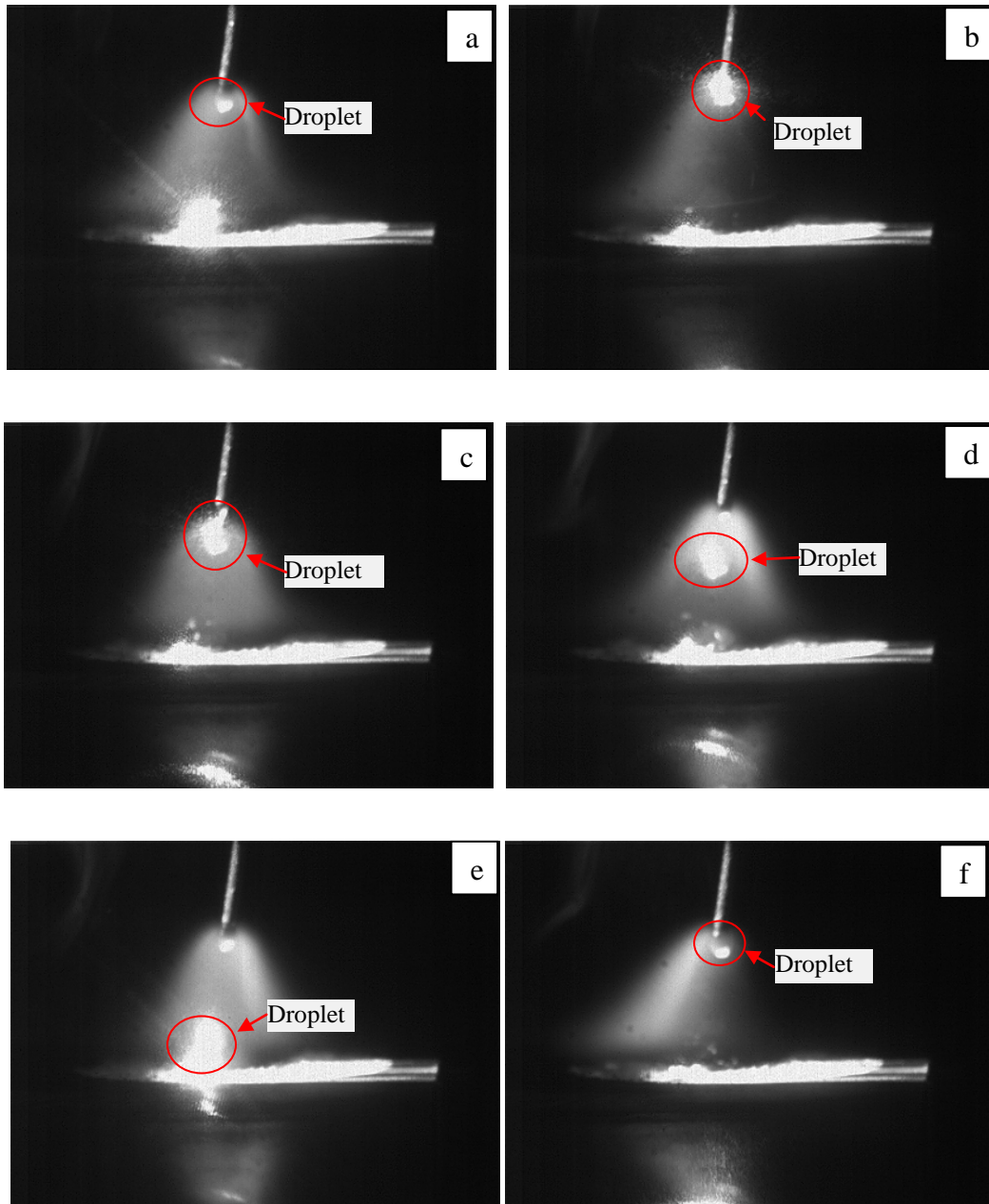


Fig. 4-6 Metal transfer in Laser Enhanced GMAW at experimental condition #4.
Consecutive images in the figure were acquired at 3000 frames per second

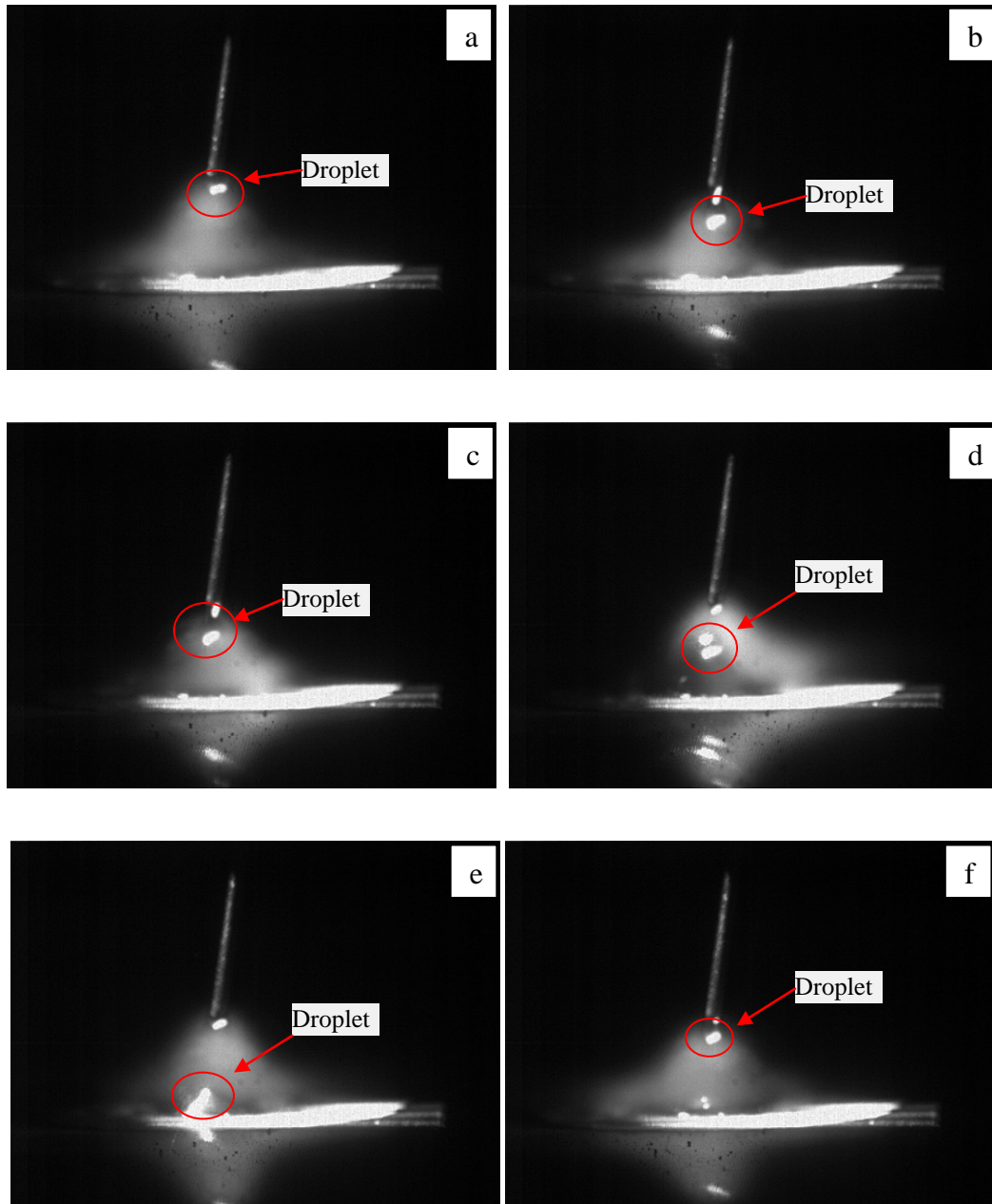


Fig. 4-7 Metal transfer in Laser Enhanced GMAW at experimental condition #5.

Consecutive images in the figure were acquired at 3000 frames per second

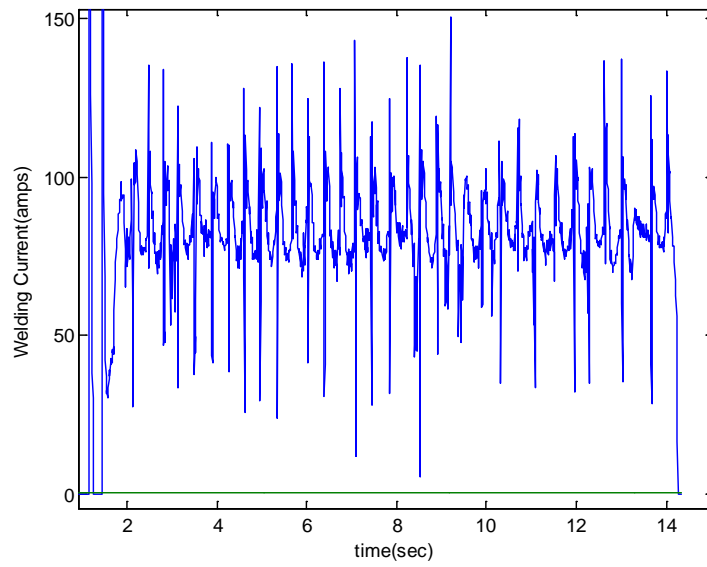
In all images, the weld pool surface illuminated by the laser beam was clearly shown as a bright line. As can be seen, the metal transfer in all experimental conditions changed to the spray transfer and the droplet detached from the wire before touched the weld pool. In particular, a direct comparison can be made between Fig. 4-4 and Fig. 4-2 that were both conducted using experimental conditions #2 in Table 1. Because of use of the laser,

the metal transfer changed from the short-circuiting transfer in Fig. 4-2 to the spray transfer in Fig. 4-4.

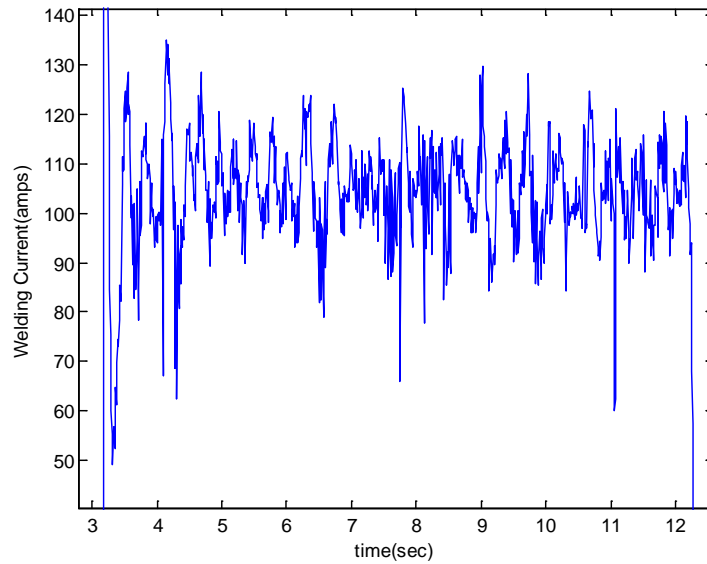
Each image series in Fig. 4-3 to Fig. 4-7 represents a complete transfer cycle under the respective conditions. Each first image represents the beginning of a metal transfer cycle. As the droplet grows, the gravitational force increases. The cross section of the laser beam intercepted by the droplet increases as the droplet thus grows. Because the intensity of the laser on the cross section is independent from the droplet, the recoil pressure of the laser acting on the droplet increases. As a result, the auxiliary force applied by the laser on the droplet and the gravitational force both increase. On the other hand, the surface tension as can be seen in Eq. (4-1) is approximately constant when the droplet grows. Hence, as the droplet grows, the detaching force increases but the retaining force remains approximately constant. As a result, once the sum of the detaching force becomes larger than the sum of the retaining force, the droplet is detached. Because the droplet is detached in all conditions listed in Table 4-1 before it may touch the weld pool, the auxiliary detaching force introduced by the laser is sufficient to implement the Laser Enhanced GMAW for the conditions listed in Table 4-1. Because the laser is applied continuously, the detachment of the droplet appears to be natural result of the balance of the forces. Because of possible variation in other forces, the diameter of the droplet being detached is not accurately controlled. To control the droplet diameter, the laser can be pulsed and be applied when the droplet needs to be detached. The control of the droplet diameter exceeds the scope of this present work.

4.2.3 Current Waveforms

Fig. 4-8 is the measured current waveforms for Laser Enhanced GMAW experiments conducted using the conditions in Table 4-1. Observation of these current waveforms shows that the current waveforms become less fluctuating when the wire feed speed or the current increases. This can also be seen from the right column in Table 4-1.

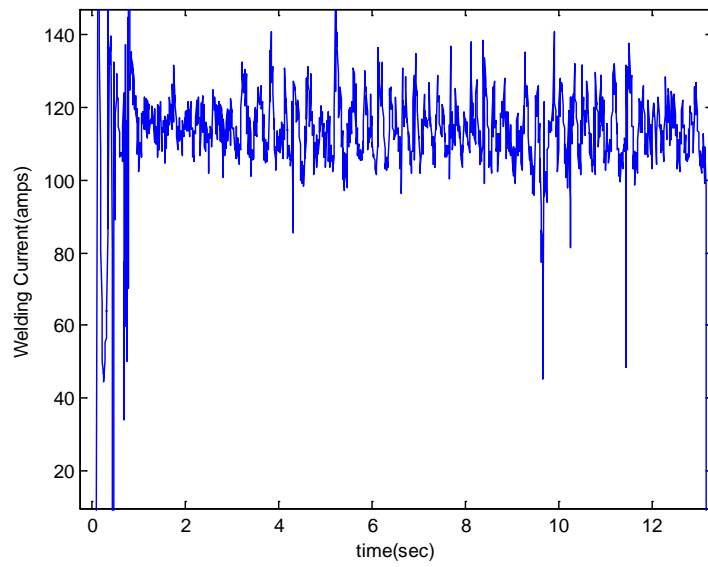


a) Experiment #1

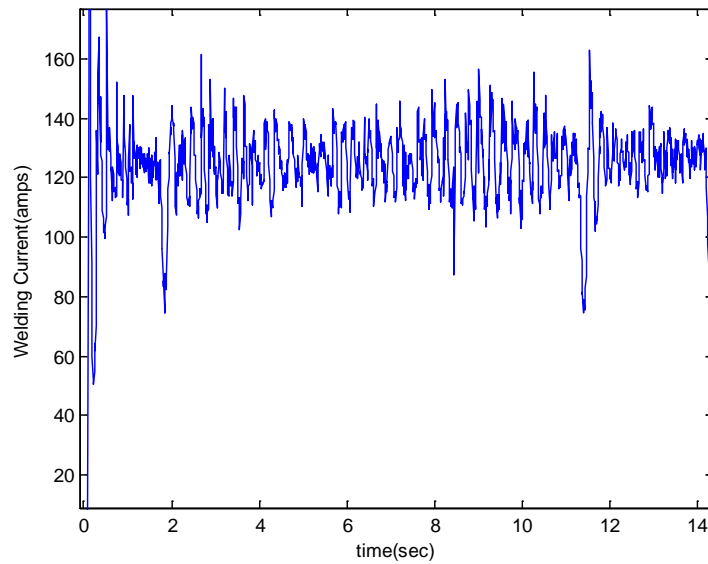


b) Experiment #2

Fig.4-8 Current waveforms in Laser Enhanced GMAW experiments: a) Experiment #1, b) Experiment #2, c) Experiment #3, d) Experiment #4, and e) Experiment #5

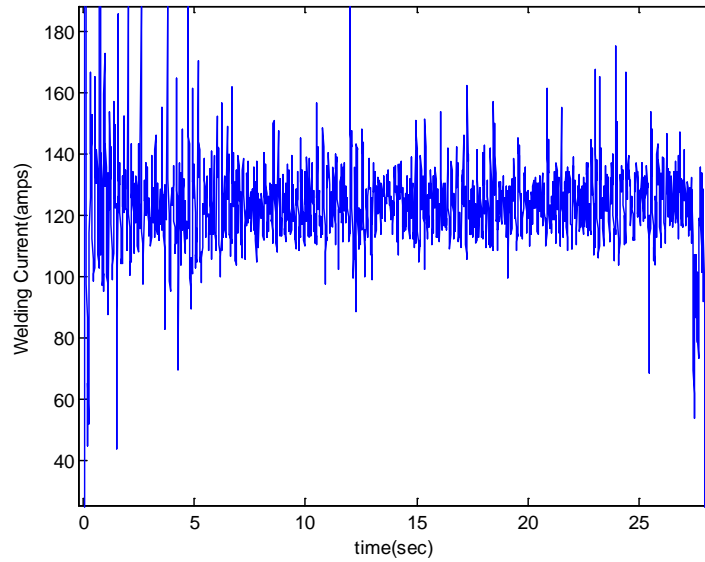


c) Experiment #3



d) Experiment #4

Fig.4-8 Current waveforms in Laser Enhanced GMAW experiments (Continued)



e) Experiment #5

Fig.4-8 Current waveforms in Laser Enhanced GMAW experiments (Continued)

As analyzed above, the detachment of the droplet under a continuous laser application is a natural result of the balance of the force. When the current increases, the electromagnetic force increases at least quadratically with the current as initially suggested by

$$F_{em} = \frac{\mu_0 I^2}{4\pi} \left(\frac{1}{2} + \ln \frac{r_i}{r_u} \right) \quad (4-8)$$

Further, the exit radius of the current path, i.e., r_i also increases as the current increases as the arc will climb toward the neck of the droplet. Hence, the electromagnetic force increases rapidly as the current increases. On the other hand, the surface tension does not change and the vapor jet force at most increases proportionally. Hence, the detaching force increases much faster than the retaining force as the current increases. The gravitational force needed to break the balance reduces. Hence, the droplet is detached at smaller diameters when the current increases in the continuous Laser Enhanced GMAW. Further, the melting speed also increases such that the period of the metal transfer is thus reduced fast. As a result, the arc length and wire extension are subject to smaller

fluctuations and variations. The current waveform thus becomes less fluctuating. To control the transfer period, droplet diameter and current fluctuation, laser pulses can be applied whenever the detachment is needed.

Fig. 4-9 is the recorded current waveform in an experiment conducted using condition #4 in Table 1. From $t = 1$ s to $t = 7$ s, no laser was applied and the process was conventional GMAW. After $t = 7$ s, the laser was applied and the process was the continuous Laser Enhanced GMAW. As can be seen, the current fluctuation was significantly reduced after the laser was applied due to that the transfer changed from the short-circuiting to spray transfer. The variance of welding current before 7 seconds was $369.21 A^2$, and dramatically reduced to $91.22 A^2$ after $t=7$ s. The standard deviation reduced from 19.21 A to 9.55 A after $t=7$ s.

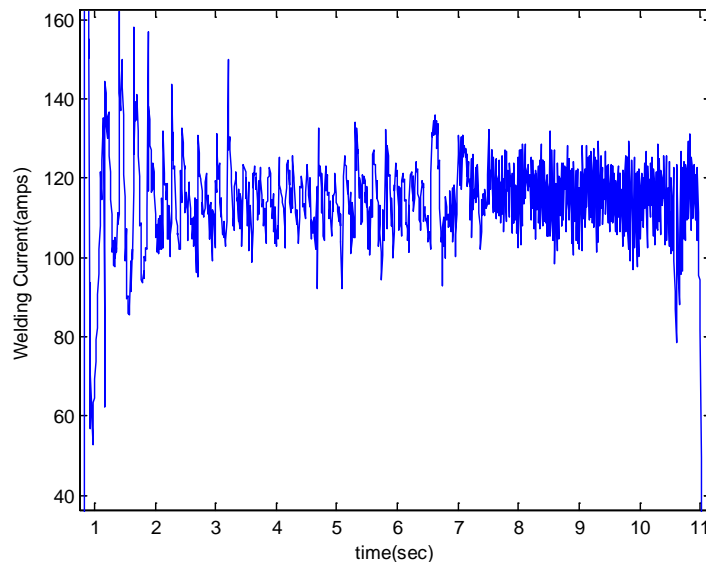


Fig. 4-9 Comparative conventional and Laser Enhanced GMAW using condition #4. The average current does not change significantly. This implies that the heat applied by the laser to the wire is insignificant for wire melting

4.2.4 Process Parameters

Welding voltage and wire feed speed are two important process parameters in addition to the laser used and the wire diameter and material.

When others parameters are the same, increasing the voltage would increase the arc length and thus allow the droplet to grow for a longer time into a larger volume. Also, when the contact-tube-to-work distance is given, the wire extension will be reduced due to the increased arc length. As the wire extension reduces, the resistive heat will reduce. For small diameter wires, such a reduction could be significant. As a result, for the same wire feed speed, the current will increase. Because the electromagnetic force as a detaching force increases faster than a quadratic speed as the current increases, the increase in the detaching force would be significant. The increased gravitational force and electromagnetic detaching force would reduce the transition current. For the experimental condition #4 in Table 4-1, if the voltage is changed to 34 V, the metal transfer will become spray mode without the application of a laser. Similarly for Laser Enhanced GMAW process, the voltage setting would also affect the metal transfer in a similar way. For the same laser, when the voltage is reduced, the transfer could be changed from a spray to short-circuiting. However, in principle, it may typically be possible for the Laser Enhanced GMAW to assure a spray transfer by increasing laser power. A pulsed laser of relatively high peak power is thus appropriate for the Laser Enhanced GMAW.

Because the wire feed speed is the major parameter to determine the current and thus the electromagnetic force, it plays a critical role in determining the laser power/intensity needed to assure the spray transfer. When the laser power/intensity and other welding parameters including the wire diameter/material and arc voltage setting are given, the droplet diameter and transfer frequency in the continuous Laser Enhanced GMAW are primarily determined by the wire feed speed. As shown in Fig. 4-10, when increasing the wire feed speed from 200 to 400 inches per minute, the welding current increases approximately linearly from 82.6 A to 131.6 A. However, because the electromagnetic force as a detaching force increases faster than a quadratic speed, the needed gravitational

force to break the force balance decreases rapidly. As a result, the time needed in each cycle to detach the droplet (i.e., the metal transfer time) decreases rapidly.

There is another important change when wire feed speed increases. When the wire feed speed is 350 or 400 inches per minute, as shown in Fig. 4-6 and Fig. 4-7, the pinch effect could be observed between the droplet and the solid wire. This pinch effect is also demonstrated in Fig. 4-11. However, as can be observed from Fig. 4-5, Fig. 4-6, and Fig. 4-7, when the wire feed speed is lower than 300 inches per minute, the pinch effect was not obvious.

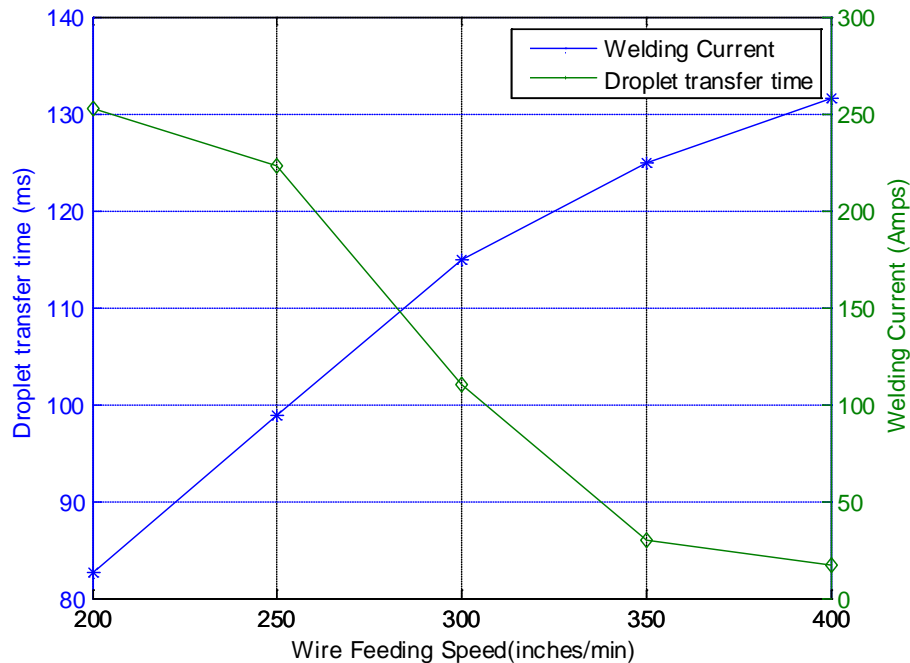


Fig. 4-10 Effect of wire feed speed on current and droplet transfer time in Laser Enhanced GMAW

4.2.5 Analysis of Laser Effect

The first question that needs to be answered through analysis is how the laser affects the metal transfer. To this end, the actual laser power applied on the droplet can be estimated first. Because the laser beam dimension is $1 \text{ mm} \times 14 \text{ mm}$ and the diameter of the droplet

can be assumed to be not greater than 1.2 mm, the actual incident power of the laser applied on the droplet should be less than 70 W. Then taking experimental condition #4 in the Table 1 as an example one may extend an analysis as follows:

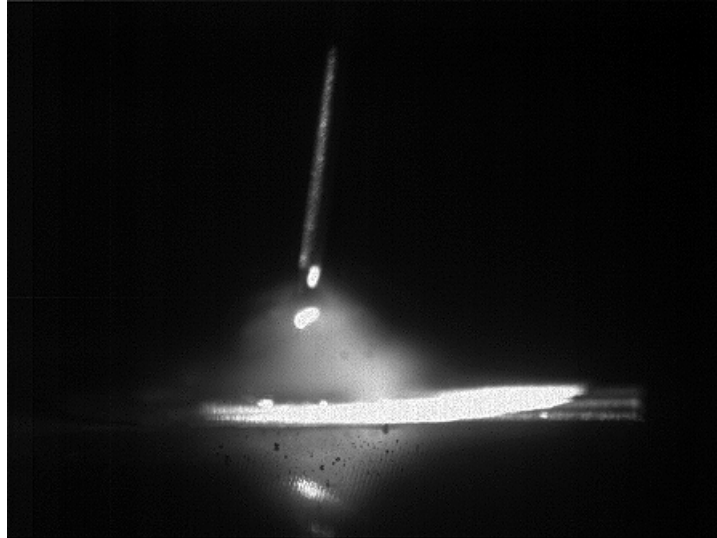


Fig. 4-11 Pinch effect in the Laser Enhance GMAW process

When the voltage was set at 30 V, the metal transfer without an application of the laser was short-circuiting and the current was 125 A approximately. When the laser was applied, the current was still 125 A approximately but the metal transfer changed to spray mode. Because the heat applied onto the droplet by the laser is insignificant in comparison with that of the arc, the change of the metal transfer must be primarily due to the force rather than the heat generated by the laser spot. In fact, in comparison with the anode arc power that melts the wire, the laser power is approximately its 4.6 percent (70 W over 125 A of current multiplied 12 V of estimated anode voltage). Due to the specular reflection of the droplet surface, no more than 50% of the incident laser power should be absorbed. That is, the application of the laser should only increase the heat by 2.3%. Unfortunately, even when the current (thus anode heat) increases 15% from 120 A to 138 A, the metal transfer would still not be the spray transfer. Hence, it is the force rather than the heat that effectively changed the metal transfer from the short-circuiting to the spray transfer during Laser Enhanced GMAW.

Secondly, how the laser force is produced needs to be understood. Basically, the pressure imposed by the laser on the droplet can be considered to have two major components: radiation pressure and recoil pressure. For the laser radiation pressure, previous studies have obtained clear results/conclusions. The radiation pressure (P) of a normally incident cw light imposed on a macro-object with a plane surface can be expressed as [78]

$$P = I(1 + R)/c \quad (4-9)$$

where c is the speed of the light, R is the reflectivity of the illuminated surface, and I is the intensity of the light. However, the radiation pressure on the object (droplet in our case) is very insignificant in comparison with the recoil pressure. For example, for a 100 W laser with 1 mm spot and $R = 0.8$, the radiation force calculated from Eq. (4-9) is in the order of 10^{-7} N while the surface tension needed to be overcome to detach the droplet is at the order of 4×10^{-3} N [79].

For the recoil pressure acting on a substrate during intense laser evaporation, Ref. 80 gave:

$$P_r = AB_0 T_s^{-1/2} \exp(-U/T_s) \quad (4-10)$$

where A is a numerical coefficient, B_0 is a vaporization constant, T_s is the surface temperature, and $U = M_a L_v / (N_a k_b)$. Here M_a is the atomic mass, L_v is the latent heat of evaporation, N_a is Avogadro's number, and k_b is the Boltzmann's constant. This equation is relatively complicated and Ref. 81 gave a simpler expression:

$$P_r = (P/A)^2 / \rho E \quad (4-11)$$

where P/A is the power density of the laser, ρ is density of the vapor, and E is the energy needed to evaporate 1 kg metal. As its authors indicated [81], when the laser intensity is about 3×10^6 W/cm², the recoil pressure will be about 10^7 Pa.

In the Laser Enhanced GMAW process, as $F_T = F_g + F_d + F_m + F_{em} + F_{recoil\ force}$, a higher F_T could be produced by adding a laser beam. . The power intensity of the laser

used is about $6.17 \times 10^3 \text{ W/cm}^2$ (864 W over the laser dimension $1 \text{ mm} \times 14 \text{ mm}$), the recoil pressure is at least at the order of 10^3 Pa . The surface of the droplet intercepting the laser beam could be estimated at the order of 10^{-6} m^2 . In this case, the force generated by laser recoil pressure will at the order of 10^{-4} N . It is at the same order of the force to detach a droplet as aforementioned.

4.3 Conclusions

- (1) Droplet detaching theories were reviewed and analyzed, and Dynamic Force Balance Theory (DFBM) was selected as the main theory to analyze the metal transfer phenomenon in laser enhanced GMAW;
- (2) An experimental system has been established and the feasibility of the novel Laser-Enhanced GMAW process was experimentally demonstrated;
- (3) The laser aiming at the droplet in Laser-Enhanced GMAW can apply an auxiliary detaching force without significant additional heat;
- (4) Spray transfer was successfully produced at continuous currents in the range from 80 A to 130 A for 0.8 mm diameter steel wire that would produce short-circuiting transfers in conventional GMAW;
- (5) Phenomena observed in Laser-Enhanced GMAW have satisfactorily analyzed by applying established theories and fundamentals;
- (6) Laser recoil pressure force was recognized as the additional detaching force in laser enhanced GMAW, and its value was estimated based on established physical fundamentals.

CHAPTER 5 METAL TRANSFER INFLUENCE

FACTORS IN LASER ENHANCED GMAW

The metal transfer phenomenon was introduced in the former Chapter, and the laser recoil pressure force was identified as the additional detaching force. To better understand the metal transfer in laser enhanced GMAW, a systematic series of experiments should be done to identify the main influence factors to change metal type.

5.1 Basic Analysis of Metal Transfer in Laser Enhanced GMAW

By adding a low power laser onto the droplet, an auxiliary detaching force will be generated. In this case, the metal transfer type will be changed. There are many factors which influence the metal process.

A key issue is that how the metal transfers largely depends on the welding current that also determines other critical parameters including heat input and arc pressure. An application may require a preferred metal transfer mode that needs to be produced using a particular welding current while this current may result in a heat input and arc pressure that are not most suitable for this application.

An example of practical value is that many applications prefer the metal transfer to take place in the spray mode but it requires a current higher than the transition current [1] to produce in conventional GMAW. In this mode, the arc pressure is [7]

$$P_a = (\mu_0 J_a^2 / 4) [R_a^2 - R^2 - 2\epsilon_0 R c \cos(\omega t) \cos(kz)] \quad (5-1)$$

where the arc current density

$$J_a = \alpha I / (\alpha \pi R^2 (\beta^2 - 1) + \pi R^2) \quad (5-2)$$

and μ_0 is the permeability, R_a is the arc current radius, R is the equilibrium radius of the droplet, ϵ_0 is the Alitude of the perturbation, ω is angular frequency, t is the time, k is a wave number, z represents the axial coordinate of a cylindrical coordinate system, α is the ratio of arc to the liquid current density, I is the current, β is the ratio of arc to the liquid radius [7]. It can be seen that the arc pressure is proportional to the square of the welding current. Increasing the welding current thus increases the arc pressure at higher ratio. An extremely high arc pressure is often not acceptable for many applications.

The metal transfer process is governed by the forces exerted on the droplet. In dynamic-force balance theory (DFBM) [25, 77], five major forces were used to analyze the metal transfer process. Surface tension is the main retaining force to support the droplet, while the gravitational force, electromagnetic force, aerodynamic drag force, and momentum force typically tend to detach the droplet. In the short-circuiting transfer mode, the detaching force, mainly the gravitational force, is not large enough to balance out the retaining force; the droplet would touch the weld pool. In this case, the merging of the droplet into the weld pool is critical that determines the production of possible spatters and the formation of the welds. For the globular transfer mode, as the repelled globular typically generates severe spatters, only the drop globular transfer may be adopted in applications. In the drop globular transfer, as the droplet cannot be detached at a reasonable small diameter, a large and oscillating droplet is expected in conventional GMAW that causes not only potential arc instability/fluctuation but also uncontrolled droplet travel directions that directly result in the merging of droplet with the weld pool at undesired locations to produce poor formations of welds. The drop spray transfer mode is usually characterized by uniform droplet diameter, regular detachment, directional droplet transfer, and it is thus widely used in the industry.

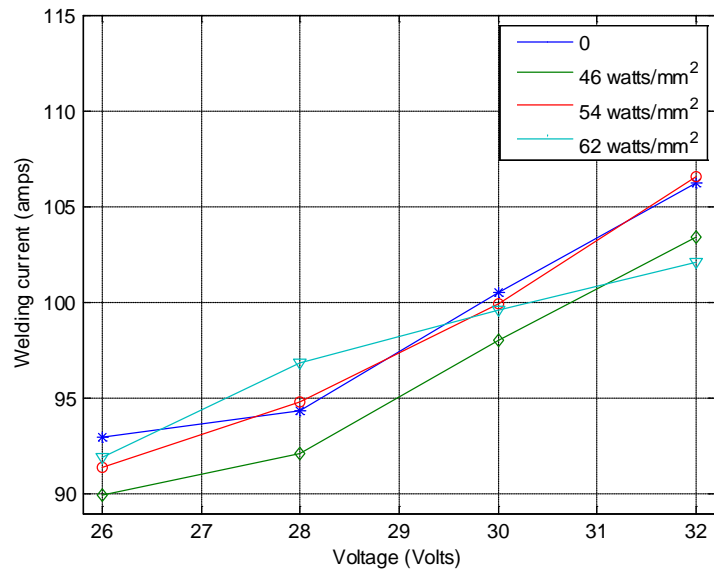
The metal transfer in GMAW has been traditionally regarded as a two stage process: first, a droplet forms at the end of the solid wire under the arc heating effect; second, the droplet detaches from the end of the welding wire and travels in the arc zone. The merging of the droplet into the weld pool after the travel in the arc-zone is also a stage in

the transfer process but has not been much studied. As has been seen above, the merging is critical as it determines the process stability (short-circuiting transfer) or the capability to produce good weld formations (drop globular or spray transfer). To emphasize, the authors add the merging as the third stage for the convenience of analysis in this dissertation.

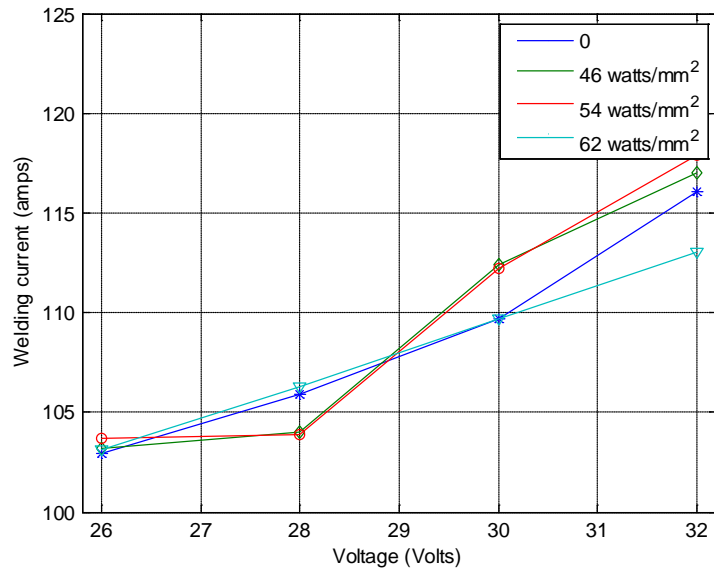
5.2 Experiment Conditions to Study Metal Transfer in Laser Enhanced GMAW

A CV (constant voltage) continuous waveform power supply was used to conduct experiments. Pure argon was used as the shield gas and the flow rate was 12L/min (25.4 ft³/h). The work-piece was mild steel and experiments were done as bead-on-plate at a travel speed 6.6 mm/s (15.6 in./min). The wire used was ER70S-6 of 0.8 mm (0.03 inch) diameter. The distance from the contact tube to the work piece was 20 mm as aforementioned.

The welding voltage was set at four levels: 26, 28, 30, and 32 V. For each voltage, four different wire feed speeds, 250, 300, 350, and 400 inches per minute, were used to produce different welding current levels resulting in 16 sets of experimental conditions. In all experiments, welding currents were not more than 135 A which will generate short-circuiting or repelled globular transfer or non-wire-axis drop globular in the conventional GMAW. The laser beam was continuously applied along the wire (solid and droplet) at four different levels of laser intensities for each of the 16 experimental conditions: 0, 46 W/mm², 54 W/mm², and 62 W/mm². There were thus totally 64 experiments conducted. For convenience, the parameters will be presented as a set (wire feed speed, voltage, laser intensity).

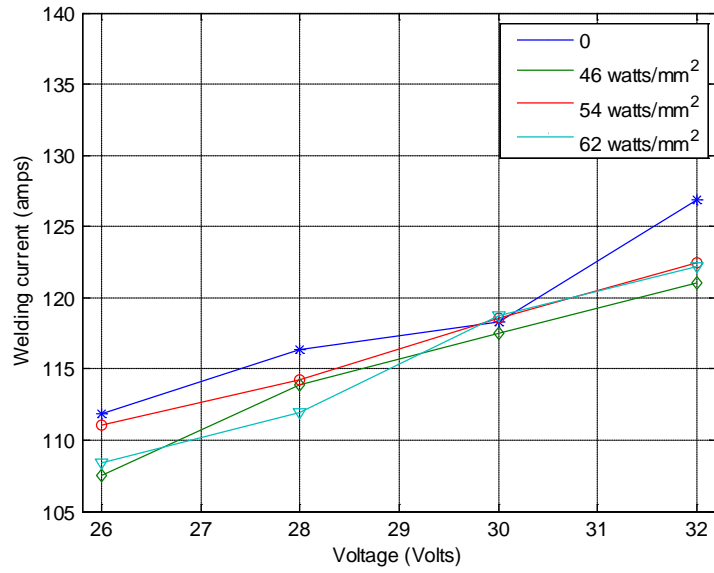


(a) W.F.S. 250

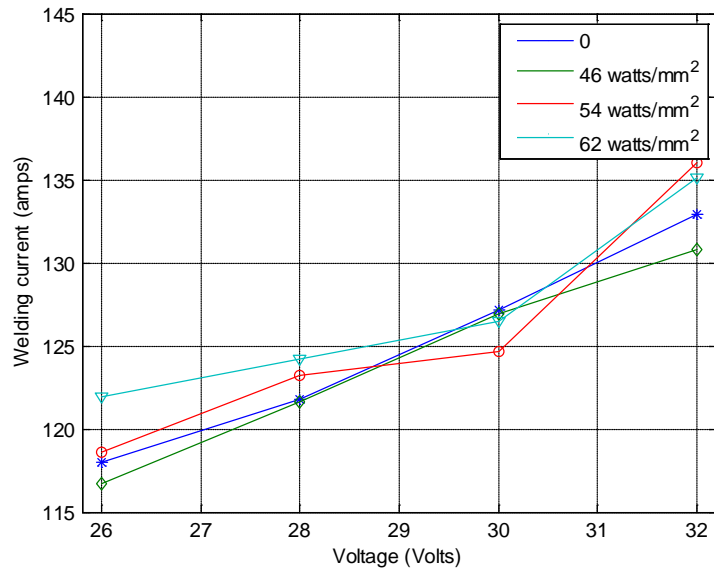


(b) W.F.S. 300

Fig. 5-1 Welding current under different wire feed speeds and different laser powers: a) W.F.S. 250, b) W.F.S. 300, c) W.F.S. 350, and d) W.F.S. 400



(c) W.F.S. 350



(d) W.F.S. 400

Fig. 5-1 Welding current under different wire feed speeds and different laser powers
(Continued)

Fig. 5-1 shows the mean current measured in all experiments. It can be seen that all the currents were lower than the transition current that is approximately 150 A [1] for the wire material and diameter. The current increases significantly as the voltage setting increases because of the reduced wire extension. However, the effect of the laser on the current is significant, no more than 5 A.

5.3 Observation and Analysis in Laser Enhanced GMAW

The diameter of the detached droplet is obtained from series of high speed images in this study. All images presented as series have the dimension scale except for those presented individually. The time interval of consecutive images in the same series is constant. Fig. 5-2 illustrates the scene in a typical metal transfer image.

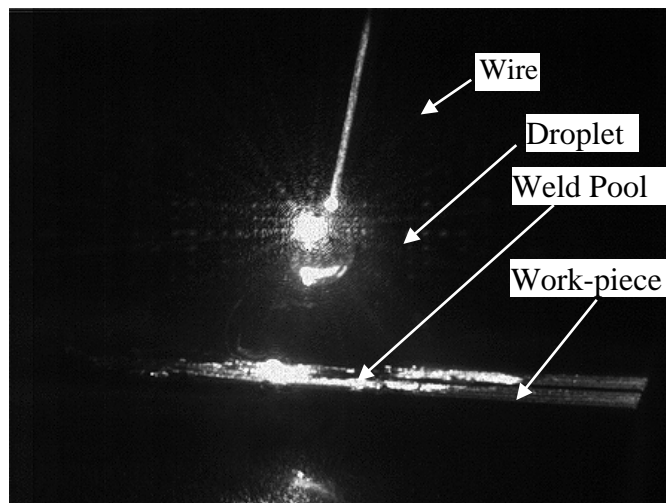


Fig. 5-2 Illustration of metal transfer image

5.3.1 Observations

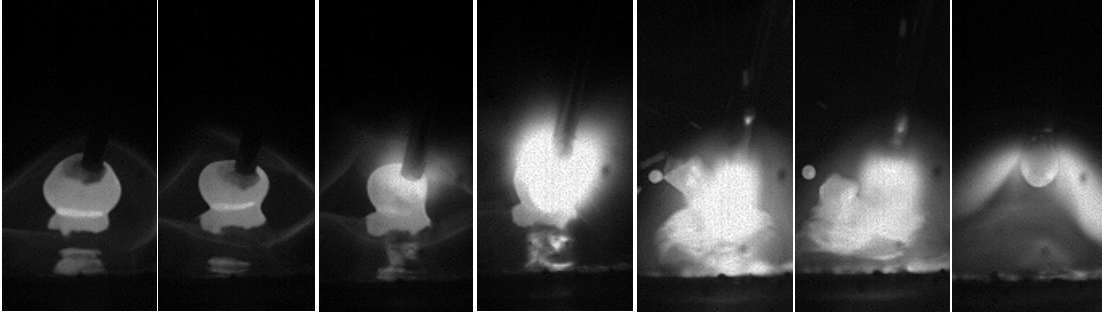
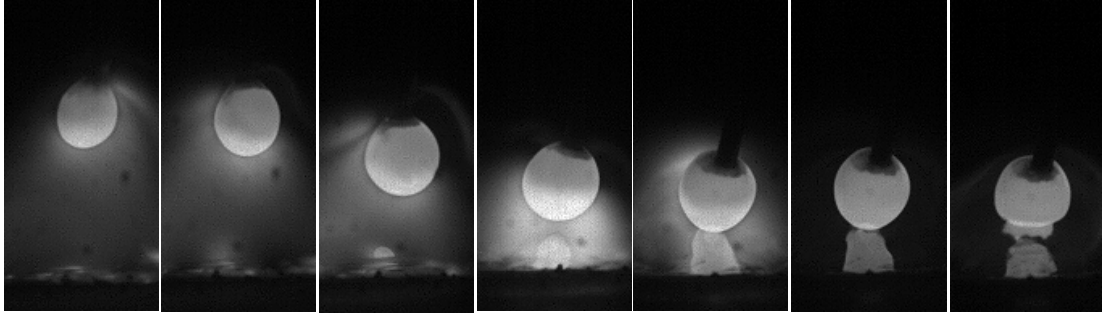
Fig. 5-3(a) shows a typical metal transfer cycle for the experiment conducted using (wire feed speed, voltage, laser intensity)=(300 in./min, 30 V, 0). This is a short-circuiting transfer in which the second and third stages of the metal transfer are combined. From Fig. 5-1, the current in this experiment is 110 A approximately. In the cycle shown in Fig. 5-3(a), the combined detaching force from the electromagnetic and gravitational force

was not sufficient enough to balance out the retaining force, i.e., the surface tension which is determined by the surface tension coefficient and diameter of the wire, before the droplet touched the weld pool. The transfer was short-circuiting and spatters were produced. Examination of recorded images during this experiment shows that the short-circuiting transfer dominated although the globular transfer also occurred occasionally.

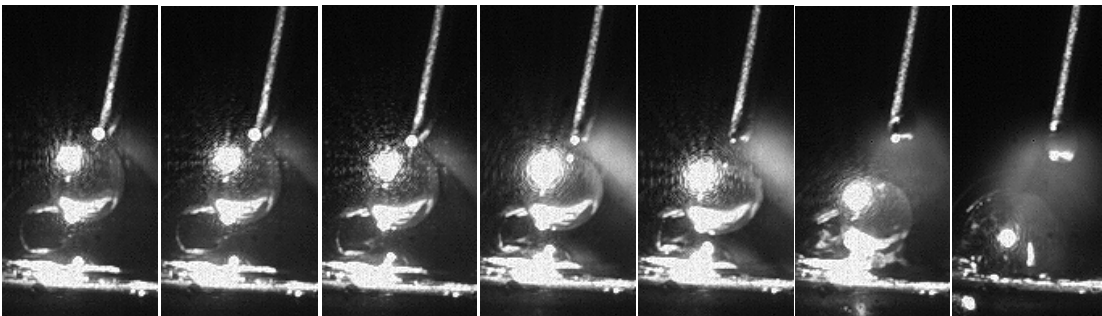
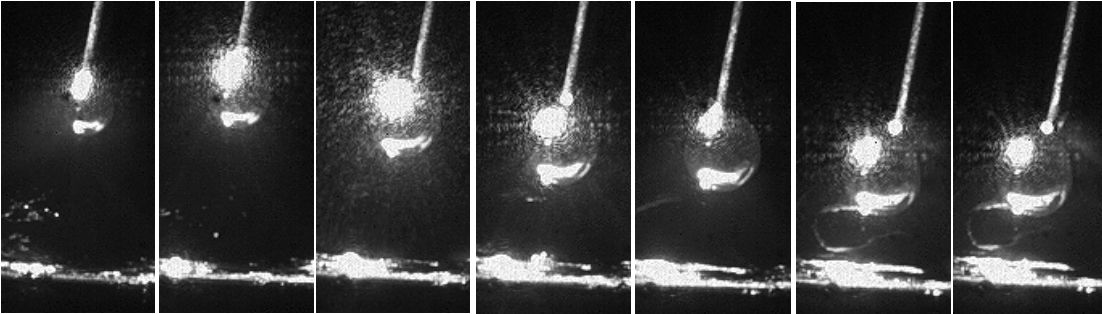
Fig. 5-3(b) is a typical metal transfer cycle from the comparative experiment with an application of the laser at intensity of 62 W/mm^2 . As can be seen, the large droplet did not touch the base metal before detached and there were no spatters produced. This is a free flight transfer type, and it is Drop Globular according to IIW classification [25, 30]. Examination of all images shows that the metal transfer all occurred as drop globular. It is apparent that it was the laser that made the difference in changing the metal transfer.

As aforementioned, the recoil pressure is the major force the laser applies to the droplet. Application of a laser beam to a droplet at an appropriate direction as in this study ensures the recoil pressure to be a detaching force. The added detaching force from the laser recoil pressure reduces the need from other sources for the detaching force. When the current thus the electromagnetic force is given, the added detaching force from the laser recoil pressure reduces the needed gravitational force to balance out the surface tension. As a result, the needed diameter of the droplet for detachment is reduced. If the needed diameter is reduced sufficiently such that the droplet can grow to this diameter before it touches the weld pool, the short-circuiting transfer changes to a free flight transfer type as observed in Fig. 5-3(b).

For these two comparative experiments, the laser does not change the mean welding current significantly as can be seen from Fig 5-1 (b). However, as the droplet does not touch the weld pool, the fluctuation of the welding current is reduced as can be seen in Fig. 5-4. Further, because the droplet is detached before touching the weld pool, the average transfer time is reduced from 183.3 ms without laser to 178.3 ms with laser. The average diameter of droplet decreases from 2.23 mm without laser to 1.89 mm with laser. The laser thus reduced the needed diameter (weight) of the droplet for detachment and changed the metal transfer type.

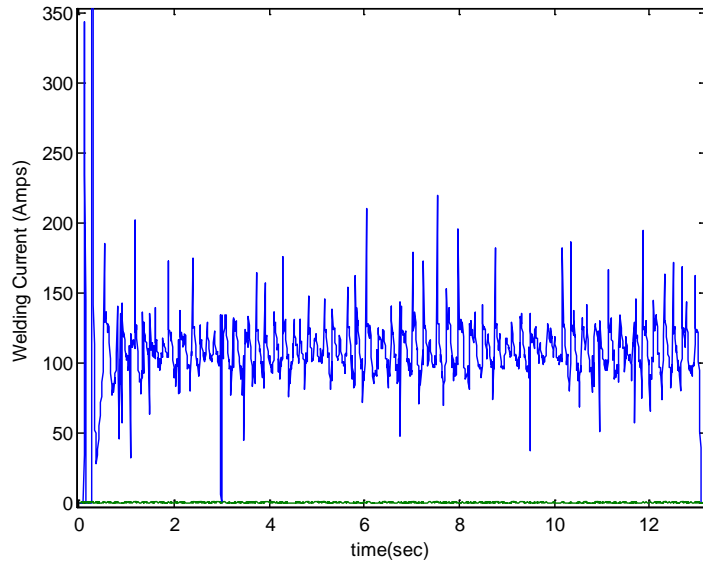


(a) Without laser

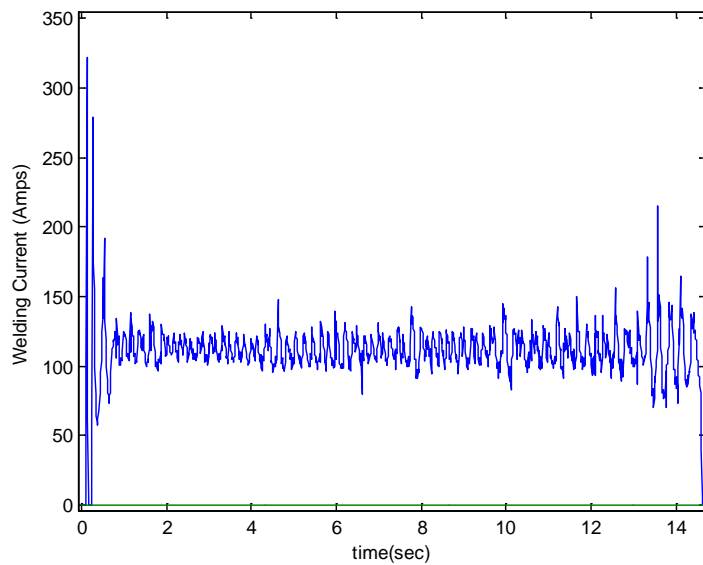


(b) Laser intensity of 62 W/mm^2

Fig. 5-3 Typical metal transfer in comparative experiments with and without laser under (300 in./min, 30 V, 0) and (300 in./min, 30 V, 62 W/mm^2)



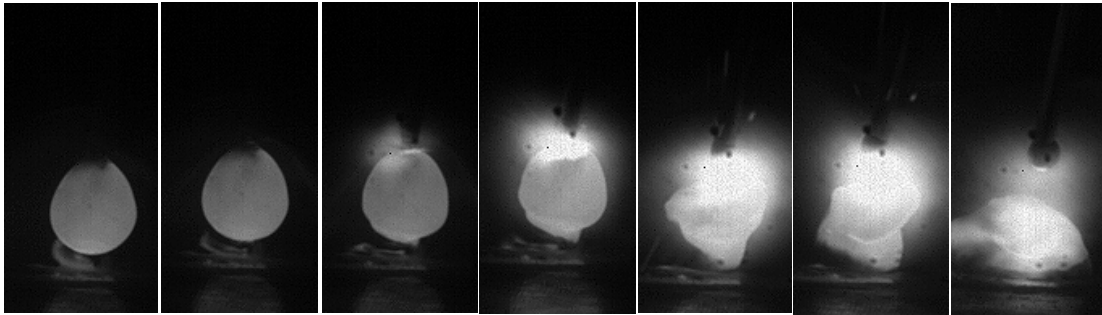
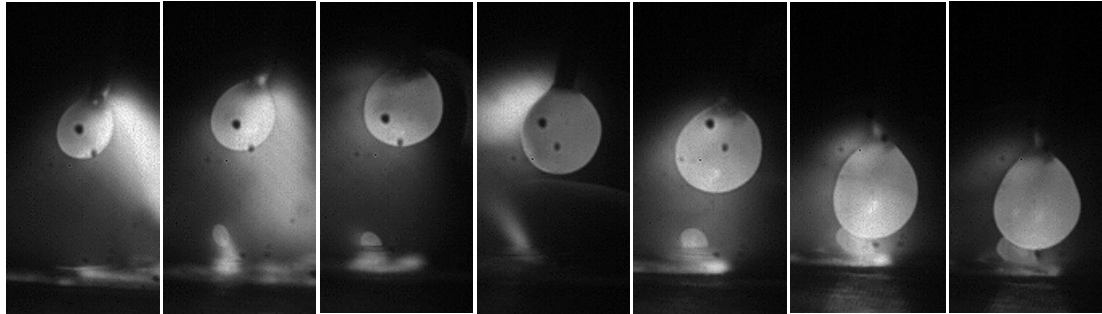
(a) No laser



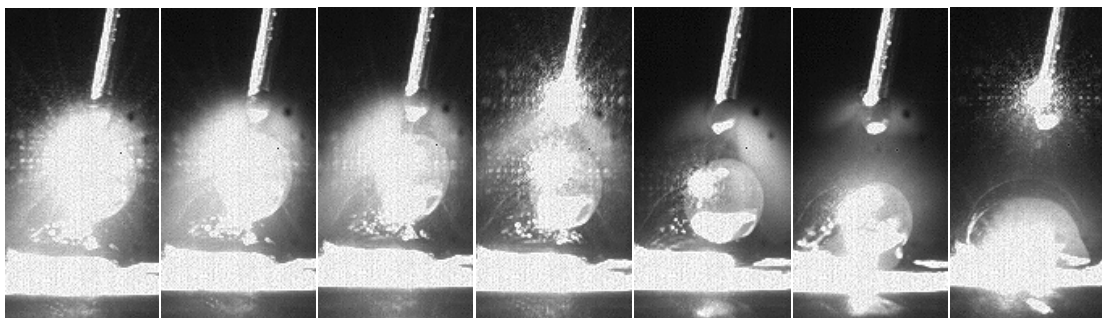
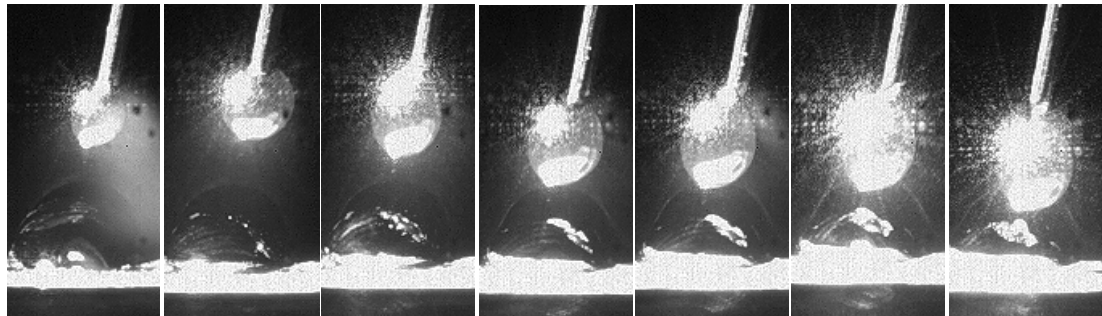
(b) Laser intensity of 62 W/mm^2

Fig. 5-4 Current waveforms for (300 in./min, 30 V, 0 W/mm^2) and (300 in./min, 30 V, 62 W/mm^2)

Figs. 5-5, Fig. 5-6, and Fig. 5-7 are typical metal images from other three additional groups of comparative experiments using other different wire feed speeds also at 30 V of voltage setting. Because of the changes in the wire feed speed, the mean current varies from experiment to experiment (shown in Fig. 5-1 (a), (c) and (d)).

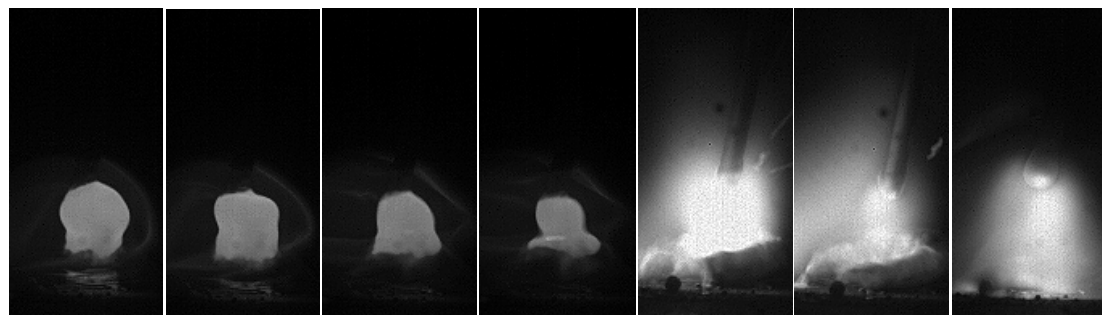
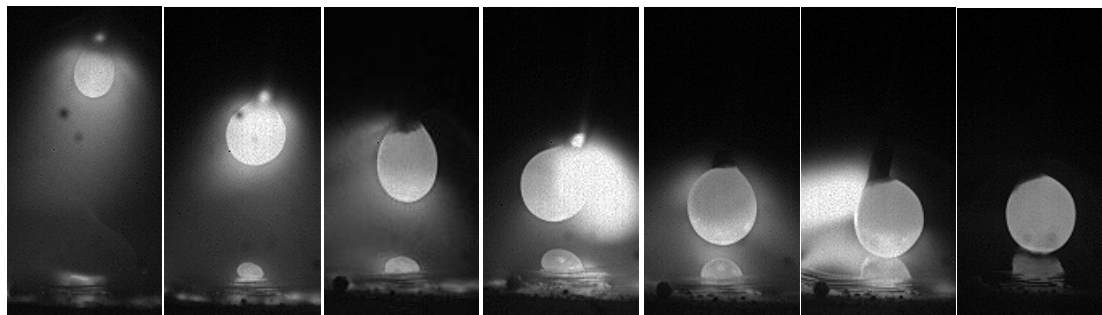


(a) Without laser

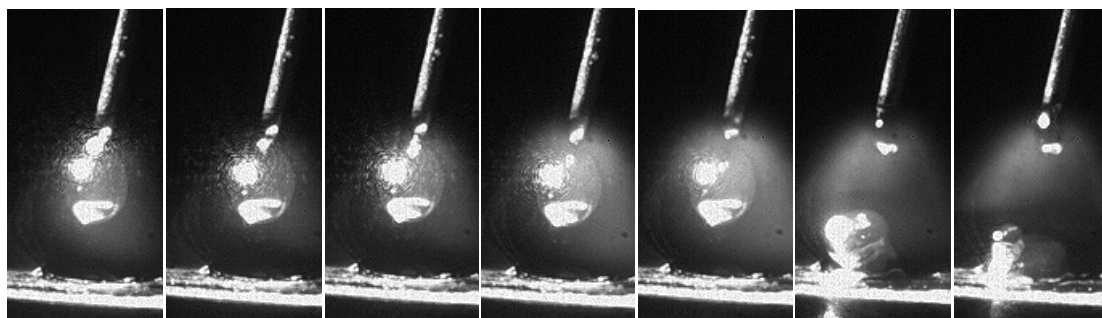
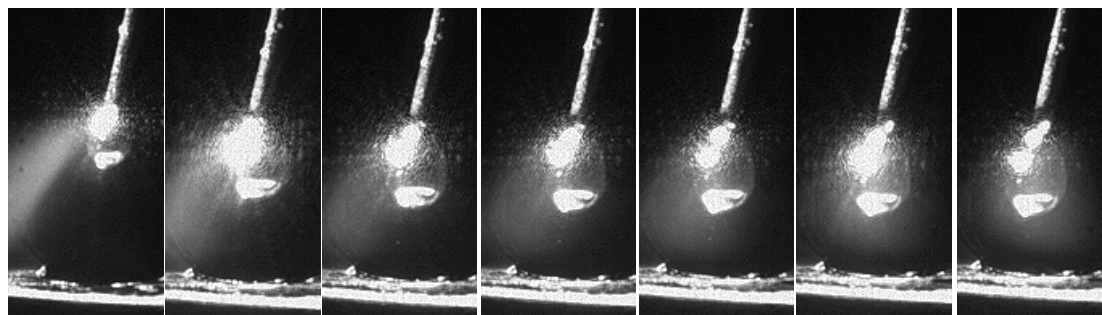


(b) Laser intensity of 62 W/mm^2

Fig. 5-5 Typical metal transfer in comparative experiments with and without laser under (250 in./min, 30 V, 0) and (250 in./min, 30 V, 62 W/mm^2)

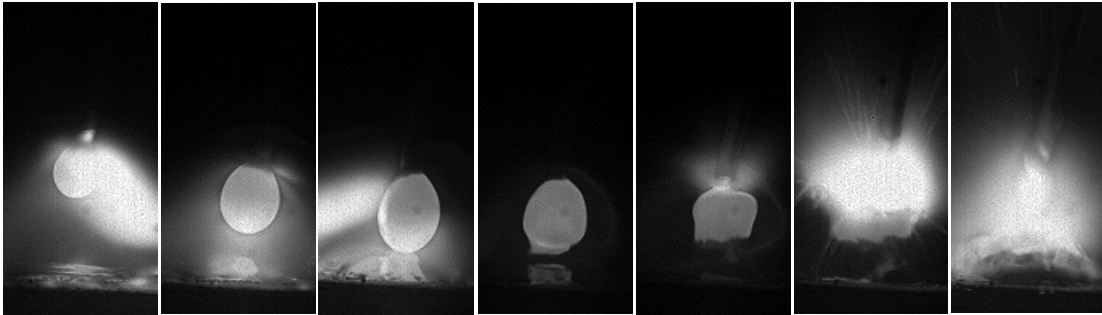
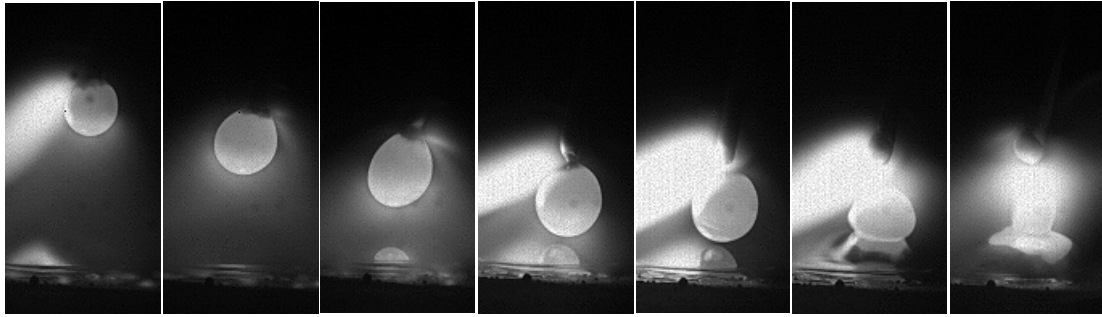


(a) Without laser

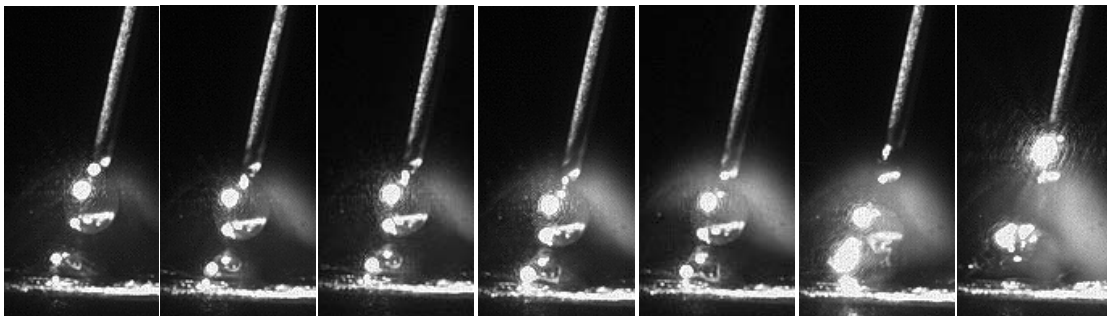
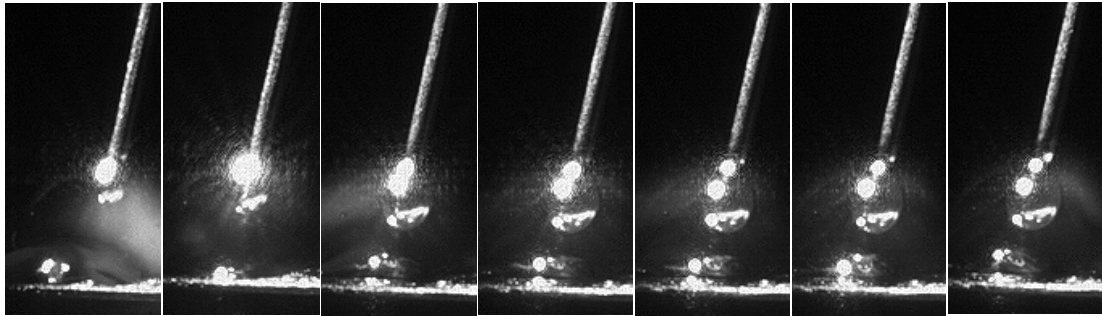


(b) Laser intensity of 62 W/mm^2

Fig. 5-6 Typical metal transfer in comparative experiments with and without laser under (350 in./min, 30 V, 0) and (350 in./min, 30 V, 62 W/mm^2)



(a) Without laser

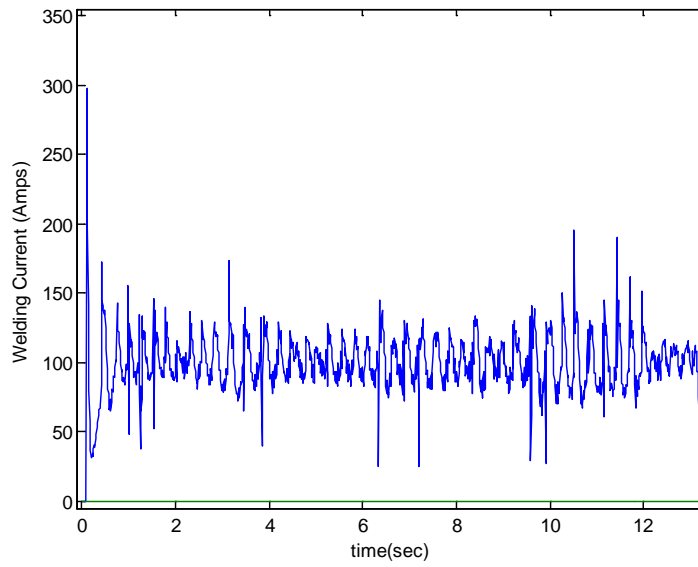


(b) Laser intensity of 62 W/mm^2

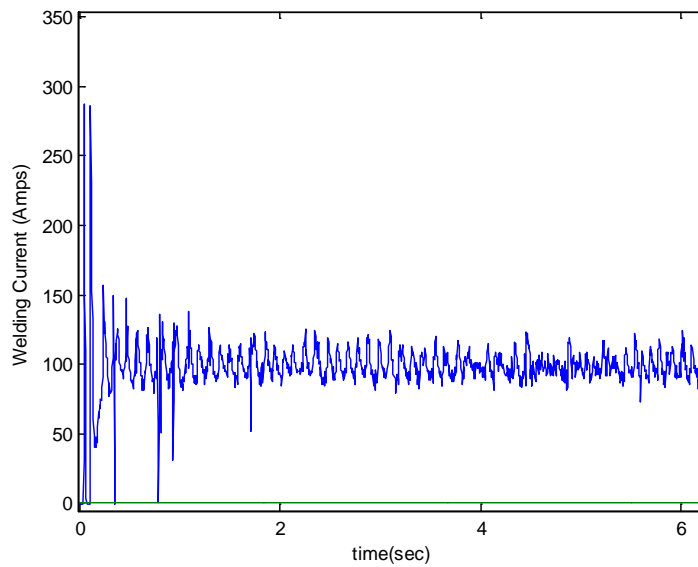
Fig. 5-7 Typical metal transfer in comparative experiments with and without laser under (400 in./min, 30 V, 0) and (400 in./min, 30 V, 62 W/mm^2)

First, the typical metal transfer process as shown in Fig. 5-5 (a) and Fig. 5-6 (a) for 250 and 350 in./min without the laser was all the short-circuiting transfer and significant amount of spatters was produced. When the laser was applied, as can be seen from Fig. 8 (b) and Fig. 5-6 (b), the metal transfer changed to the drop globular transfer and spatters were not found. As the mean welding current did not increase (Fig. 5-1 (a) and (c)), it was the authors' opinion that it was the laser recoil pressure that effectively changed the type of the metal transfer type. In addition, the changes in the metal transfer resulted in less fluctuating welding current as shown in Fig. 5-8 and Fig. 5-9 and the metal transfer process was thus more stable.

Second, when the wire feed speed increased to 400 in./min such that the current increased, the short-circuiting transfer no longer dominated. Fig. 5-7 (a) shows a consecutive transfer process where a short-circuiting transfer followed a drop globular transfer. This was typical in the experiment with 400 in./min without the laser, different from other experiments in the series at the same voltage but lower wire feed speeds where the shorting circuiting transfer dominated. The increased mean current was the major reason for the frequent occurrence of the drop globular transfer but the fluctuation of the welding current into relatively low levels (see Fig. 5-10(a)) also produced short-circuiting transfers from time to time. When the laser was introduced, short-circuiting transfers no longer occurred and transfers became totally free flight ones, as shown in Fig. 5-7(b). The diameter of droplet became similar as that of the electrode wire and the transfer is close to the drop spray. As can be seen in Fig. 5-1(d) and Fig. 5-10, the mean current and current levels did not increase by the laser. It was the laser recoil pressure that effectively changed the metal transfer mode from a mix of short-circuiting and drop globular to the drop spray and reduced the fluctuation in the welding current.

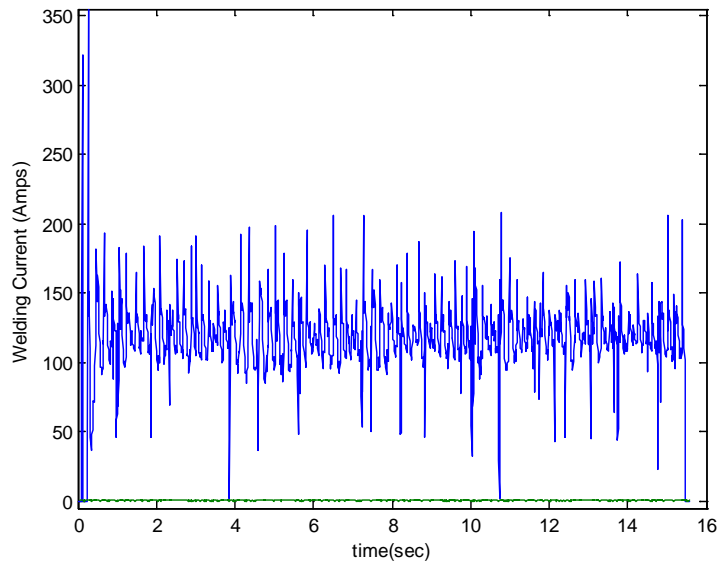


(a) No laser

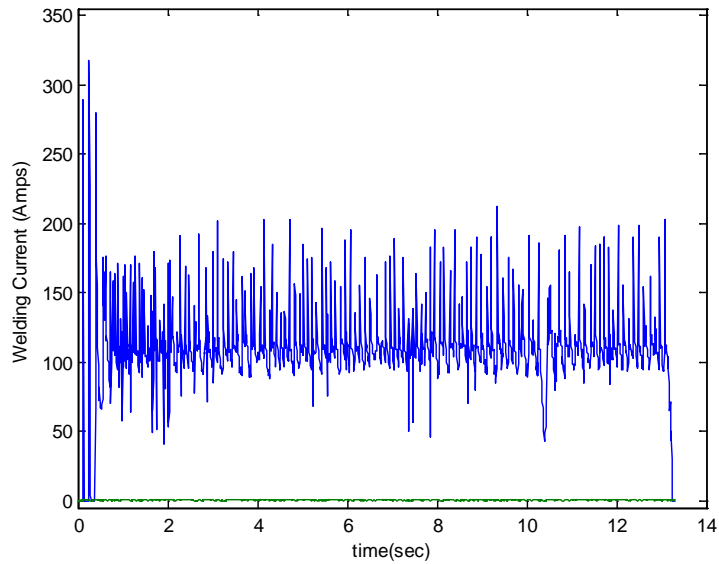


(b) Laser intensity of 62 W/mm²

Fig. 5-8 Current waveforms for (250 in./min, 30 V, 0 W/mm²) and (250 in./min, 30 V, 62 W/mm²)

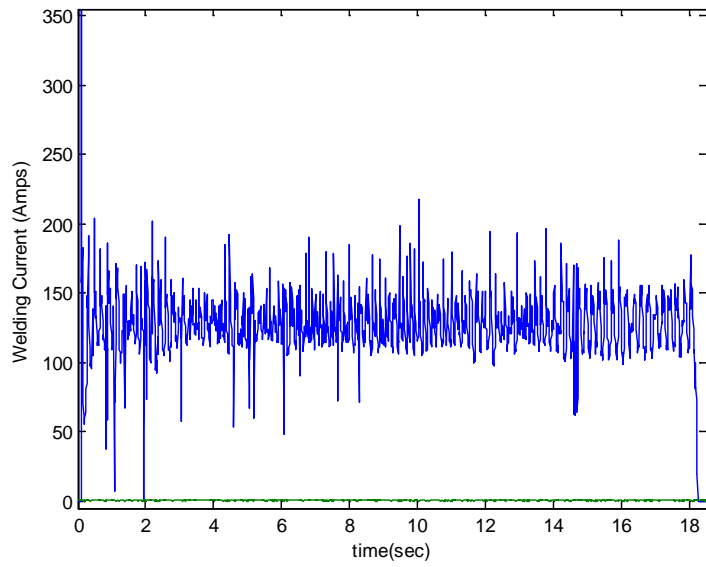


(a) No laser

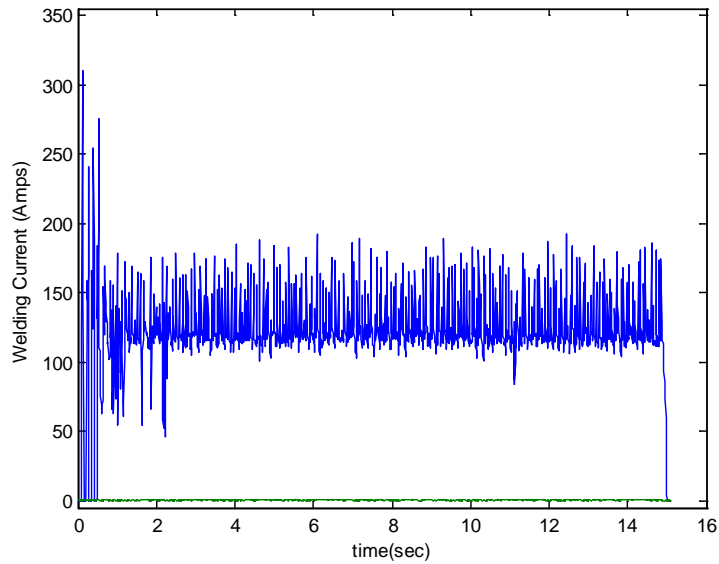


(b) Laser intensity of 62 W/mm^2

Fig. 5-9 Current waveforms for (350 in./min, 30 V, 0 W/mm^2) and (350 in./min, 30 V, 62 W/mm^2)



(a) No laser



(b) Laser intensity of 62 W/mm^2

Fig. 5-10 Current waveforms for (400 in./min, 30 V, 0 W/mm^2) and (400 in./min, 30 V, 62 W/mm^2)

5.3.2 Analysis

As has been observed above, the application of the laser changed the metal transfer. If the metal transfer in conventional GMAW is short-circuiting, the application of the laser at the intensity used could change it to the drop globular transfer. (The authors believe that it may further change to the spray transfer as long as the intensity of the laser is sufficient.) When a mix of short-circuiting and globular transfers dominates, it may change to the drop spray even with the laser intensity used. When the drop globular could be obtained, the laser reduces the diameter of the droplet detached. In all cases, the diameter of the detached droplets was decreased as further shown in Fig. 5-11. The laser recoil pressure was identified the major cause of these observed changes.

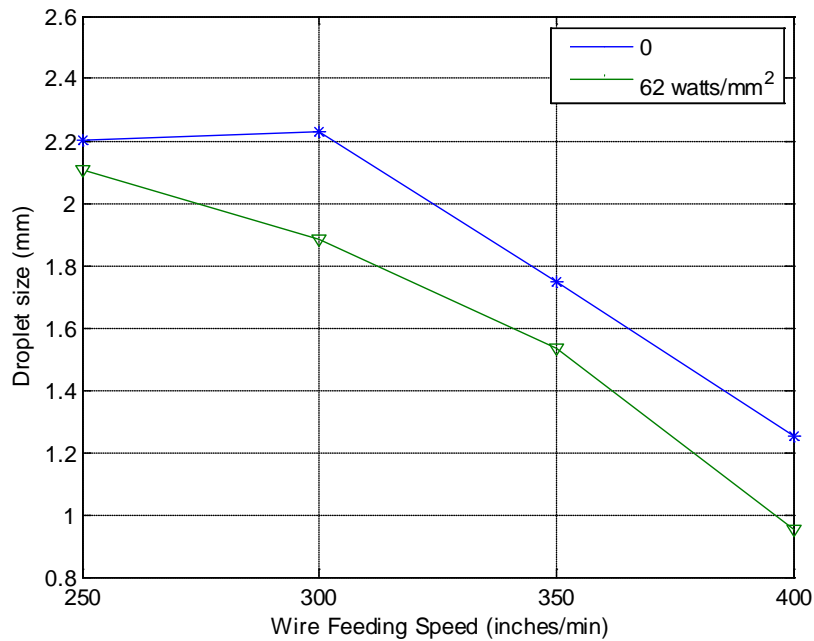


Fig. 5-11 Droplet sizes with welding voltage 30 V under different wire feed speeds

To analyze further, let's recall that in conventional GMAW, the major sources of the detaching force are the gravitational, electromagnetic, aerodynamic drag, and momentum forces, while the major retaining force is the surface tension at the interface of the solid wire and liquid droplet [25, 77]. When the diameter of the wire and material are given, this surface tension can be considered constant because the temperature at the interface

aforementioned is the melting point and changes with neither the welding current nor the application of the laser. When the welding current is lower than the transition current such that the current exits from the droplet around its bottom, the electromagnetic force as a detaching force is relatively small. The aerodynamic drag force and momentum force are typical relatively small and are often negligible in analysis such that there is a need for a large gravitational force to balance out the surface tension for detachment. In this case, as shown in Fig. 5-3, Fig. 5-5, Fig. 5-6 and Fig. 5-7, the diameter of droplet is larger than that of the wire.

More specifically, when the wire feed speed is low, such as 250 to 300 in./min, the droplet needs to grow sufficiently large to acquire a sufficient mass needed to produce a sufficient gravitational force to balance out the surface tension. However, before this large mass is obtained, the droplet touches the weld pool because of the relatively slow growth (due to the relatively small current and arc heat). The metal transfer is dominated by the short-circuiting transfer. When the wire feed speed/welding current increases, for example to 350 in./min, such that the welding current and electromagnetic force increases, the needed mass to balance out the surface reduces. However, if this reduced mass needed is still not achieved before the droplet touches the weld pool, the transfer will still be short-circuiting. In Laser Enhanced GMAW, the laser recoil pressure is added to the detaching force and the needed mass is reduced. If the needed mass is produced before the droplet touches the weld pool, the metal transfer would change from short-circuiting to drop globular or effectively reduce the diameter of the droplet detached. As shown in Fig. 5-11, all the diameters of droplet in Laser Enhanced GMAW are smaller than their respective counterparts in conventional GMAW. As long as there is a large enough laser recoil pressure (laser intensity), the drop globular and, the authors believe, drop spray would be obtained. To verify the latter, a larger intensity laser is needed.

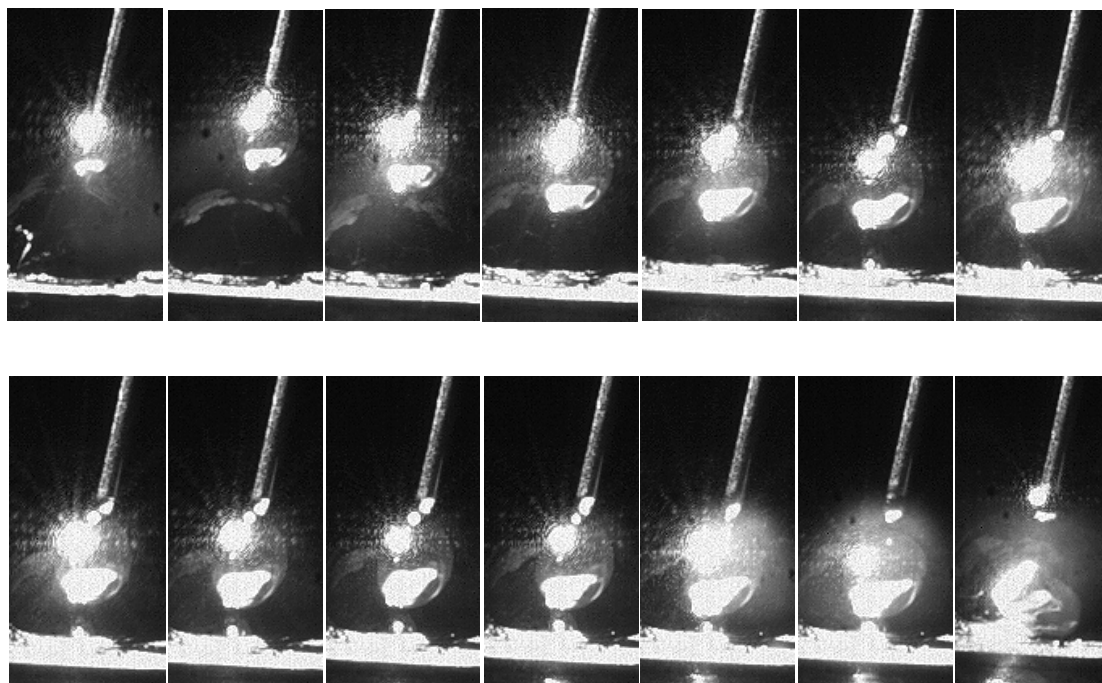
Further, when the wire feed speed further increases, such as to 400 in./min, the transfer will be dominated by a mix of globular and short-circuiting transfer in conventional GMAW. For the laser intensity applied, the short-circuiting transfer in conventional GMAW will change to drop globular in Laser Enhanced GMAW. The drop globular in conventional GMAW could remain or change to the drop spray. In both cases, the

diameter of droplet detached reduces in Laser Enhanced GMAW and the drop spray occurs when the diameter reduces to a level close to that of the wire.

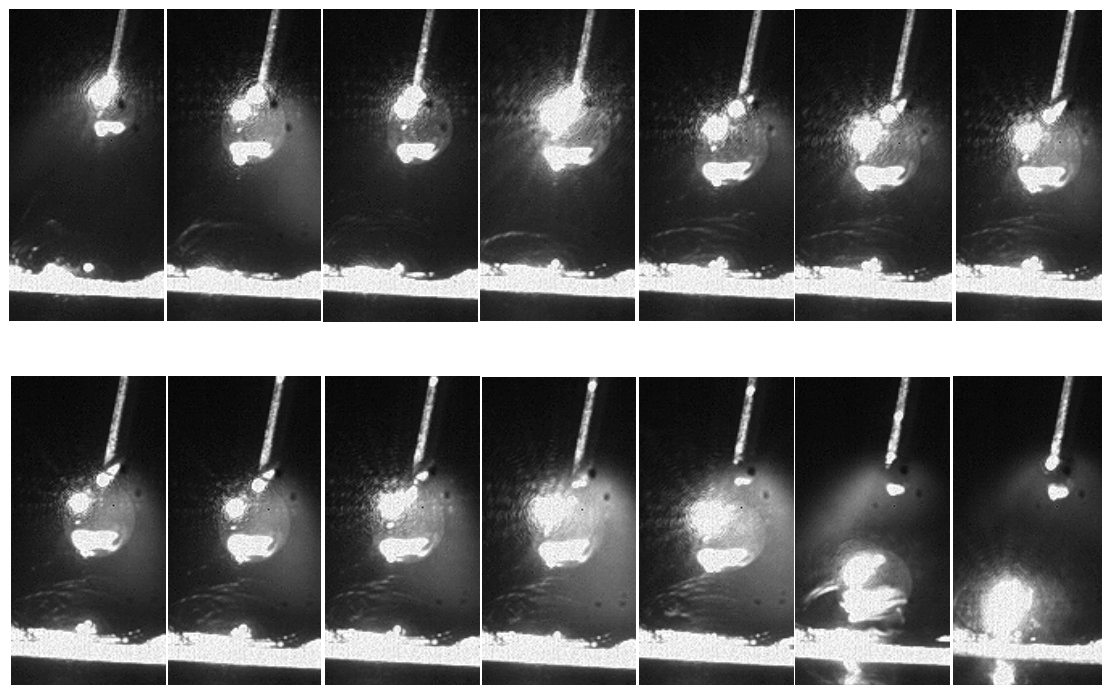
5.4 Laser Intensity

The major parameter of the laser in the Laser Enhanced GMAW is the recoil pressure that is determined by the laser intensity and the cross section of the droplet that intercepts the laser. To study the effect of the laser intensity, three levels of laser power have been used: 645, 754 and 862 W. The laser beam used in this study is $1\text{mm} \times 14\text{mm}$. The corresponding intensity is thus 46, 54 and 62 W/mm^2 . Because the laser is applied along the wire axis direction, if the diameter of the droplet is smaller than 1 mm, the interception area aforementioned increases quadratically with the droplet diameter; however, for the majority of the experiments studied in this paper, the droplet detached has a diameter greater than 1 mm and the interception area increases with the droplet diameter linearly, the interception area increases linearly with the diameter of the droplet.

Fig. 5-12 together with Fig. 5-3 and shows the metal transfer at the different laser intensity levels for (300 in./min, 30 V, 0- 62 W/mm^2). When the laser intensity was zero (Fig. 5-3(a)), the metal transfer was short-circuiting. (For shorting-circuiting transfer, the diameter of the droplet such as that given in Fig. 5-13 is measured right before the droplet touches the weld pool.) When it increased to 46 W/mm^2 , the transfer was a mix of short-circuiting and drop globular approximately at 50%-50%, but the droplet was typically detached right before the droplet touches the weld pool. Hence, in Fig. 5-13, its droplet diameter is the same as that without the laser. (One should note that the diameter of the droplet detached under a short-circuiting condition differs from that under a drop globular transfer. Hence, the same droplet diameter observed in Fig. 5-13 for without laser and laser intensity= 46 W/mm^2 is reasonable.) When the laser intensity increased to 54 W/mm^2 , the metal transfer became drop globular (Fig. 5-12); when the laser intensity further increased to 62 W/mm^2 , the diameter of the droplet detached further reduced (Fig. 5-3(b)).



(a) Laser intensity of 46 W/mm^2



(b) Laser intensity of 54 W/mm^2

Fig. 5-12 Typical metal transfer in comparative experiments with and without laser under (300 in./min, 30 V, 46 W/mm^2) and (300 in./min, 30 V, 54 W/mm^2)

As can be seen in Fig. 5-2(b), the current approximately remained unchanged. The increase in the laser intensity thus did not increase the electromagnetic force. Fig. 5-13 clearly shows the tendency that the droplet diameter reduces as the laser intensity increases. The increased laser intensity decreased the need for a larger diameter for a larger interception area and large mass.

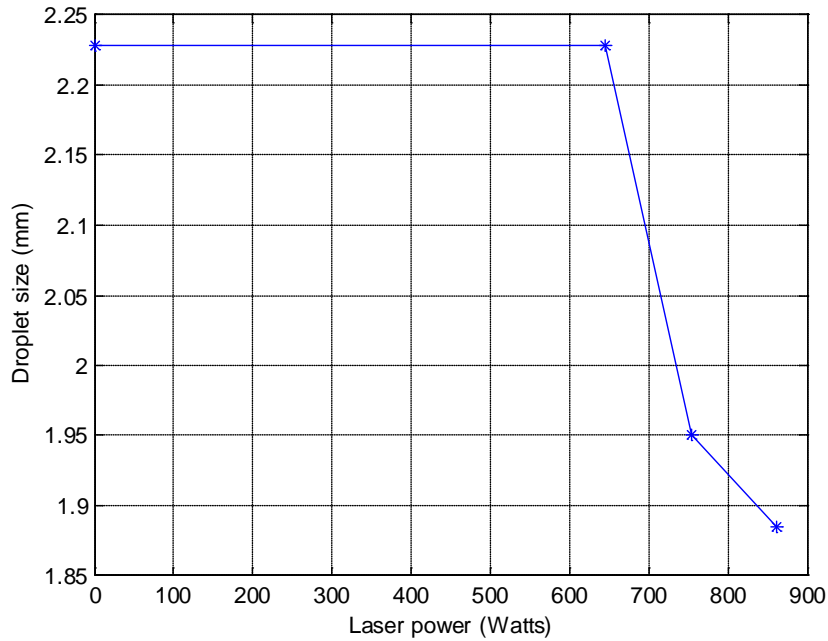
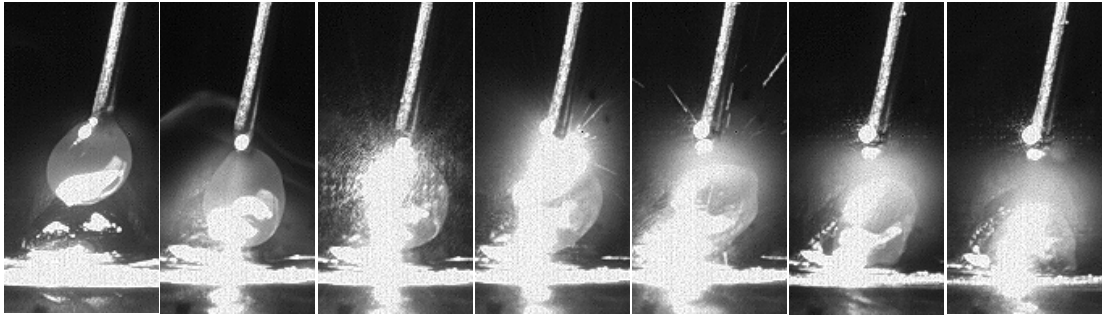
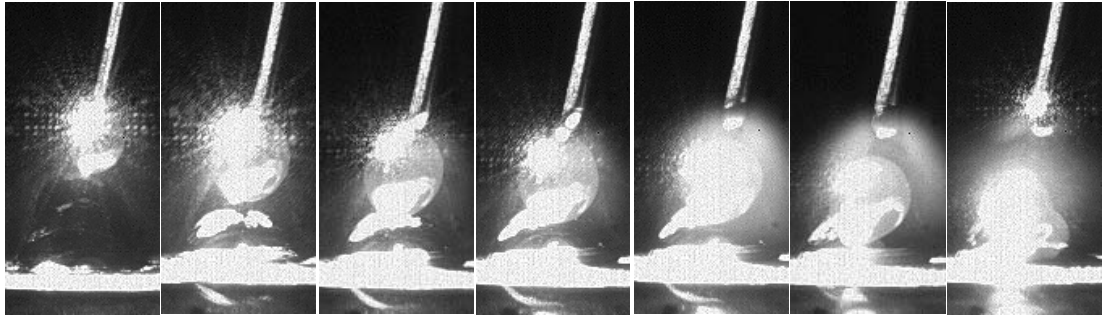
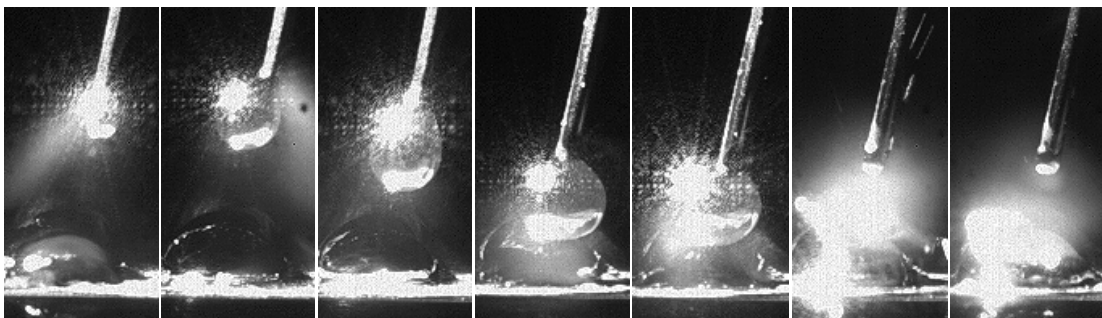
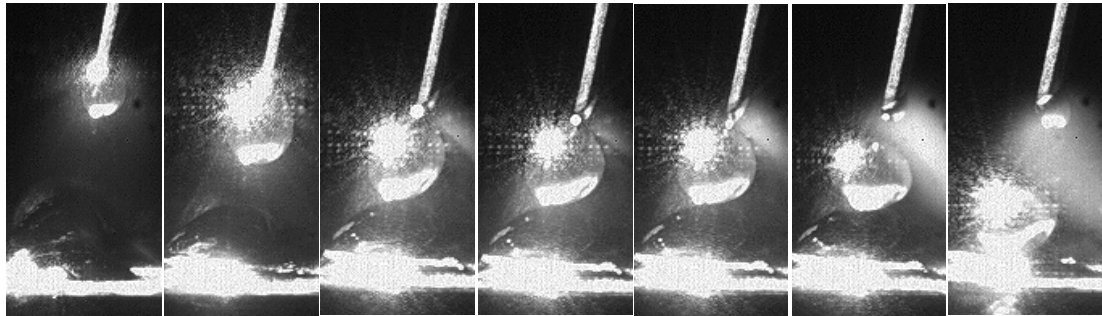


Fig. 5-13 Droplet diameter with 30 V and 300 in./min under different laser power levels. The droplet diameter is the mean of the diameter of the droplet that is detached or touches the weld pool.

Metal transfer images in additional experiments at laser intensity of 46 W/mm^2 and 54 W/mm^2 are added in Fig. 5-14, Fig. 5-15, and Fig. 5-16 to those previously presented for laser intensity at zero (without laser) and 62 W/mm^2 to form a complete set of data to examine the effect of laser intensity at 30 V of the voltage setting. The complete set of data is illustrated in Fig. 5-17 where same tendency how the laser intensity affects the droplet diameter as in Fig. 5-13 is also observed. However, there are details that deserve attention and are discussed below.

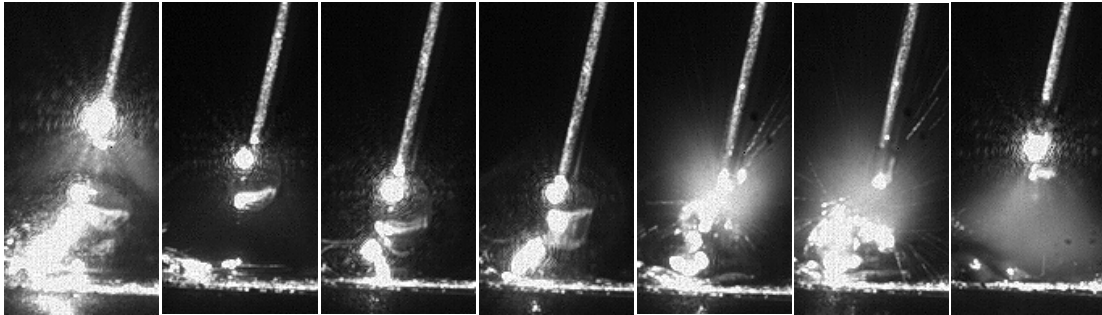
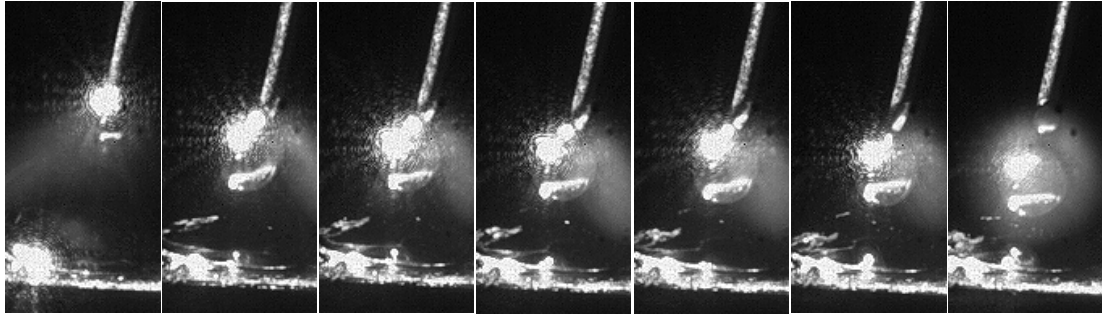


(a) Laser intensity of 46 W/mm^2

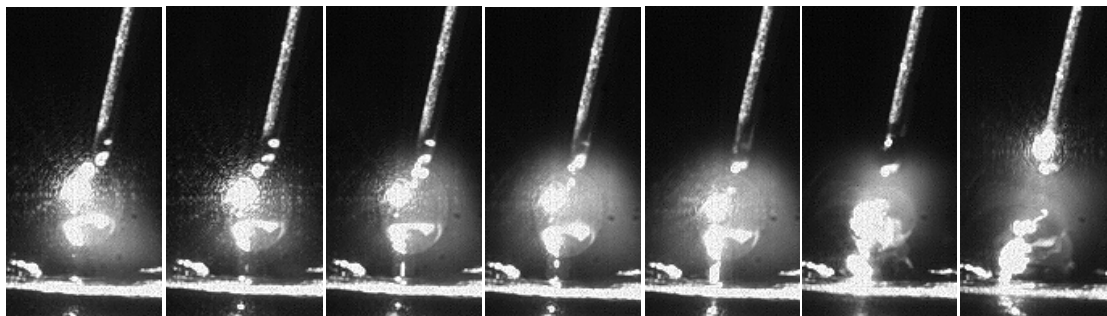
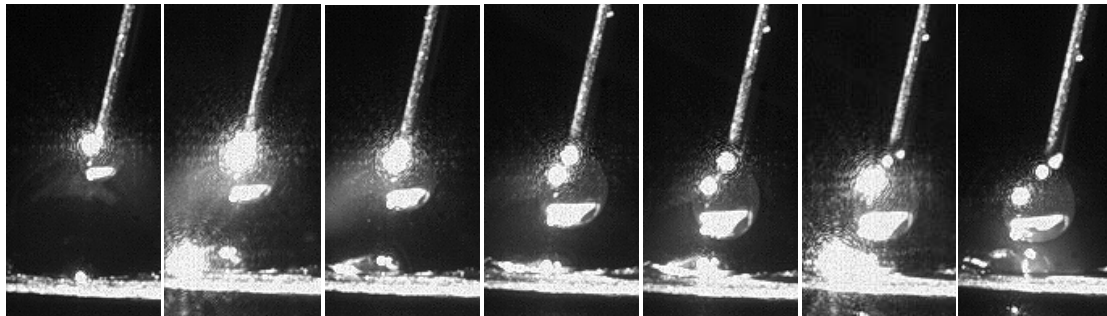


(b) Laser intensity of 54 W/mm^2

Fig. 5-14 Typical metal transfer in comparative experiments with and without laser under (250 in./min, 30 V, 46 W/mm^2), and (250 in./min, 30 V, 54 W/mm^2)

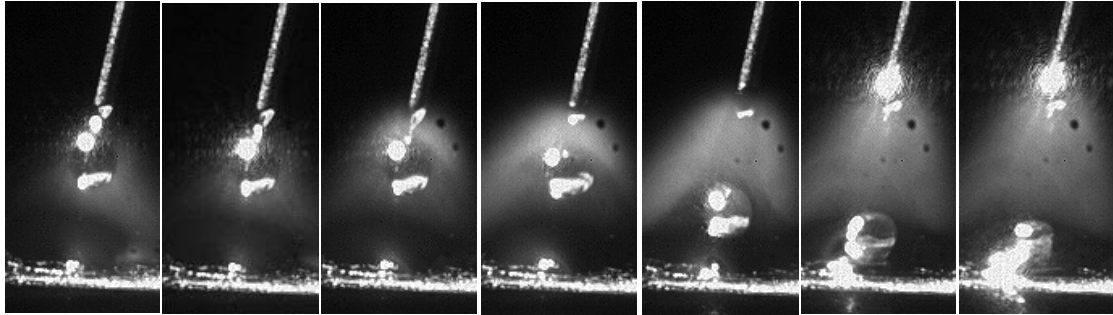
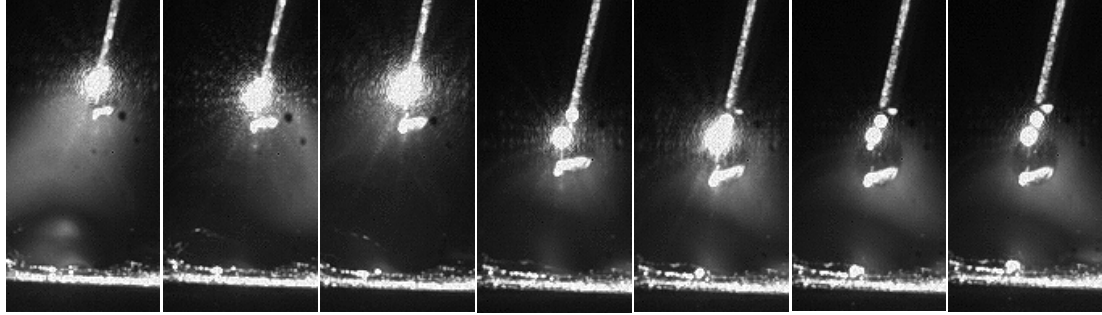


(a) Laser intensity of 46 W/mm^2

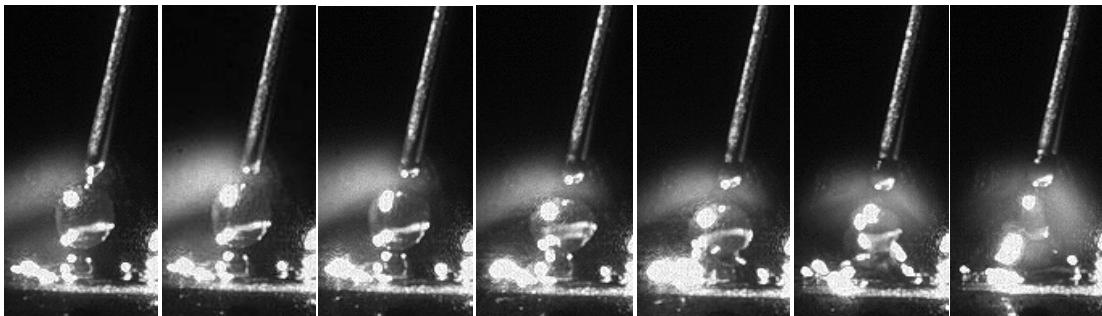
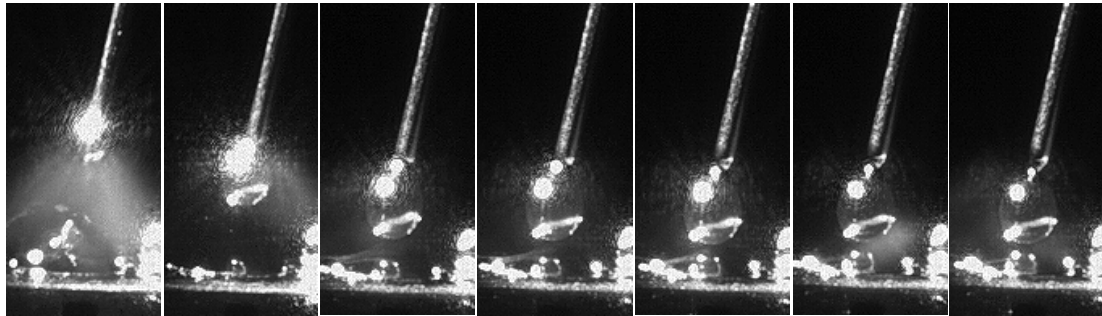


(b) Laser intensity of 54 W/mm^2

Fig. 5-15 Typical metal transfer in comparative experiments with and without laser under (350 in./min, 30 V, 46 W/mm^2), and (350 in./min, 30 V, 54 W/mm^2)



(a) Laser intensity of 46 W/mm^2



(b) Laser intensity of 54 W/mm^2

Fig. 5-16 Typical metal transfer in comparative experiments with and without laser under (350 in./min, 30 V, 46 W/mm^2) and (350 in./min, 30 V, 54 W/mm^2)

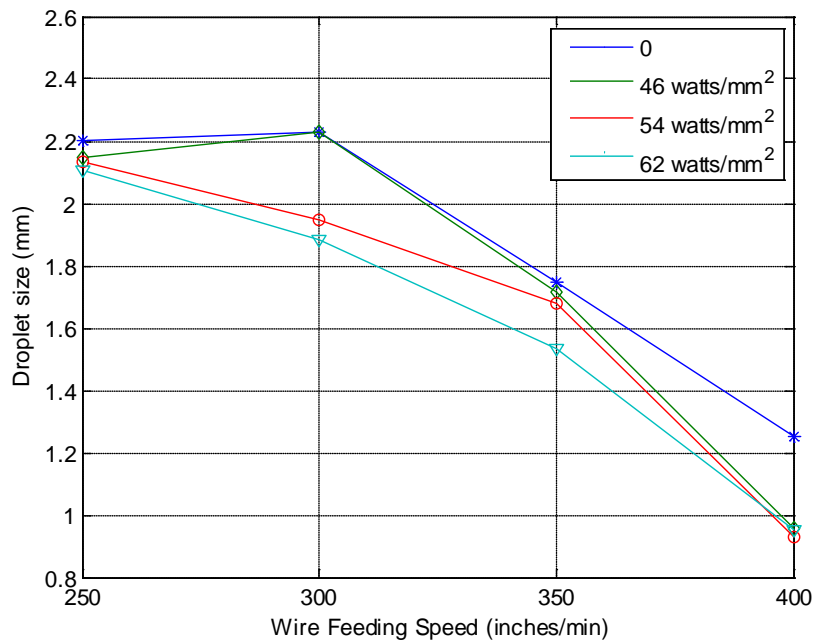


Fig. 5-17 Droplet diameter with 30 V under different wire feed speed laser power levels. The droplet diameter is the mean of the diameter of the droplet that is detached or touches the weld pool.

Let's first examine the experiment series associated with 250 in./min, i.e., (250 in./min, 30 V, 0-62 W/mm²), as shown in Fig. 5-5(a), Fig 5-14(a), Fig. 5-14(b), and Fig. 5-5(b). It is seen that the transfer with 46 W/mm² (Fig. 5-14 (a)) is a mix of short-circuiting and drop globular but the droplet diameter is almost the same as the one without laser (Fig. 5-5 (a)) as can be seen from Fig. 5-17. In these two cases, the laser recoil pressure (if any) is not large enough to compensate for the lack of gravitational force for a complete free flight transfer and a relatively large gravitational force is still needed to detach the droplet. In this mixed mode, short-circuiting transfer dominated but the drop globular transfer also occurred.

In this series of experiments, an interesting phenomenon can be observed from Fig. 5-5 (a) and Fig. 5-14(a) that the laser enhanced short-circuiting transfer (Fig. 5-14(a)) still produced spatters but at a much reduced amount from conventional GMAW (Fig. 5-5 (a)). Careful observation shows that the short-circuiting time was reduced approximately 20%

by the laser at the intensity of 46 W/mm^2 . This may possibly be the cause that reduced the spatters.

Then examine the experiment series associated with 350 in./min , i.e., (350 in./min , 30 V , $0-62 \text{ W/mm}^2$), as shown in Fig. 5-6(a), Fig 5-15(a), Fig. 5-15(b), and Fig. 5-6(b). With laser intensity of 46 W/mm^2 (Fig. 5-15(a)), the drop globular dominated and short-circuiting transfer seldom occurred. For 54 W/mm^2 (Fig. 5-15 (b)), the transfer is a stable drop globular process but the droplet diameter is larger than that with 62 W/mm^2 (Fig. 5-6 (b)).

For the experiment series associated with 400 in./min , i.e., (400 in./min , 30 V , $0-62 \text{ W/mm}^2$), as shown in Fig. 5-7(a), Fig 5-16(a), Fig. 5-16(b), and Fig. 5-7(b). the metal transfer mode is different from the two aforementioned. As shown in Fig 5-16(a), Fig. 5-16(b), and Fig. 5-7(b), the metal transfer mode is the drop spray transfer. Increasing laser intensity, the diameter of droplet will decrease though this change is not obvious.

As summarized in Fig. 5-17, for all the wire feed speeds, the diameter of droplet in each Laser Enhanced GMAW experiment is smaller than its respective counterpart in conventional GMAW experiment. If the diameter for an increased laser intensity is the same with or very close to one for a lower laser intensity (or without laser), they both must be either short-circuiting or very close to short-circuiting (i.e., the droplet is detached right before it touches the weld pool). Of course, all these phenomena can be well explained based on force analysis as has been done earlier.

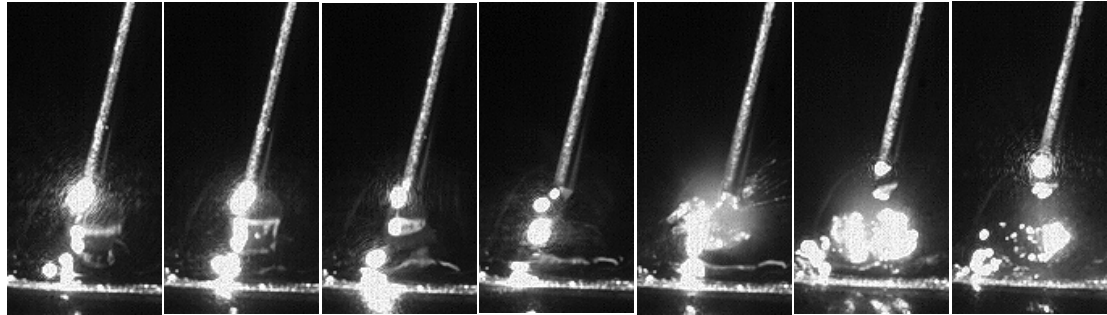
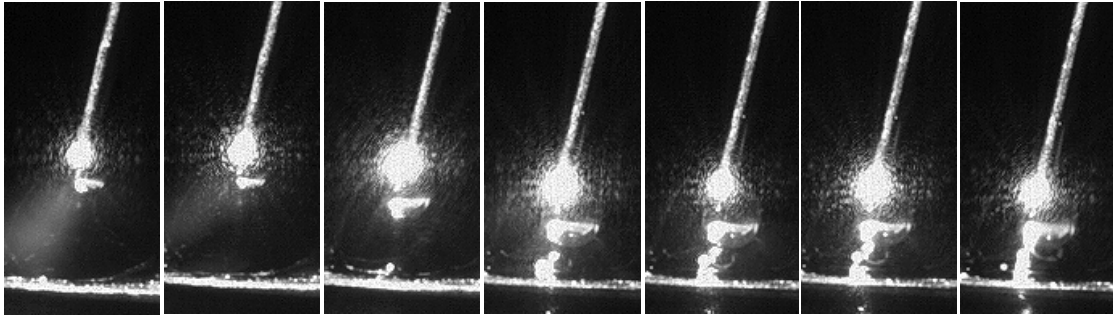
5.5 Arc Length

The voltage setting on the metal transfer affects the metal transfer through its effect on the arc length, i.e., increasing/decreasing the voltage increases/decreases the arc length. The change in the arc length affects the metal transfer through (1) an increased arc length reduces the wire extension such that the welding current increases when using a constant voltage power supply as in this study; (2) an increased arc length provides a longer gap to allow a longer time for a new droplet to develop after a droplet detachment. (This gap,

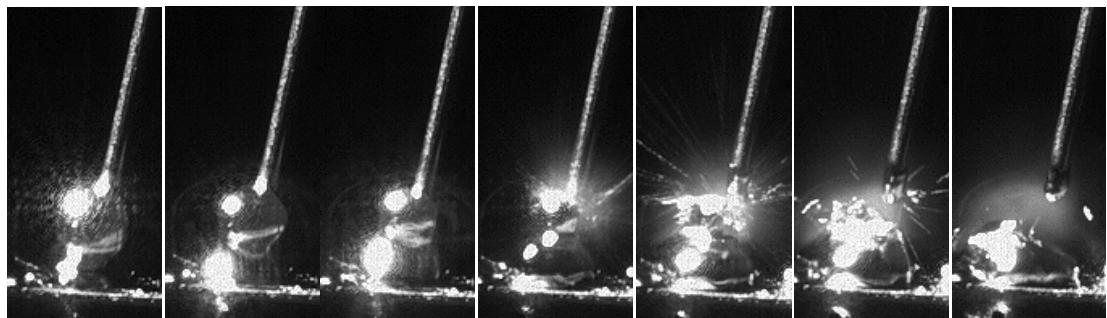
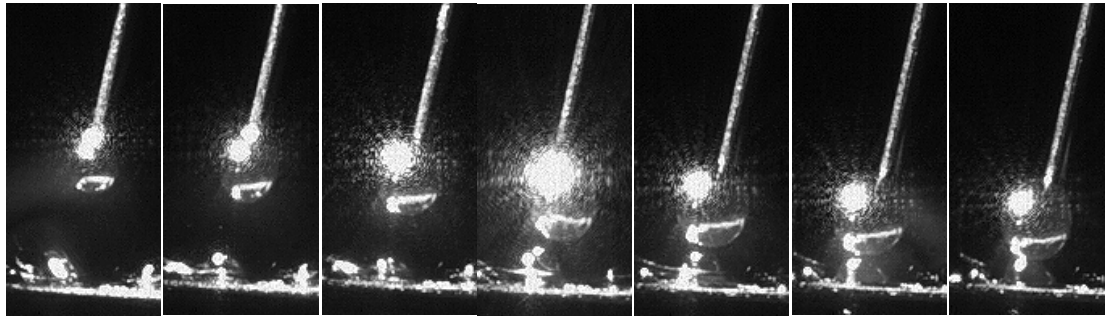
the distance from the bottom of the new droplet to the weld pool surface right after a droplet is detached, is referred to as the development gap hereafter in this study.) In Laser Enhanced GMAW, an increased laser intensity does not increase the welding current, as shown in Fig. 5-3. (Instead, it reduces the current slightly). However, when the voltage increased by 6 V, the welding current increased by 10 to 15 A (shown in Fig. 5-3). Because the electromagnetic force as a detaching force increases faster than a quadratic speed as the current increases, the increase in the detaching force would be significant.

Let's take the experiment series with 350 in./min wire feed speed (Fig. 5-6 and Fig. 5-18) as an example to illustrate how the voltage setting affects the metal transfer. When the voltage was 26 V, as shown in Fig. 5-18 (a), even if the laser power was 62 W/mm^2 , the metal transfer was still short-circuiting. This is because the development gap was short such that there was not enough time to grow the droplet. As a result, its small gravitational force together with the detaching electromagnetic force and laser recoil pressure force was not still sufficient to balance out the surface tension before the droplet touched the weld pool. When the voltage increased to 28 V (Fig. 5-18 (b)), the development gap increased for the droplet to grow longer. In addition, the electromagnetic force increased. However, those increases were still not sufficient and the metal transfer was still short-circuiting. When the voltage increased to 30 V (Fig. 5-6 (b)), the metal transfer changed to drop globular. When it further increased to 32 V, the droplet diameter is further reduced to a level comparable with that of the wire (Fig. 5-18 (c)) due to the increased current/electromagnetic detaching force.

Fig. 5-19 plots how the droplet size changed with the voltage setting for the experiment series analyzed above. The observed droplet size increase from 26 V to 28 V was due to the increased development gap that provided a longer time for the droplet to grow. The increased electromagnetic force should have tended to help detach the droplet. However, since the droplet was not detached (still short-circuiting transfer), the electromagnetic force played no role in determining the droplet size. Hence, it was the increased development gap that contributed to increasing the droplet size before short-circuiting.

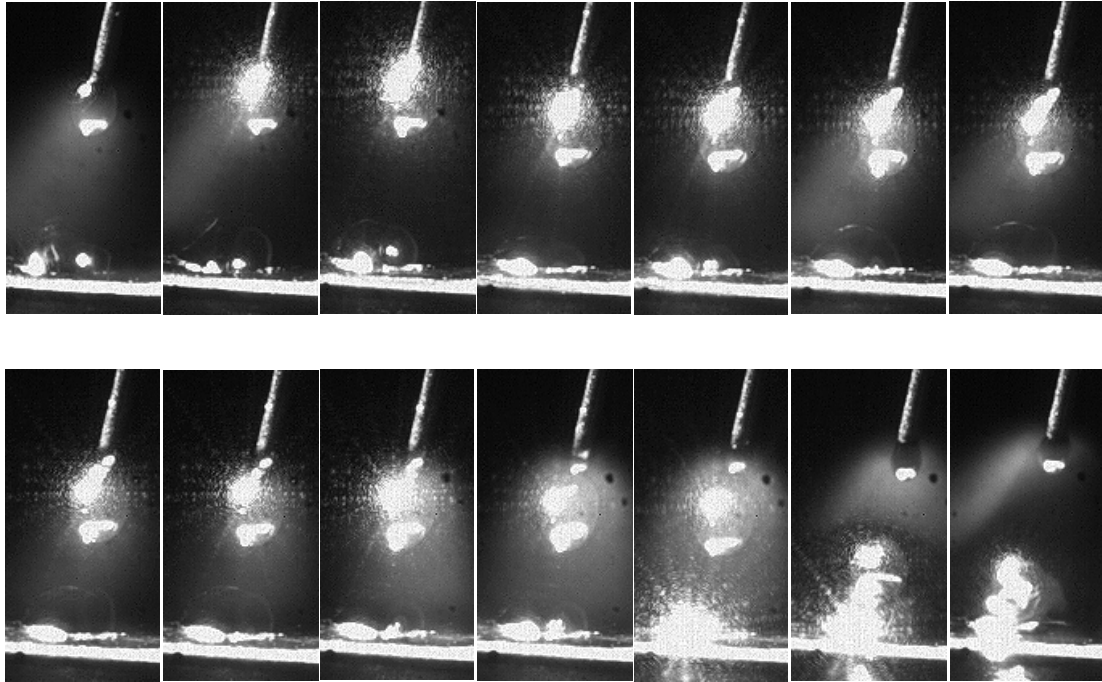


(a) Voltage of 26 V



(b) Voltage of 28 V

Fig. 5-18 Typical metal transfer in comparative experiments with laser under (350 in./min, 26 V, 62 W/mm²), (350 in./min, 28 V, 62 W/mm²) and (350 in./min, 32 V, 62 W/mm²)



(c) Voltage of 32 V

Fig. 5-18 Typical metal transfer in comparative experiments with laser under (Continued)

The droplet size decreases when increasing from 28 V to 30 V and from 30 V to 32 V were both due to the respective increase in the current/electromagnetic force and the increased development gap played no role in resulting in this decrease. The laser may only help reduce the droplet size further or affect help the transfer to change from short-circuiting to drop globular or drop spray.

Similar analysis can be done to understand how the voltage affects the metal transfer process for other wire feed speeds such as for 400 in./min wire feed speed (Fig. 5-7 and Fig. 5-20). Despite the change in the current that directly affect the electromagnetic force, the voltage setting still affects the metal transfer through its associated current change and development gap change.

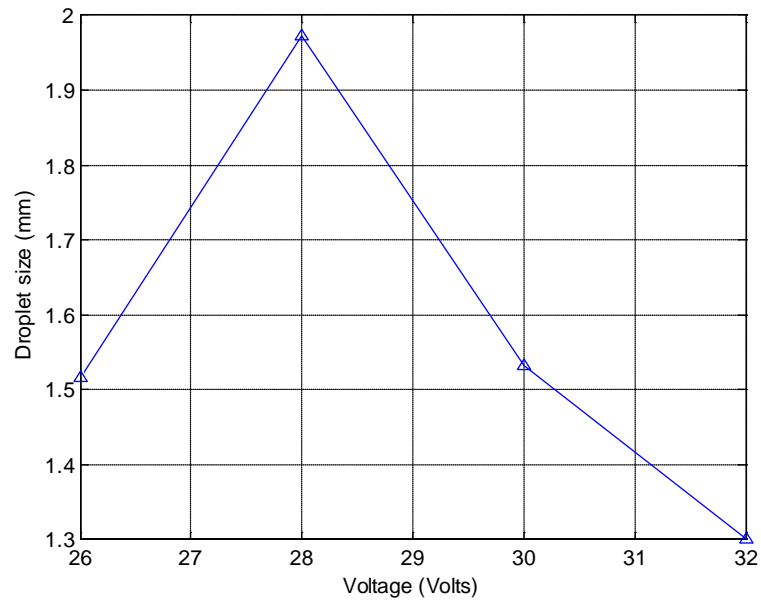
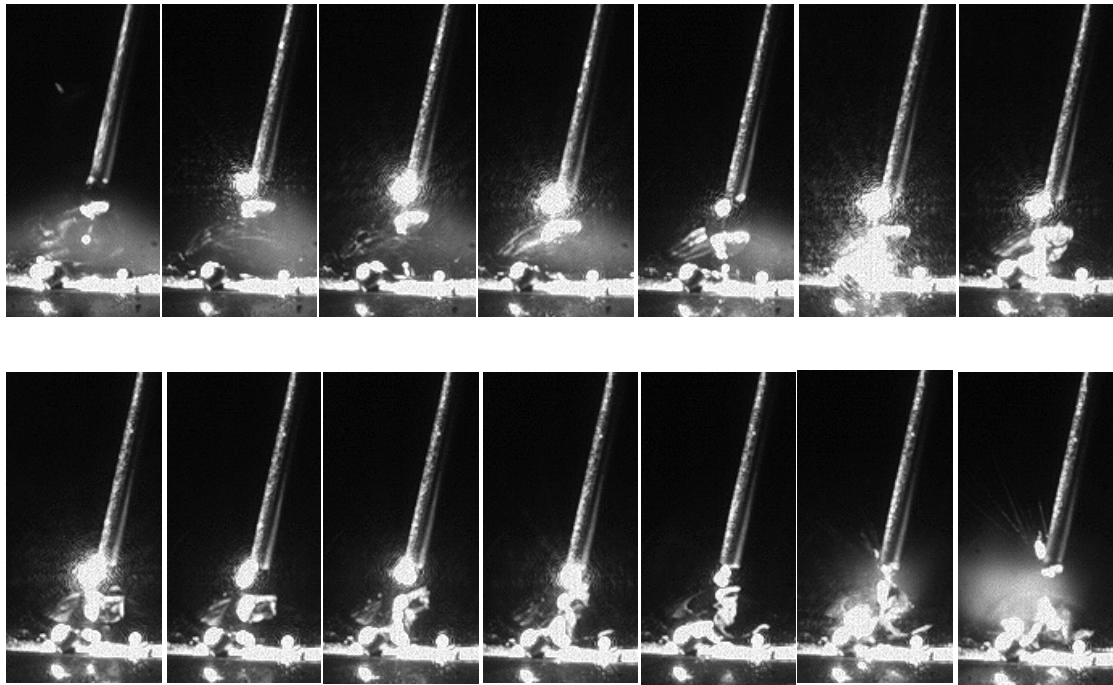


Fig. 5-19 Droplet sizes with welding feed speed 350 in./min under different voltages

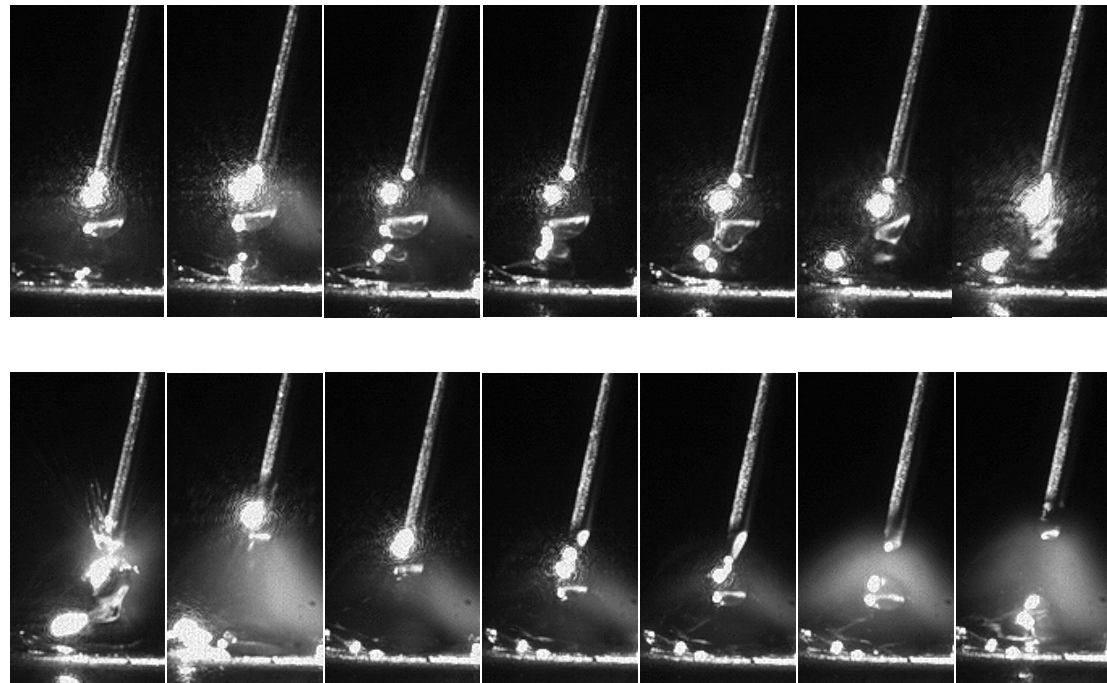
In summary, a higher voltage setting increases the current and development gap. The increased development gap may help change the metal transfer from short-circuiting to drop globular or even drop spray but it plays neither role in affecting the size of the droplet detached under free-flight transfers nor role in changing the transfer from drop globular to drop spray. The increased current affects the metal transfer by increasing the electromagnetic detaching force.

5.6 Laser Recoil Pressure Force Estimation

In laser enhanced GMAW, estimating the laser recoil pressure is a key issue for the further feedback control of this process. To better understand the physics fundamentals of the method, the forces affecting metal transfer are analyzed first. It is well known that in conventional GMAW, the major forces acting on the droplet include the gravitational force, electromagnetic force (Lorentz force), aerodynamic drag force, surface tension, and momentum force [20-25].

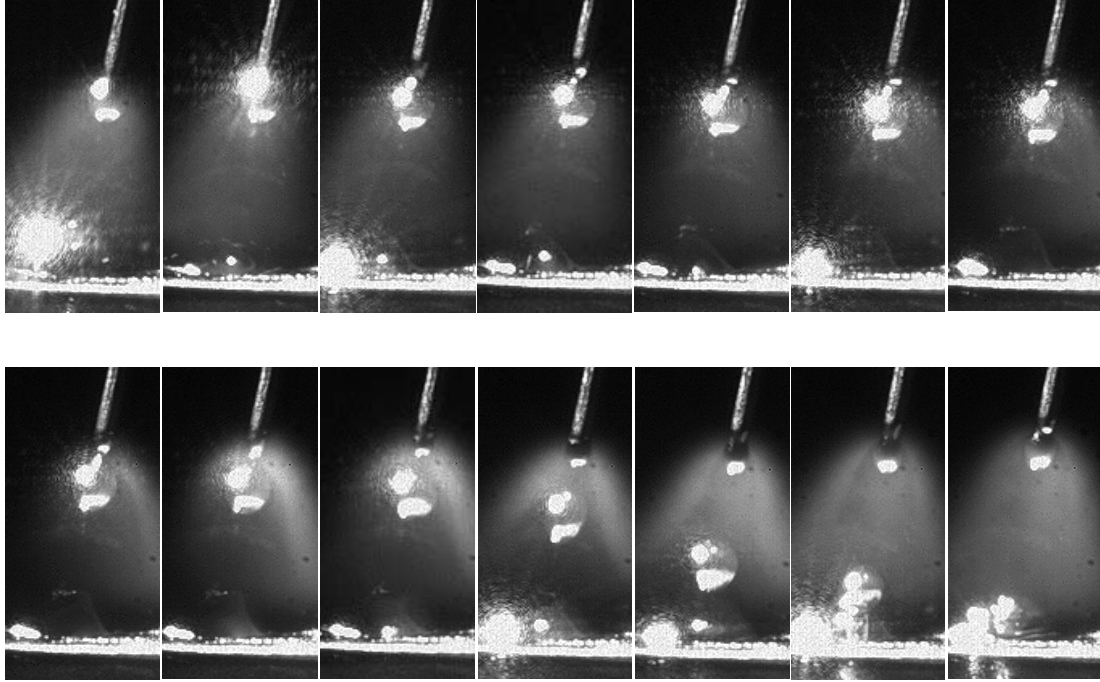


(a) Voltage of 26 V



(b) Voltage of 28 V

Fig. 5-20 Typical metal transfer in comparative experiments with laser under (400 in./min, 26 V, 62 W/mm²), (400 in./min, 28 V, 62 W/mm²) and (400 in./min, 32 V, 62 W/mm²)



(c) Voltage of 32 V

Fig. 5-20 Typical metal transfer in comparative experiments with laser under (Continued)

In Laser Enhanced GMAW, a laser is applied and an additional force is introduced as shown in Fig. 4-1. To be simple, the dynamic-force balance theory (DFBM) [20-25, 77] is used in this paper to conduct preliminary analysis of the forces for the Laser enhanced GMAW.

In laser enhanced GMAW, the total detaching force F_T will be expressed by

$$F_t = F_g + F_d + F_m + F_{em} + F_{laser\ recoil\ force} \quad (5-3)$$

When the total detaching force F_T could balance the surface tension, the droplet will be detached. However, the laser recoil pressure force $F_{laser\ recoil\ force}$ is unknown because there is less accurate calculation theory to achieve this value. In this case, the author proposes a calculating method to estimate this force.

As the radius of welding wire and surface tension coefficient are constant, the surface tension is fixed and it indicates that the retaining force keeps constant. To calculating

aerodynamic drag force, the area of the drop seen from above A_d should be calculating first. A_d can be given by

$$A_d = \pi(r_d^2 - r_w^2) \quad (5-4)$$

Take the case (Wire feed speed at 300 in./min, laser power intensity at 62 W/mm² and welding voltage at 30V) as an exAle to analyze this force. The experiment results (shown in Fig. 5-11) shows that the largest radius of droplet with these welding parameters is about 0.95mm. In this case, the largest aerodynamic drag force is about 8×10⁻⁵N. It could be neglected when estimating the laser recoil pressure. The calculating constants used are shown in Table. 5-1 [82-85].

Table 5-1 Constants used for laser recoil pressure force estimation

Symbol	Value	Unit	Description
C_1	2.885e-10	m ³ /(A s)	Melting Rate Constant
C_2	5.22e-10	m ³ /(A Ω s)	Melting Rate Constant
r_w	0.0004	m	Wire Radius
v_p	10	m/s	Relative fluid to drop velocity
C_d	0.44		Drag coefficient
ρ_p	1.6	Kg/m ³	Plasma density
ρ_r	0.7836	Ω/m	Resistivity of the electrode
ρ_w	7860	Kg/m ³	Electrode density
μ_0	1.25664e-6	(kg m)/(A ² s ²)	Permeability of free space
σ	1	N/m ²	Surface Tension Coefficient

To estimate the momentum force, as the wire feed speed is a constant, the change of the droplet mass \dot{m}_d should be estimated first. \dot{m}_d can be expressed by

$$\dot{m}_d = \pi\rho_w(C_1I + C_2\rho_r l_s I^2) \quad (5-5)$$

By calculating, it is found that the maximum momentum force is around $5 \times 10^{-5} \text{N}$. It could be also neglected when estimating the laser recoil pressure force.

To estimate the electromagnetic force, similar as the definition in Ref. 20, f_2 is defined as

$$f_2 = \ln \sin \theta - \frac{1}{4} - \frac{1}{1 - \cos \theta} + \frac{2}{(1 - \cos \theta)^2} \ln \frac{2}{1 + \cos \theta} \quad (5-6)$$

In this case, the electromagnetic force could be expressed as

$$F_{em} = \frac{\mu_0 I^2}{4\pi} \left(\ln \frac{r_d}{r_w} + f_2 \right) \quad (5-7)$$

In the laser enhanced GMAW, the half-angle subtended by the arc root at the centre of the droplet θ is in the range from 90° to 150° [20-25]. As shown in Fig. 5-21, the value of f_2 does not change significantly when the half-angle varies from 90° to 150° . So the selection of half-angle will not influence the estimating results. Let's recall the exAle case to analyze. As the mean welding current is a constant, the electromagnetic force will not change significantly in a certain time interval between the moment with and without laser.

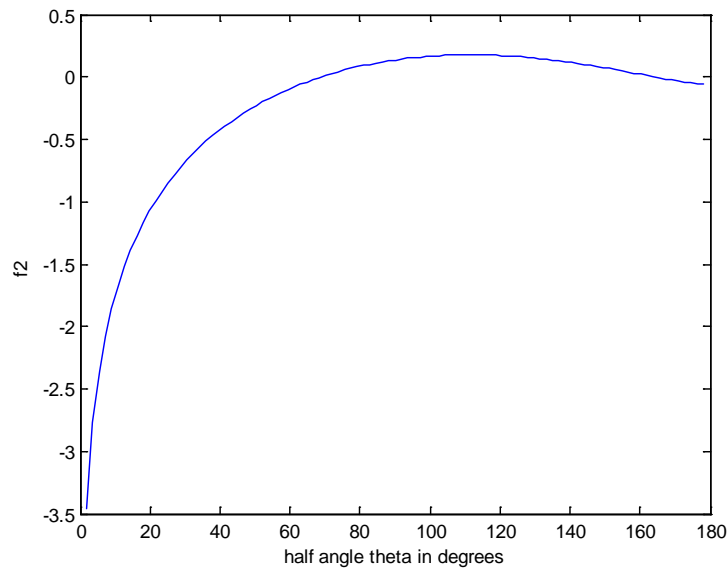


Fig. 5-21 Variation of f_2 as the function of half-angle θ

As Fig. 5-11 shown, the diameter of the droplet will reduce when the laser is adopted in GMAW. As other main detaching force almost keeps the same, the change should be mainly due to the existence of laser pulse. In this case, the gravitational force value difference could be considered as the estimating laser recoil pressure force. The gravitational forces in conventional GMAW and laser enhanced GMAW is shown in Fig. 12. When wire feed speed at 300 in./min, laser power intensity at 62 W/mm² and welding voltage at 30V, the value difference of gravitational force is about 1.75×10⁻⁴ N. Considering the estimating errors and other force value changes, the maximum laser recoil pressure force could be about 2.5×10⁻⁴ N.

For the further control consideration, the laser recoil pressure force estimating equation could be expressed as

$$F_{laser\ recoil\ force} = \eta \times r_d \quad (5-8)$$

where η is the laser recoil pressure force coefficient, and it is about 0.15 to 0.30 N/m.

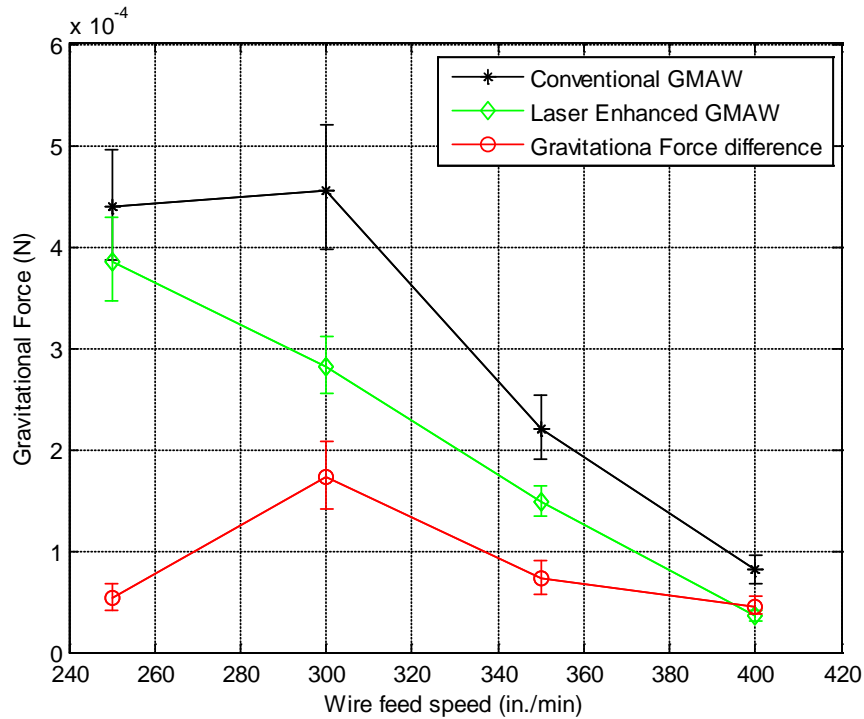


Fig. 5-22 Gravitational forces in conventional GMAW and laser enhanced GMAW

5.7 Conclusions

- (1) An experimental system has been established and a series of 64 sets of experiments have been designed and conducted to symmetrically study the Laser Enhanced GMAW;
- (2) The laser aiming at the droplet in Laser Enhanced GMAW applies an auxiliary detaching force on the droplet without a significant change in the heat current;
- (3) Free flight transfers could be successfully produced at continuous currents from 90 A to 135 A with a 0.8 mm diameter steel wire without spatters;
- (4) Laser enhanced metal transfer process is also governed by the established physics of metal transfer except for there is a need to include the additional detaching force generated by the laser;
- (5) If the metal transfer is short-circuiting transfer in conventional GMAW, Laser Enhanced GMAW may change it to drop globular transfer; if conventional and Laser Enhanced GMAW both produce drop globular, the latter reduces the diameter of the droplet; if the metal transfer is short-circuiting or drop globular transfer in conventional GMAW, Laser Enhanced GMAW may become the drop spray; the established physics of metal transfer can explain all these changes by counting the additional detach force introduced by the laser.
- (6) Laser intensity and arc voltage are major factors affecting the metal transfer in Laser Enhanced GMAW.
- (7) The enhancement of the laser increases as the laser intensity increases and the droplet size could be effectively controlled by changing the laser intensity in an appropriate range.
- (8) An increased arc voltage increases the current and can affect the metal transfer through an increased electromagnetic force.
- (9) An increased arc voltage also increases the arc gap and possible time interval for the droplet to develop to reduce the chances for short-circuiting transfer or repelled drop globular transfer.
- (10) Droplets can be detached at a given/desired diameter in a reasonable range by applying an appropriate laser intensity under a given current (arc variable) in a

reasonable range and the needed laser intensity is determined by the desired droplet diameter and the used welding current (arc variable).

- (11) The dynamic balance force theory could be used to explain the detaching phenomenon in laser enhanced GMAW. The gravitational force difference due to the mass change when laser was adopted could be used to estimate the laser recoil pressure force, and the result had a reasonable accuracy.

Copyright © Yi Huang 2011

CHAPTER 6 PULSED LASER ENHANCED

GMAW

In laser enhanced GMAW developed in the former Chapters, a constant low power laser was applied onto the molten droplet. To better utilize the energy and force from laser, pulsed laser will be used. Wire melting in laser enhanced GMAW is important for the future control of the droplet size at given arc variables.

6.1 Laser Enhanced GMAW with Pulsed Laser Power

Adding a lower power laser could change the metal transfer mode in laser enhanced GMAW. In this case, spatters could be reduced or eliminated, and it will reduce the clean-up cost after welding and save much metal. In the experimental results aforementioned, a continuous laser was used to prove this proposal. Actually a continuous power laser was not necessary in the Laser Enhanced GMAW. From the former analysis, the laser was only used to generate the recoil pressure as an additional detaching force which was actually not needed before the detaching instant. To this end, the laser radiation could be activated onto the droplet only at the moment when the droplet grew to the desired size. The continuous laser will be replaced with a pulsed laser. Further smaller laser power energy will be adopted in laser enhanced GMAW.

Fig.6-1 shows the experimental results with welding voltage 30 V and wire feed speed 350 inches per minute. Different from the results shown in Ref. 2, the laser power was not continuous, but pulsed instead. The frequency was 16 Hz with duty cycle 30%, and the peak laser power intensity was set as 62 W/mm^2 with base intensity was 0. In this case, when the droplet did not grow to the desired size, not laser was projected onto the droplet. The wire melts mainly due to resistance heat and arc heat. Because the detaching

force, mainly electromagnetic force and gravitational force, could not balance the retaining force, surface tension, the droplet would not detach. When it grew to desired size, the laser pulse was introduced to generate an additional detaching force exerting onto the droplet to compensate the lack of detaching force. The droplet would be detached to realize a free flight transfer instead of short-circuiting transfer. No spatters were generated in this process. Less electric energy was used, and it also reduced the clean-up cost after welding. All these properties of laser enhanced GMAW made it a sustainable future industrial process.

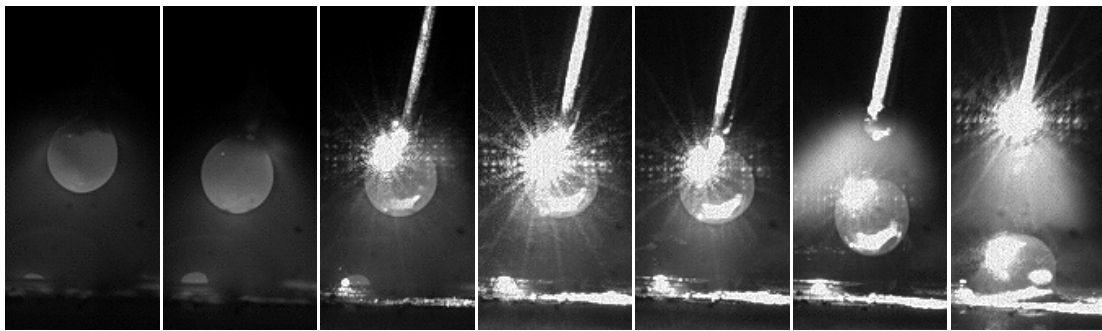


Fig. 6-1 Typical metal transfer in pulsed laser enhanced GMAW

Pulsed laser was adopted in laser enhanced GMAW, and the welding current waveform was almost the as the one with continuous laser, shown in Fig. 6-2. It also indicated that the laser did not influence the welding current, but generated an additional detaching force.

6.2 Laser Enhanced GMAW with Pulsed Laser Power and Welding Current

When pulsed laser was adopted in the proposed novel laser enhanced GMAW, less laser power was used. However, as the laser power pulse was not well controlled, the laser may be not exerted on the suitable instant when the desired droplet was obtained. As CV welding power source was adopted in this research, the fluctuation of welding current was expected to occur. In this case, the time to grow a droplet was not consistent. The

laser pulse duration may be a little long or short. To solve this problem, laser enhanced GMAW with pulsed welding current and pulsed laser power will be proposed.

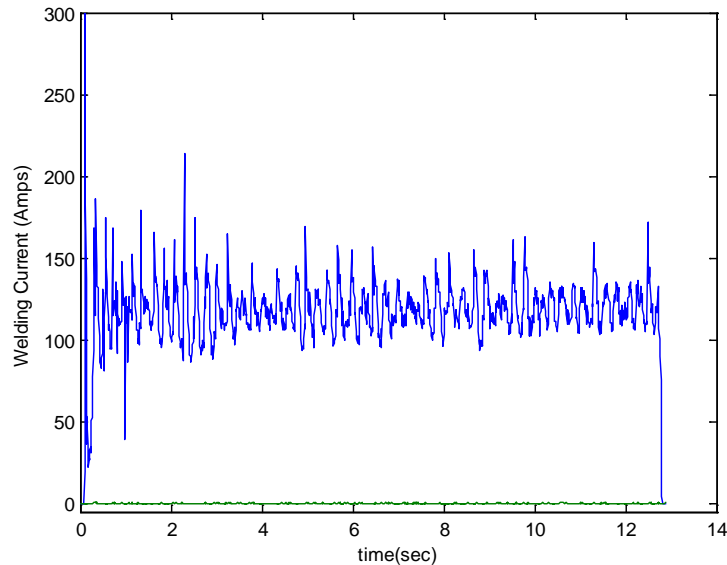


Fig. 6-2 Welding current waveform in pulsed laser enhanced GMAW.

A Constant Current (CC) was adopted in this experiment. The welding current could be controlled by the remote control of the welder power. The PC controller will send a pulsed welding current to the welder power, and the welder power will exert a pulsed welding current to the work-piece. The laser pulse should be combined to the pulsed welding system, and the two pulses should be active at the same time to ensure maximum detaching effect on the droplet. Fig. 6-3 shows the welding current waveform and the laser power intensity waveform. As can be seen, the two pulses were exerted simultaneously. In this experiment, the base welding current was 118A, and the peak current was 135A which was below the transition one. The selection of base current was based on the experiment result shown in Fig. 5-1. The fluctuation of welding voltage was not large, and the mean welding voltage was about 30V. The relative welding voltage will ensure the stable of arc length.

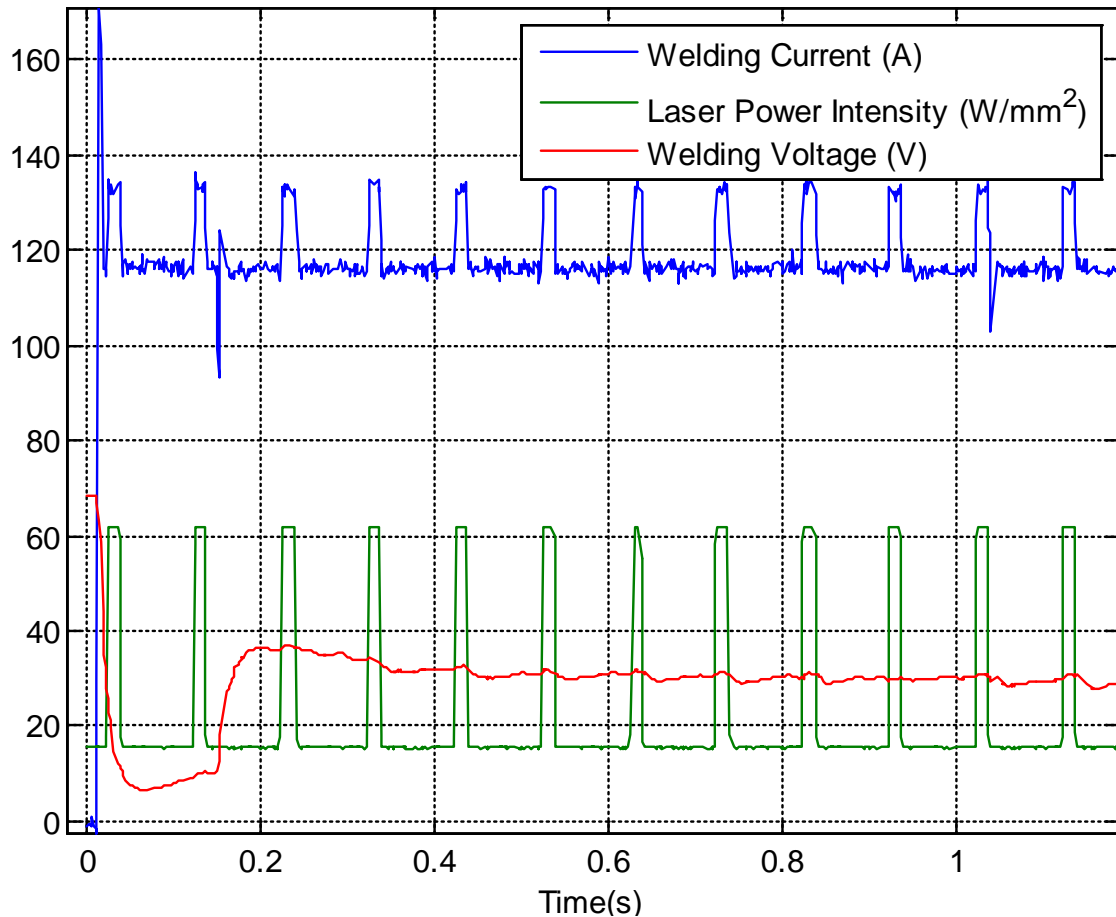


Fig. 6-3 Welding current waveform and laser power intensity waveform in pulsed laser enhanced GMAW

Although the pulsed welding current is adopted here, this process is still different from the pulsed GMAW. In traditional pulsed GMAW, the peak welding current will be higher than the transition one. The base current is used to keep the arc, while the peak current is used to melt welding wire and detach the droplet. In pulsed laser enhanced GMAW, the base current is used to melt the welding wire, while the peak current is used to detaching the droplet. As the electromagnetic force increases quadratically with the increase of welding current, a slight increase of welding current will cause the increase electromagnetic force. Combined with laser recoil pressure force, the droplet detachment will be controlled at an ideal level.

6.3 Conclusions

Pulsed laser enhanced GMAW was developed. As pulsed laser power was used, it would save much energy and the droplet detachment will be not affected. The laser pulse and welding current pulse were activated simultaneously which will ensure the detaching of droplet.

Copyright © Yi Huang 2011

CHAPTER 7 CONTROLLED DROPLET TRANSFER AND FULL PENETRATION USING LASER ENHANCED GMAW

Laser enhanced GMAW has been well developed and the metal transfer phenomenon was explained based on the established fundamentals. As the metal transfer is controlled by the laser recoil pressure force, the formation of welds will be improved. As the heat input to the work-piece is reduced, full penetration of thin plate could be obtained.

7.1 Controlled Droplet Transfer in Laser Enhanced GMAW

The metal transfer type was changed when laser was introduced to GMAW. The formation of welds was also improved. The trajectory of droplet is controlled by the laser beam so that the improved formation of welds broadens the range of application of laser enhanced GMAW.

7.1.1 Surface Quality

Surface quality is an important aspect to test the reliability of the laser enhanced GMAW. Three aspects of the surface quality of the welds will be evaluated, and they are the smoothness of the welds, spatters, and the uniformity of the weld along the welding direction. The experimental results are shown in Fig. 7-1, Fig. 7-2, Fig. 7-3 and Fig. 7-4. As 1 inch (25.4 mm) width work-piece was adopted in this research, and no accurate work plane equipment was used, some welds may not be in the middle of the work-piece. To the experiment with 250 inches per minute, shown in Fig. 7-1, if no laser in the GMAW, many spatters will be generated, and no weld will be exactly along the welding

direction. Ripple weld is the main appearance of the result. In laser Enhanced GMAW, when voltage is low, although metal transfer mode is still short-circuiting, the amount of spatters decreases, and all the welds will be along the welding direction. Ripple welds still exist, but they are smoother than the one without laser.



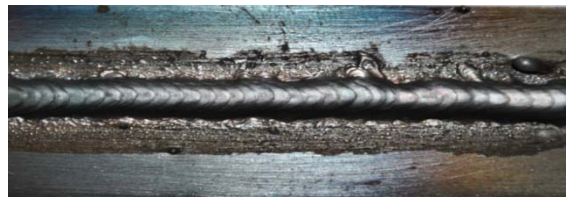
(a) 26V, 0 W



(b) 26V, 862 W



(c) 28V, 0 W



(d) 28V, 862 W



(e) 30V, 0 W



(f) 30V, 862 W



(g) 32V, 0 W



(h) 32V, 754 W

Fig. 7-1 Surface appearance of the weld beads with 250 in./min under different voltages and different laser power levels

Increasing wire feed speed to 300 or 350 inches per minute, as shown in Fig. 7-2 and Fig. 7-3, in conventional GMAW, welds are almost along the welding direction. Spatters are still severe, and no smooth welds could be acquired. Some welds seem not along the welding direction. As welding current increases (increasing voltage or wire feed speed), ripple will gradually disappear, but still there. In laser enhanced GMAW with lower welding voltage, welder is smoother than the one before. Spatters will be lessened due to the laser recoil pressure. When the metal mode is changed to projected drop globular, welds will be much smoother, as shown Fig. 7-2 (f), (h), (i) and Fig. 7-3 (f) (h). The Fig. 7-3 (i) shows the welds with spray metal transfer, and obviously it is the best welds which could be obtained used the same wire feed speed. No spatter will be generated, and ripple is almost disappearing.

If the wire feed speed is 400 inches per minute, as shown in Fig. 7-4, all the welds will be along the welding direction as higher electromagnetic force will be generated. In laser GMAW, spray transfer will be obtained when voltage is higher than 28 V. Compared to the welds results from conventional GMAW, weld beads will be smooth and straight. The appearance looks like the welds which are acquired with welding current more than transition current, and that is 150 A. In this case, good welds could be acquired at low welding current, and at the same time droplet size could be controlled by adjusting laser power and voltage.

7.1.2 Controlled Drop Globular Transfer

In Laser Enhanced GMAW experiments conducted in this study, drop globular is a major metal transfer mode. The authors found the drop globular transfer with an enhancement from a laser behaves differently from those without a laser enhancement in conventional GMAW.



(a) 26V, 0 W



(b) 26V, 862 W



(c) 28V, 0 W



(d) 28V, 862 W



(e) 30V, 0 W



(f) 30V, 754 W



(g) 32V, 0 W



(h) 32V, 754 W



(i) 32V, 862 W

Fig. 7-2 Surface appearance of the weld beads with 300 in./min under different voltages and different laser power levels



(a) 26V, 0 W



(b) 26V, 862 W



(c) 28V, 0 W



(d) 28V, 862 W



(e) 30V, 0 W



(f) 30V, 754 W



(g) 32V, 0 W



(h) 32V, 645 W



(i) 32V, 862 W

Fig. 7-3 Surface appearance of the weld beads with 350 in./min under different voltages and different laser power levels



(a) 26V, 0 W



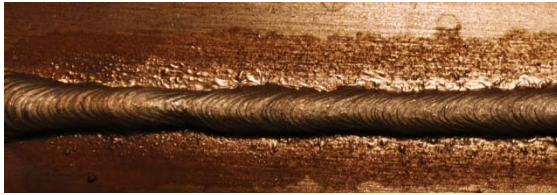
(b) 26V, 862 W



(c) 28V, 0 W



(d) 28V, 862 W



(e) 30V, 0 W



(f) 30V, 754 W



(g) 32V, 0 W



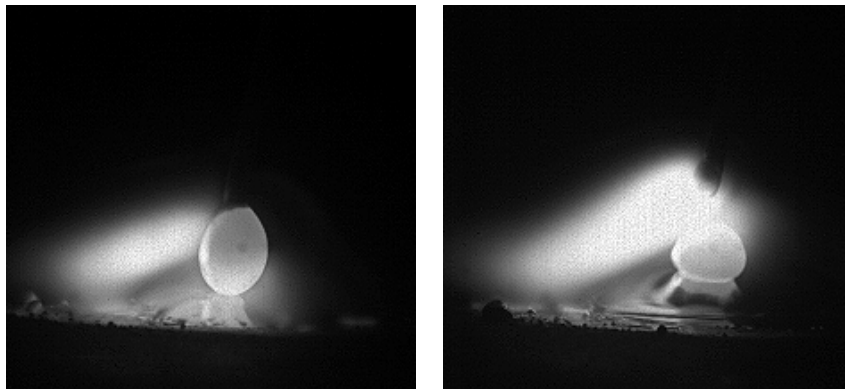
(h) 32V, 645 W



(i) 32V, 862 W

Fig. 7-4 Surface appearance of the weld beads with 400 in./min under different voltages and different laser power levels

Fig. 7-5 shows two images in a cycle of drop globular transfer in conventional GMAW under (400 in./min, 30 V, 0). Fig. 7-5 (a) is the image of the droplet shortly before its detachment. It is found that the center of the sphere of the droplet is not exactly along the axis of the wire. In fact, as long as the droplet is not detached, the center of the sphere oscillates, as shown in Fig. 5-7 (a). The trajectory of the detached droplet is thus not fixed; it may not be along the axis of the wire and change from cycle to cycle. As a result, the transverse location where the detached droplet merges with the weld pool is not fixed and may change from cycle to cycle. The images in Fig. 7-5 (a) and (b) demonstrate this uncontrollability of the droplet merging location associated with a droplet globular transfer in conventional GMAW. This type of drop globular is referred to as uncontrolled drop globular transfer in this study.



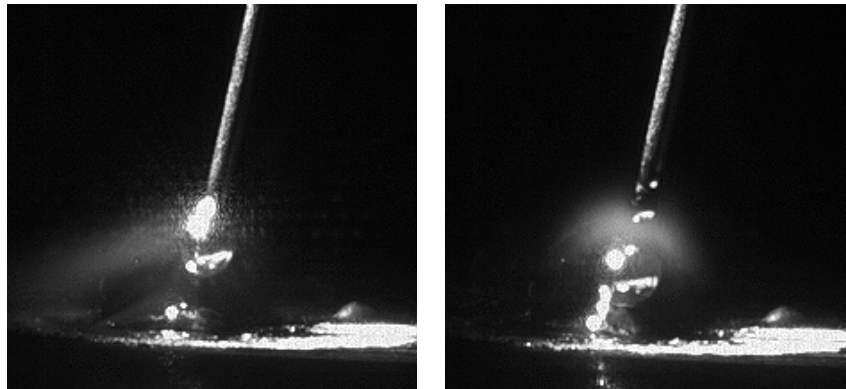
(a) Before detachment

(b) Merging to welding pool

Fig. 7-5 Images of Uncontrolled drop globular process

Fig. 7-6 are counterpart images, of those in Fig. 7-5, under (400 in./min, 30 V, 62 W/mm²). They show the droplet shortly before its detachment and merging into the weld pool in drop globular transfer with a laser enhancement. It is apparent that this laser enhanced drop globular transfer differs from its counterpart in conventional GMAW: its center of the droplet sphere is approximately along the axis of the wire. There is indeed a slight deviation of this center from the axis but observation and analysis of images in different cycles shows (1) its magnitude and direction are both consistent in different cycles; (2) this slight consistent deviation is away from the direction of laser application.

It is apparent that this deviation is caused by the laser recoil pressure. Because the droplet is approximately along the axis and the slight deviation is consistent in magnitude and direction, the transverse location of the merging is also consistent, slightly away from the axis of the wire. As can be seen, the application of the laser brings certain controls to the drop globular transfer and the resultant drop globular becomes a controlled drop globular.



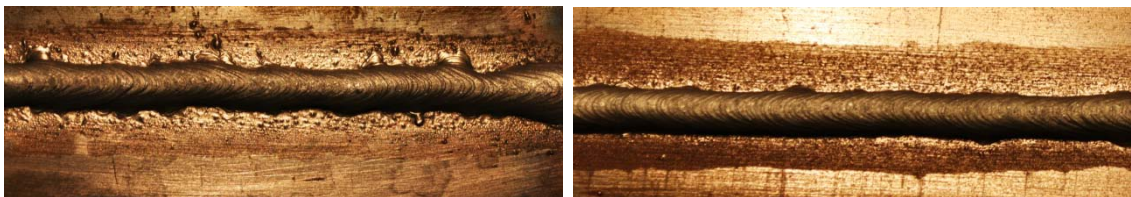
(a) Before detachment (b) Merging to weld pool

Fig. 7-6 Images of controlled drop globular process

Drop globular is seldom used in industry [1-3] and its unfixed droplet trajectory in a natural/uncontrolled form may have been the major reason. However, there is a lack of effective solutions in literature. In Laser Enhanced GMAW, the trajectory of the droplet is controlled by the laser recoil pressure and the merging of the droplet in drop globular transfer becomes controllable. It is the laser that made the drop globular become controllable in this study. Laser enhanced drop globular transfer is a controlled drop globular but it is possible that a controlled drop globular may also be achieved using other means.

Compared to uncontrolled drop globular process, a controlled drop globular process produces welds more consistently because of the controlled/consistent droplet trajectory and transverse merging location. As can be seen in Fig. 7-7(a), a typical weld produced by uncontrolled drop globular lacks control on the transverse direction. Spatters are also found because some droplets may merge into the weld pool at edges [1]. Rough weld

surfaces are also found because of the unfixed positions where large droplets merge into the weld pool. In Laser Enhanced GMAW, all issues, weld direction inconsistency, spatters and rough weld surfaces, are resolved by the controlled/consistent droplet trajectory, controlled/consistent/appropriate merging location and reduced droplet size, as shown in Fig. 7-7(b). Quality welds may thus be produced by the Laser Enhanced GMAW at a controlled drop globular transfer and drop globular thus may become a valid process for applications where the current requires desired waveforms or need to be below the transition current.



(a) Without laser

(b) Laser intensity of 62 W/mm^2

Fig. 7-7 Typical surface appearance in comparative experiments with and without laser under (400 in./min, 30 V, 0) and (400 in./min, 30 V, 62 W/mm^2)

As observed in Fig 7-7 (b), the metal shading surface, associated with heat affect zone, was asymmetric in the Laser Enhanced GMAW. This was apparently caused by the part of the laser that was not blocked by the wire and droplet.

7.2 Full Penetration

Full penetration is an important requirement in welding applications, such as butt joints, groove joint welding. For the weld joints in closed containers, such as boiler, aerospace, incomplete penetration may lead to cracks and rupture. Achieving full penetration is always a focus in welding research and applications. When GMAW is used, it is much difficult to obtain full penetration. There are many physical mechanisms unknown so that it is very difficult to control the full penetration using GMAW. Many works have been done to reach this goal, but not an effective method is found [86-90].

To obtain full penetration without padding at the back is much more difficult as the formation of the back seam is mainly determined by the gravitational force and surface tension. The thermal field is also very important but difficult to control in real time. The formation welds, both the front and back, and the welding angle are the basic standards to test the achievement of full penetration. Fig. 7-8 shows the qualified and unqualified full penetration bead with grooves. In this research, thin plate without groove is the objective to achieve full penetration.

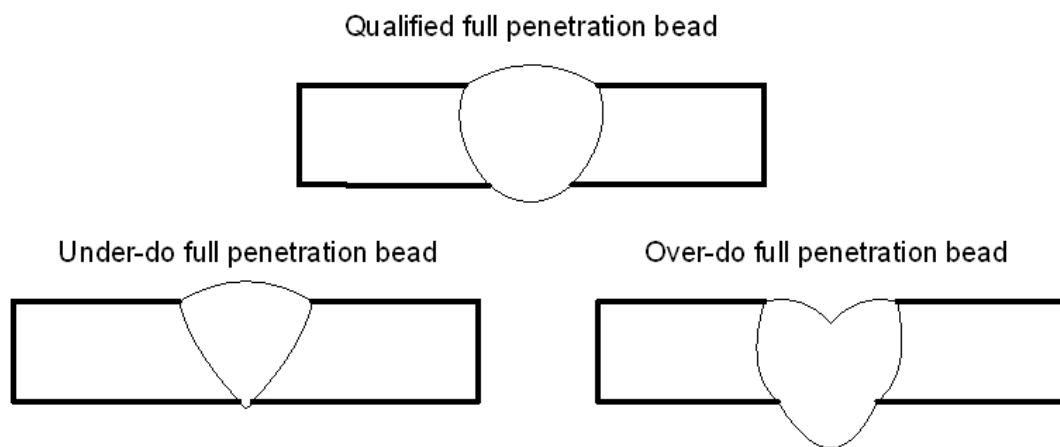


Fig. 7-8 Different full penetration levels

For the thin plate, if the welding current is relative high, such as higher than the transition current, burn-through will occur. When lower welding current is adopted, short-circuiting is expected to occur. There are many spatters generated in this process, and in this case good formation of weld bead can sometimes not been obtained.

Laser enhanced GMAW is an effective way to achieve the free flight metal transfer with welding current under transition one as aforementioned. Good formation of welds could also be obtained. Laser enhanced GMAW will be an effective welding method to achieve full penetration on thin plate without back padding and groove. To clearly illustrate the achievement of full penetration, the bead-on-plate welds will be introduced first, and then butt joint.

7.2.1 Bead on Plate Welds

A CC (constant current) continuous waveform power supply was used to conduct these experiments. Pure argon was used as the shield gas and the flow rate was 12L/min (25.4 ft³/h). The work-piece was mild steel and experiments were done as bead-on-plate at a varied travel speed. The thickness of weld plate is 1/8 inch (3.2mm). The wire used was ER70S-6 of 0.8 mm (0.03 inch) diameter. The distance from the contact tube to the work piece was 20 mm as aforementioned.

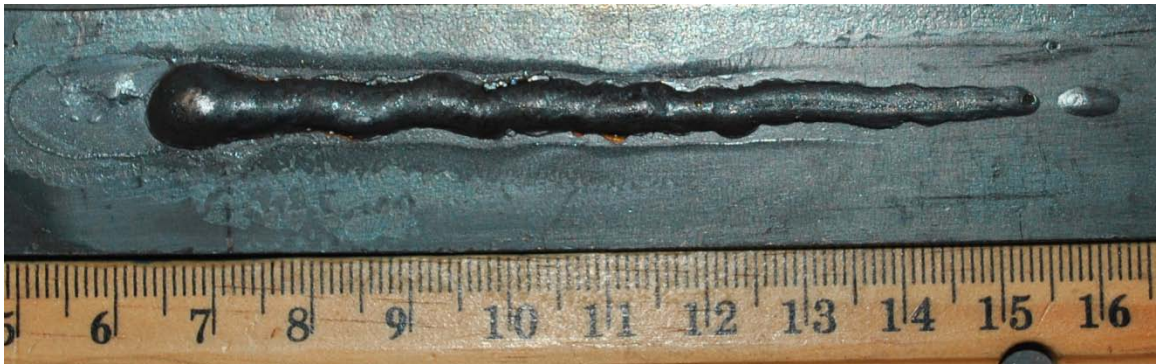
The welding current was set at four levels: 125, 130, and 135 A. The wire feed speed was selected as 400 inches per minute. In all experiments, welding currents were not more than 135 A which will generate short-circuiting or repelled globular transfer or non-wire-axis drop globular in the conventional GMAW. The laser beam was continuously applied along the wire (solid and droplet) at laser intensities 62 W/mm². The travel speed was from 4.0 to 4.5 mm/s.

Travel speed is one of the most important parameters to obtain full penetration. It will influence the heat input to the work-piece. If the travel speed is fast, partial penetration will be obtained. Meanwhile when the travel is slow, over-do penetration will be achieved due to the excessive heat input. Burn through is also expected to occur if the travel speed is further reduced.

When the travel speed is at 4.0 mm/s, shown in Fig. 7-9, too much heat input will be taken to the work-piece. The back metal is too much, and the height of the welds is a little too high. It also influences the formation of front seam as the total molten metal from welding wire is a constant. Increasing travel speed to 4.1 mm/s shown in Fig. 7-10, the tendency to obtain too high back seam is reduced. As the heat input is lower than the one with travel speed at 4.0 mm/s, the good formation of full penetration could be obtained occasionally.



(a) Front image



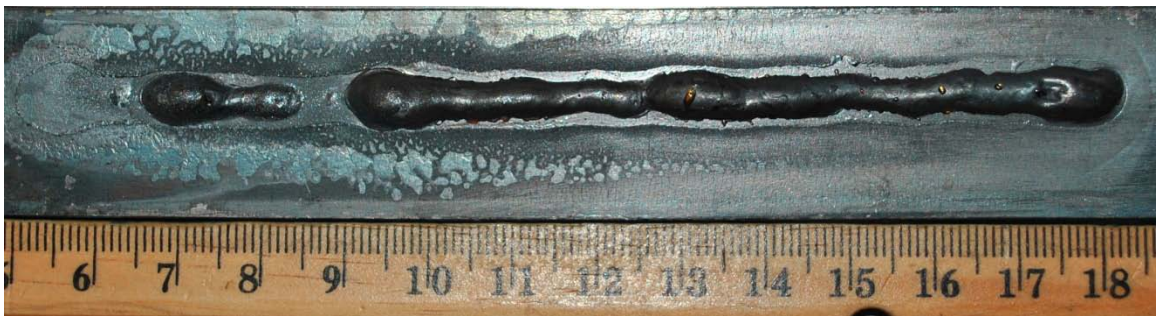
(b) Back image

Fig. 7-9 Full penetration with travel speed at 4.0 mm/s and welding current 125A: a) front image, b) back image

When the travel speed increases to 4.2mm/s, as shown in Fig. 7-11, both the front and back of welds will have good formation. The penetrated metal is moderate although there is some place with excessive metal occasionally. As the travel speed increases, the heat input is further reduced, but not too much, it will benefits to control the flow of molten metal.



(a) Front image



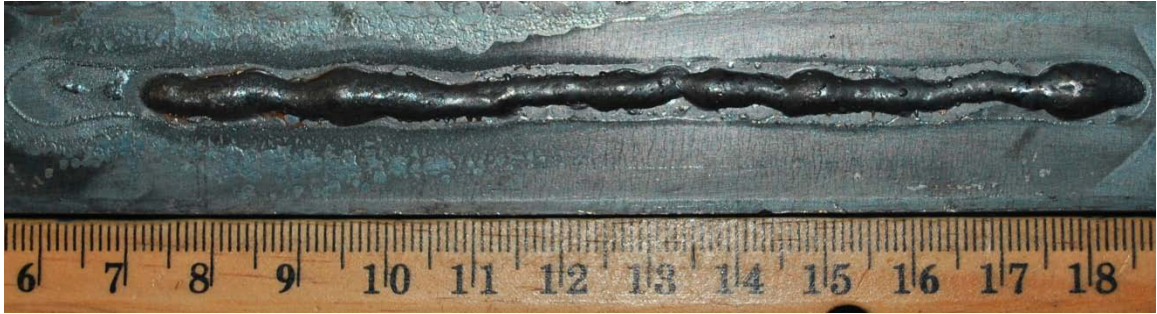
(b) Back image

Fig. 7-10 Full penetration with travel speed at 4.1 mm/s and welding current 125A: a) front image, b) back image



(a) Front image

Fig. 7-11 Full penetration with travel speed at 4.2 mm/s and welding current 125A: a) front image, b) back image



(b) Back image

Fig. 7-11 Full penetration with travel speed at 4.2 mm/s and welding current 125A
(Continued)

If the travel speed further increases, such as to 4.3mm/s and 4.4mm/s as shown in Fig. 7-12 and Fig. 7-13, as the heat input is further reduced, the back seam is not continuous. However, the good formation of front seams is still achieved. It depends on the characteristics of laser enhanced GMAW.



(a) Front image



(b) Back image

Fig. 7-12 Full penetration with travel speed at 4.3 mm/s and welding current 125A: a) front image, b) back image



(a) Front image



(b) Back image

Fig. 7-13 Full penetration with travel speed at 4.4 mm/s and welding current 125A: a) front image, b) back image

There is no spatter in all these experiment results as the free flight metal transfer is obtained. To be mentioned, the back seam is still not consistent when the travel speed is moderate. There are many reasons to cause this phenomenon, such as electric network fluctuation. To obtain a stable and consistent back welds, a closed-loop control system should be built.

Welding current determines the heat input directly to the work-piece. As the mean welding current is lower than the transition one, the variation of welding current is small. Fig. 7-14, Fig. 7-15, and Fig. 7-16 show the front and back image of welding seams with welding current at 130A. As shown in Fig. 7-14, if the travel is still 4.2mm/s, a little excessive molten metal is expected to be cumulated at the back of welds. Increasing travel speed could reduce this tendency, but also reduces the consistency of welds.



(a) Front image



(b) Back image

Fig. 7-14 Full penetration with travel speed at 4.2 mm/s and welding current 130A: a) front image, b) back image



(a) Front image

Fig. 7-15 Full penetration with travel speed at 4.35 mm/s and welding current 130A: a) front image, b) back image



(b) Back image

Fig. 7-15 Full penetration with travel speed at 4.35 mm/s and welding current 130A
(Continued)



(a) Front image



(b) Back image

Fig. 7-16 Full penetration with travel speed at 4.5 mm/s and welding current 130A: a)
front image, b) back image

When the welding current is 135A, the heat input from welding power supply is much higher. Over-do full penetration will be much easier to be obtained, as shown in Fig. 7-17 and Fig. 7-18. A little higher travel speed may lead to an acceptable penetration welds (Fig. 7-19). To achieve a moderate full penetration welding seam, the travel speed and mean welding current should be controlled at a reasonable level.



(a) Front image



(b) Back image

Fig. 7-17 Full penetration with travel speed at 4.2 mm/s and welding current 135A: a) front image, b) back image

7.2.2 Butt Joint

To obtain a further usability of laser enhanced GMAW on full penetration, a butt joint welds was conducted. As there is a seam between the two plates, the heat input to achieve full penetration will be reduced. The wire feed speed is reduced to 350 inch/min. The

other parameters were set as the ones with bead on plate welds. Welding current was set as 125A.



(a) Front image



(b) Back image

Fig. 7-18 Full penetration with travel speed at 4.35 mm/s and welding current 135A: a) front image, b) back image



(a) Front image

Fig. 7-19 Full penetration with travel speed at 4.45 mm/s and welding current 135A: a) front image, b) back image



(b) Back image

Fig. 7-19 Full penetration with travel speed at 4.45 mm/s and welding current 135A
(Continued)

Fig. 7-20, Fig. 7-21 and Fig. 7-22 show the front and back image of butt joint full penetration results. It was found that the penetrated metal increased as the travel speed reduced. To achieve the same penetration result, the travel speed is a little slower than the one with bead on plate. No spatters are generated in these processes which will reduce the clean-up cost after welding.



(a) Front image



(b) Back image

Fig. 7-20 Full penetration with travel speed at 4.05 mm/s and welding current 125A: a) front image, b) back image



(a) Front image



(b) Back image

Fig. 7-21 Full penetration with travel speed at 4.15 mm/s and welding current 125A: a) front image, b) back image



(a) Front image



(b) Back image

Fig. 7-22 Full penetration with travel speed at 4.27 mm/s and welding current 125A: a) front image, b) back image

It should be mentioned that in the industrial application of full penetration on butt joint, swinging torch is always used. Seam tracking technology is also adopted. In this case, the welding seam will be just along the joining line of the two plates. As a preliminary research in this dissertation, these methods are not adopted.

From the results shown above, it was found that full penetration was sensitive to the welding current and travel speed. It was determined by the heat input to the work-piece. To achieve a stable and consistent full penetrated welding seam, much work should be done. It is a research focus in the welding field.

7.3 Conclusions

- (1) Good formation of welds could be obtained in laser enhanced GMAW, and no spatters were generated.
- (2) Controlled drop globular transfer in Laser Enhanced GMAW offers desirable metal transfer characteristics that benefit formation of quality welds.
- (3) Controlled drop globular transfer extends the capability of the productive GMAW process into the range of constant current that conventionally produces undesirable drop transfer that is not most suitable for practical use.
- (4) Laser enhancement provides an effective method to achieve a controlled drop globular and to empower the GMAW to use a constant current in a much increased range to meet the requirements from different applications.
- (5) Full penetration could be obtained both bead on plate and butt joint welding, and the results were sensitive to the mean welding current and travel speed.

CHAPTER 8 NONLINEAR CONTROL

MODELING OF DYNAMIC METAL

TRANSFER IN LASER ENHANCED GMAW

In laser enhanced GMAW, free flight metal transfer could be obtained. To achieve a much more stable welding process, the metal transfer process should be well controlled. To this end, the control algorithm should be developed for the future closed-loop real time control.

8.1 Nonlinear Modeling of Dynamic Metal Transfer

To fully control the GMAW process, many models were proposed and developed for the GMAW process. PI control strategy could be developed for maintaining the desired heat and mass by regulating the current [91]. A steady-state model for heat and mass transferred from the electrode to the work-piece was established [92-99]. In the later research, robustness is also taken into account [94-102]. An adaptive multi-input multi-output (MIMO) scheme was developed to control both geometrical and thermal characteristics of a weld based on lumped parameter and distributed parameter modeling and identification [93-108]. However, GMAW is a complex process, and it has many parameters to be monitored and controlled. The relationship between them can not be considered linearly. The nonlinearities of GMAW should be considered when building model for this process.

The laser recoil pressure force is the main effect to change the metal transfer in laser enhanced GMAW different from the conventional GMAW. It has been estimated in the Chapter 5. The Eq. (5-8) gives an estimation of laser recoil pressure force with moderate

accuracy. By analyzing the electric system of laser enhanced GMAW and the forces acting on the droplet, a nonlinear model is developed to simulate the dynamic metal transfer process in laser enhanced GMAW.

8.1.1 Nonlinear Model Setup

Modeling of GMAW process is very important for the process control. Based on the physical fundamental analysis of GMAW process, a nonlinear model has been set up [82-85] for traditional GMAW. In laser enhanced GMAW, all the properties are the same as the ones in conventional GMAW except laser pulse which will be taken into account to the referred modified nonlinear model for the laser enhanced GMAW.

First, a numbers of inputs, outputs, and states for the model should be defined. These are given as below.

States:

$x_1 = I$, Welding current;

$x_2 = l_s$, Wire extension;

$x_3 = x_d$, Droplet displacement;

$x_4 = v_d$, Droplet velocity;

$x_5 = m_d$, Droplet mass;

Outputs:

$y_1 = I$, Welding current;

$y_2 = r_d$, Droplet radius;

Inputs:

$u_1 = U_c$, Welding voltage;

$u_2 = WFS$, Wire feed speed;

$u_3 = r_d \text{ desired}$, Desired droplet radius;

Now, laser enhanced GMAW can be described by the following nonlinear system.

$$\dot{x} = f(x) + g(x)u \quad (8-1)$$

$$y = h(x) \quad (8-2)$$

$$x = t(x), \text{ if } L(x, u) \geq 0 \quad (8-3)$$

Now let's examine the electric circuit of the GMAW, as shown in Fig. 8-1. The electric relationship of welding current with other parameters could be expressed by

$$i = \frac{U_c - R_L I - U_{arc} - R_s I}{L_s} \quad (8-4)$$

Where $U_{arc} = U_0 + R_a I + E_a(L - l_s)$ and $R_L = \rho_r(l_s + \frac{1}{2}(r_d + x))$. L is the distance from contact tube to work-piece. As discussed in the former section, it is selected as 20mm in this paper.

In this nonlinear system, the nonlinear state equations are listed below.

$$\dot{x}_1 = \frac{1}{L_s} [u_1 - (R_a + R_s)x_1 - U_0 - E_a(L - x_2) - \rho_r(x_2 + \frac{1}{2}(r_d + x_3))x_1] \quad (8-5)$$

$$\dot{x}_2 = u_2 - MR/(\pi r_w^2) \quad (8-6)$$

$$\dot{x}_3 = x_4 \quad (8-7)$$

$$\dot{x}_4 = \frac{1}{x_5} (-K_d x_3 - B_d x_4 + F_t) \quad (8-8)$$

$$\dot{x}_5 = (C_1 x_1 + C_2 \rho_r x_2 x_1^2) \rho_w \quad (8-9)$$

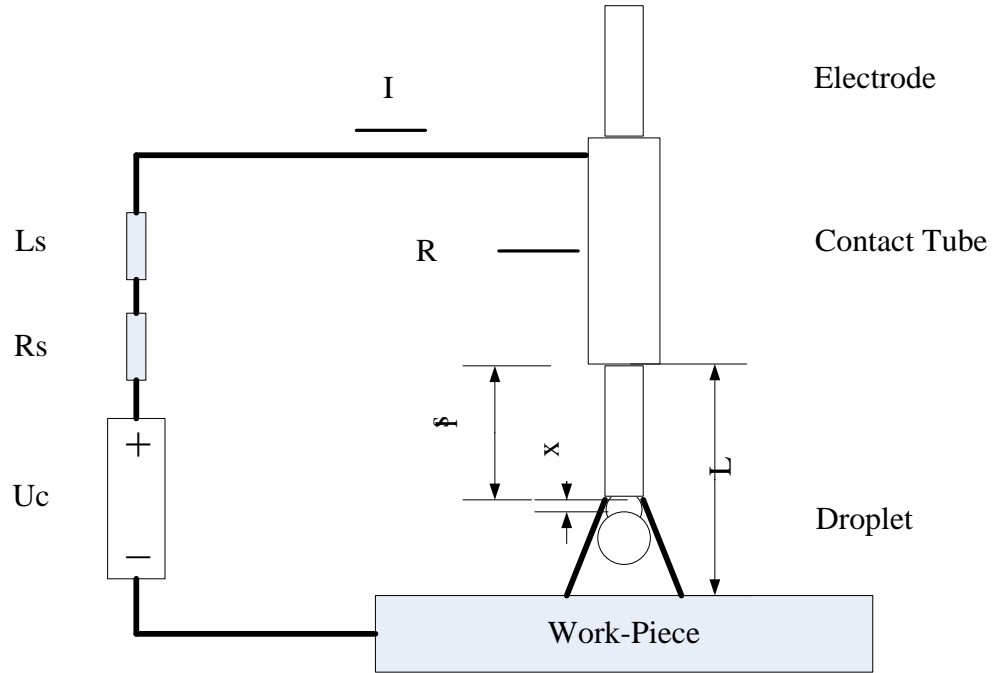


Fig. 8-1 Schematic image of GMAW process

Based on the physics fundamentals of laser enhanced GMAW, some equations used are stated below.

$$r_d = \left(\frac{3x_5}{4\pi\rho_w} \right)^{1/3} \quad (8-10)$$

$$MR = C_1x_1 + C_2\rho_r x_2x_1^2 \quad (8-11)$$

$$F_{laser\ recoil\ force} = \eta r_d \quad (8-12)$$

$$F_m = MR * \rho_w * WFS = \rho_w u_2 (C_1x_1 + C_2\rho_r x_2x_1^2) \quad (8-13)$$

$$F_g = gx_5 \quad (8-14)$$

$$F_d = \frac{1}{2} C_d \pi (r_d^2 - r_w^2) \rho_p v_p^2 \quad (8-15)$$

$$F_{em} = \frac{\mu_0 x_1^2}{4\pi} \left(\ln \frac{r_d}{r_w} + f_2 \right) \quad (8-16)$$

Combined with Eq. (4-1) and (4-7), these equations could be used to calculate the states equations.

In the laser enhanced GMAW, laser recoil pressure force plays a significant role to determine the detachment of droplet. In this case, modified dynamic force balance theory was used to decide whether the droplet is detached. The reset condition can be expressed by

$$F_t = F_g + F_d + F_m + F_{em} + F_{laser\ recoil\ force} > F_\sigma \quad (8-17)$$

If the detachment criterion fulfilled,

Then

$$x_1 = x_1 \quad (8-18)$$

$$x_2 = x_2 \quad (8-19)$$

$$x_3 = \left(\frac{3x_5}{4\pi\rho_w} \right)^{1/3} \quad (8-20)$$

$$x_4 = 0 \quad (8-21)$$

$$x_5 = \frac{x_5}{2} \left(\frac{1}{1+\exp(-100x_4)} + 1 \right) \quad (8-22)$$

Otherwise,

$$x_1 = x_1 \quad (8-23)$$

$$x_2 = x_2 \quad (8-24)$$

$$x_3 = x_3 \quad (8-25)$$

$$x_4 = x_4 \quad (8-26)$$

$$x_5 = x_5 \quad (8-27)$$

The relative constants in these equations are shown in Table 8-1 [82-85].

Table 8-1 Constants used for nonlinear model

Symbol	Value	Unit	Description
U_0	15	V	Arc Voltage Constant
L_s	2.5e-5	H	Source Inductance
B_d	0.0008	Kg/s	Drop DAing Coefficient
C_1	2.885e-10	m ³ /(A s)	Melting Rate Constant
C_2	5.22e-10	m ³ /(A Ω s)	Melting Rate Constant
E_a	636	V/m	Arc Length Coefficient
K_d	3.5	N/m	Drop Spring Constant
r_w	0.0004	m	Wire Radius
R_a	0.022	Ω	Arc Current Coefficient
R_s	0.004	Ω	Welding Wire Resistance
v_p	10	m/s	Relative fluid to drop velocity
C_d	0.44		Drag coefficient
ρ_p	1.6	Kg/m ³	Plasma density
ρ_r	0.7836	Ω/m	Resistivity of the electrode
ρ_w	7860	Kg/m ³	Electrode density
μ_0	1.25664e-6	(kg m)/(A ² s ²)	Permeability of free space
σ	1	N/m ²	Surface Tension Coefficient

8.1.2 Simulation Results

A simulation program for laser enhanced GMAW was developed in Simulink. It was based on the model described in the former Section. To validate the proposed model, the simulating results should be compared to the experimental results.

Let's recall the exAle case again. Wire feed speed u_2 will be set at 300 in./min (0.127m/s), laser power intensity at 62 W/mm² and welding voltage u_1 at 30V. To simulate the practical experiment environment, a Gaussian noise will be added to the welding voltage. The noise is with noise power at 0.00001, and the sAling time was selected at 0.0001. Other constants used in this model were listed in Table. 1.

Choose 1 second as the time interval to analyze. The continuous laser power was adopted. The welding current and wire extension were shown in Fig. 8-2 and Fig. 8-3. From Fig. 8-2, it was found that the mean welding current was about 110A. This result agreed with the result shown in Fig. 5-1 and Fig. 5-4. The wire extension was about 8mm. The arc length will be about 8mm. By carefully analyzing the images shown in Fig. 3 (b), it was found that the arc length was about 6mm, and the wire extension was about 10mm in the experiments. There are several reasons to cause this simulation error. In this nonlinear model, some conditions which restricted the laser enhanced GMAW were neglected. The welding pool height above the work-piece was also not considered.

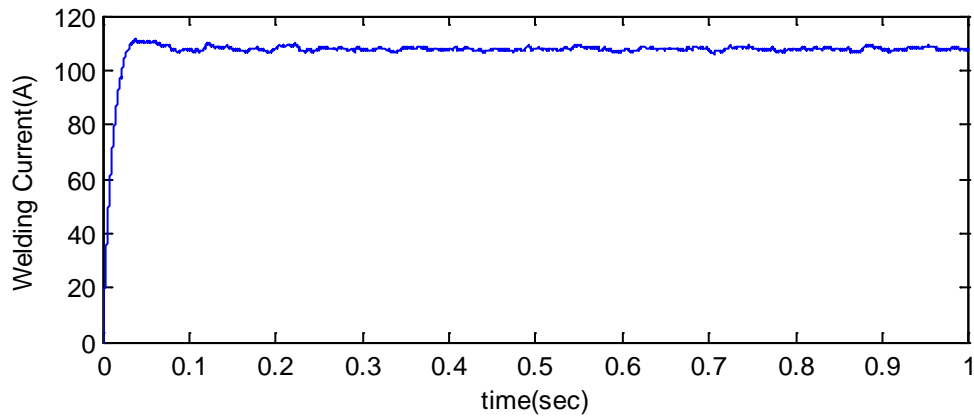


Fig. 8-2 Welding current waveform simulation result

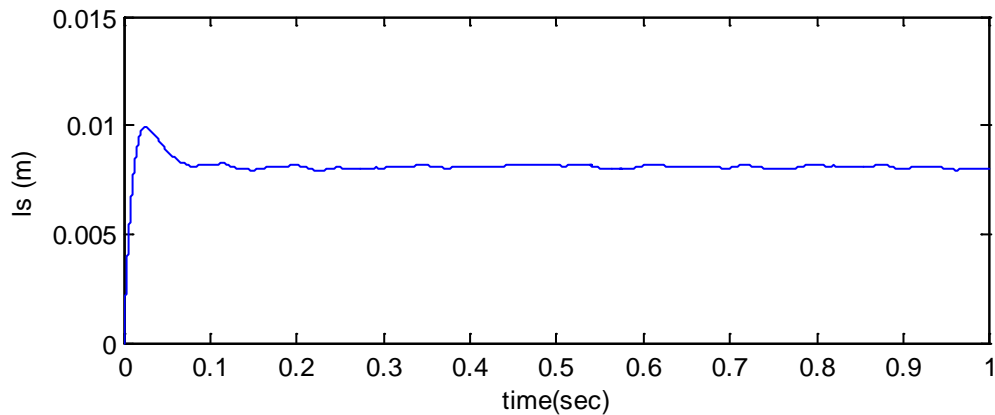


Fig. 8-3 Wire extension simulation result

The most important simulation result is the droplet mass and size. Fig. 8-4 and Fig. 8-5 show the simulating droplet radius and droplet mass. In conventional GMAW, as the welding current is lower than the transition current, droplet needs to grow to a relative large size to achieve enough gravitational force to compensate the lack of detaching force. Short-circuiting metal transfer always occurs. When laser was adopted, droplet does not need to grow to such a large size. As shown in Fig. 8-4, the radius of droplet is about 0.95mm. Although it is a little larger than the radius of welding wire, free flight transfer was obtained. The simulation result agrees with the experiments results very well.

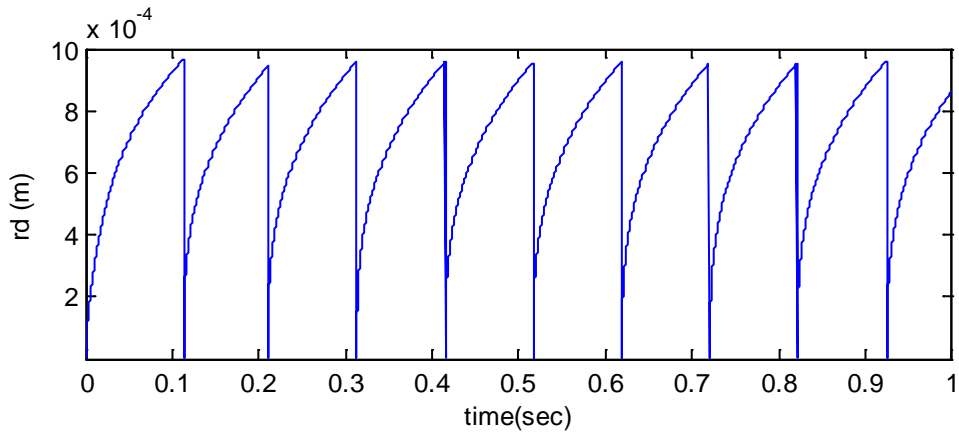


Fig. 8-4 Droplet radius simulation result

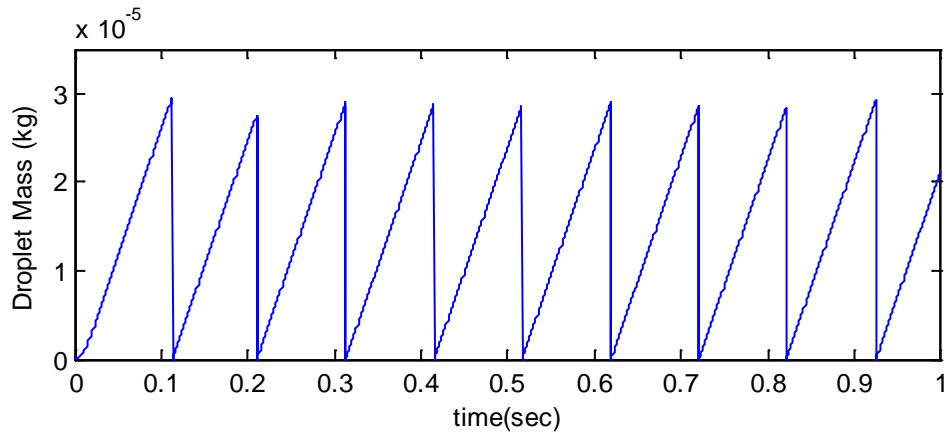


Fig. 8-5 Droplet mass simulation result

To better understand the metal transfer process, the forces acting on the droplet will be analyzed. Fig. 8-6, Fig. 8-7, Fig. 8-8, Fig. 8-9, Fig. 8-10 and Fig. 8-11 show the simulating results of detaching forces. As shown in Fig. 8-6 and Fig. 8-7, the aerodynamic drag force and momentum force acting on the droplet were very small. For the momentum force, it was almost a constant during the welding process. The electromagnetic force was still the main detaching force in the laser enhanced GMAW, and it will compensate most of surface tension. The gravitational force increases with the increase of droplet mass, and the simulating result shows that it is an important detaching force.

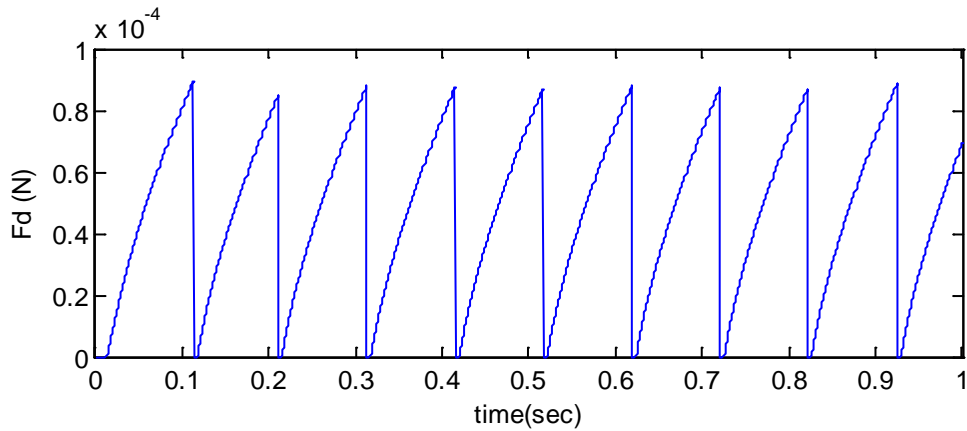


Fig. 8-6 Aerodynamic drag force simulation result

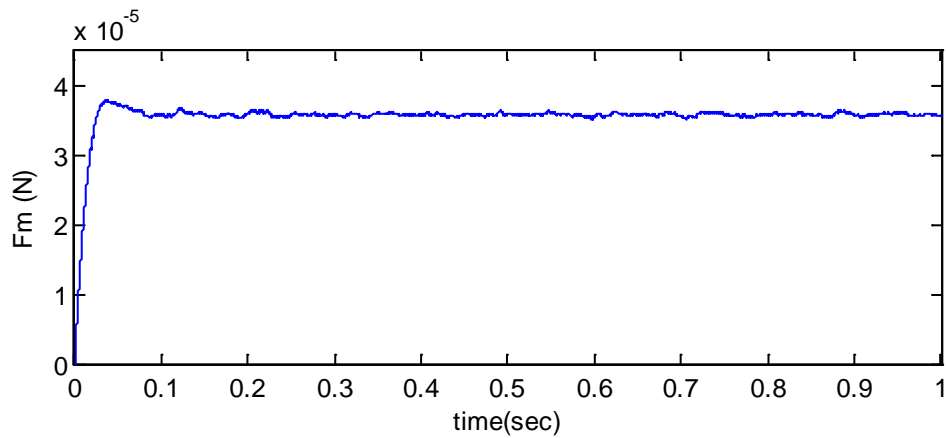


Fig. 8-7 Momentum force simulation result

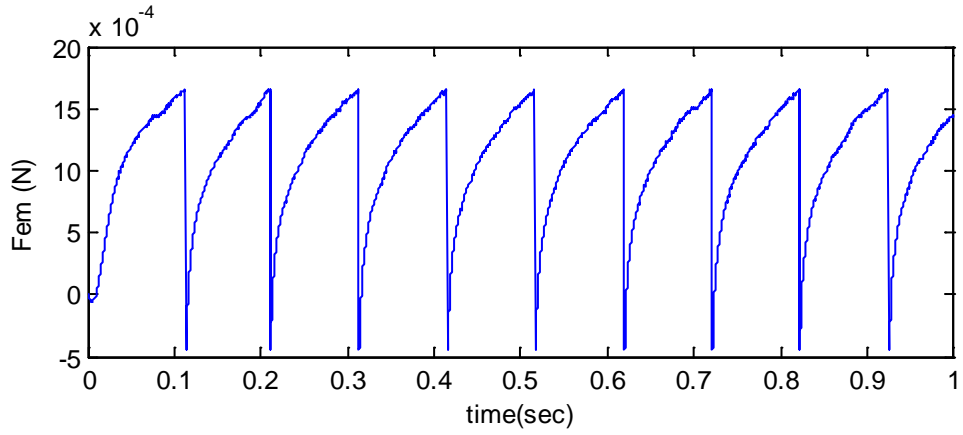


Fig. 8-8 Electromagnetic force simulation result

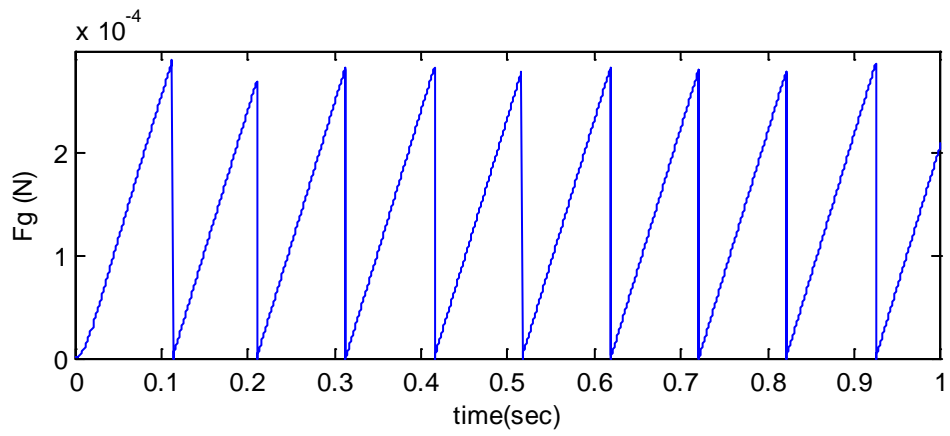


Fig. 8-9 Gravitational force simulation result

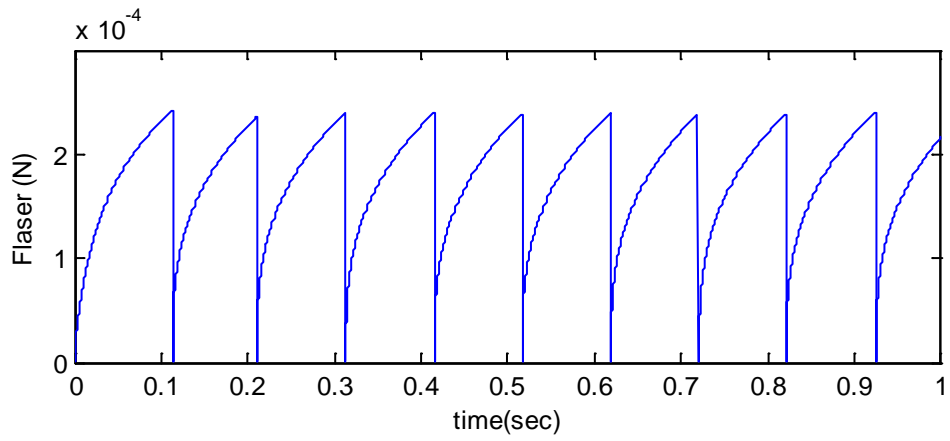


Fig. 8-10 Laser recoil pressure force simulation result

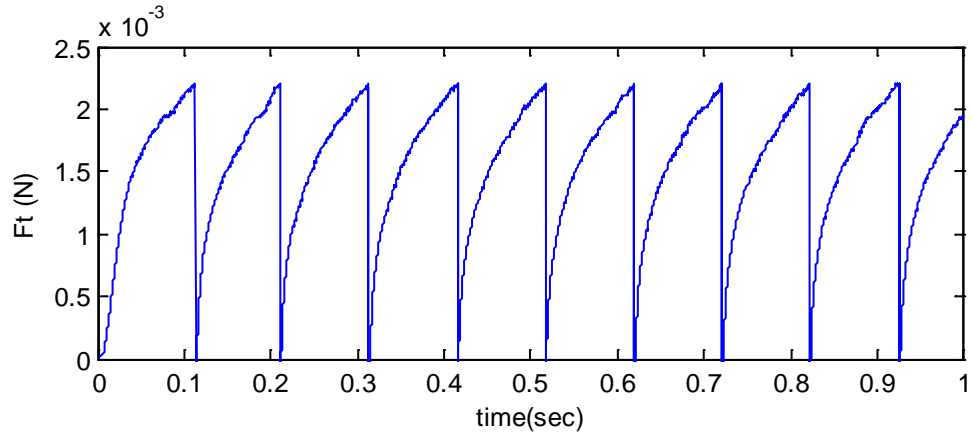


Fig. 8-11 The total detaching force simulation result

Laser recoil pressure force was an additional detaching force in laser enhanced GMAW compared to conventional GMAW. Compared the results shown in Fig. 8-9 and Fig. 8-10, it was found that the magnitude of laser recoil pressure force is closed to the gravitational force. It indicates that laser recoil pressure force was another main detaching force to determine the droplet detaching process. Fig. 8-11 shows the total detaching force.

The droplet displacement and velocity results are shown in Fig. 8-12 and Fig. 8-13.

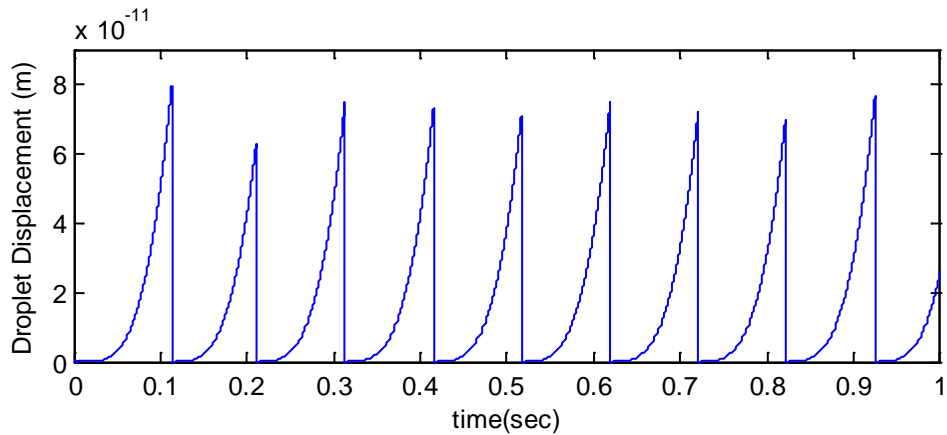


Fig. 8-12 The droplet displacement simulation result

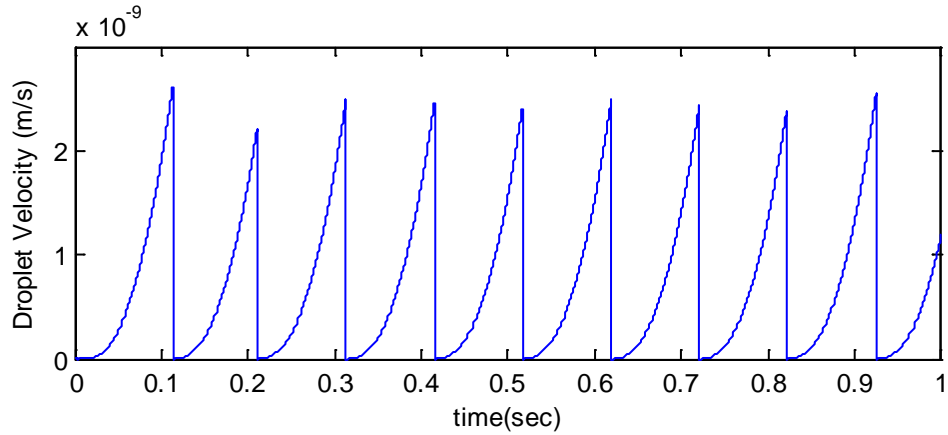


Fig. 8-13 The droplet velocity simulation result

As discussed in the former Section, to better utilize the laser power, pulsed laser will be used. In this nonlinear model, the pulsed laser recoil pressure force was controlled by the droplet radius. When the desired droplet radius was fulfilled, laser will exert an additional detaching force on the droplet. The laser recoil pressure force did not affect the welding current (Refs. 1-3), so the welding current will be kept the same with and without laser pulse. As shown in Fig. 8-14, the droplet radius was also the same as the one with constant laser shown in Fig. 8-4. Examining the wire extension (seen in Fig. 8-15 and Fig. 8-3), the same result was obtained. It indicated that the laser did not influence the wire melting, but only exerted an auxiliary detaching force onto the droplet.

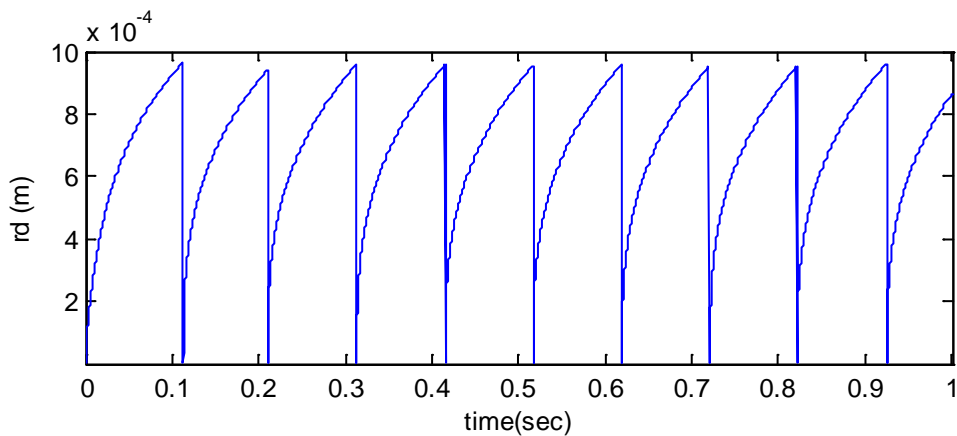


Fig. 8-14 Droplet radius simulation result with pulsed laser

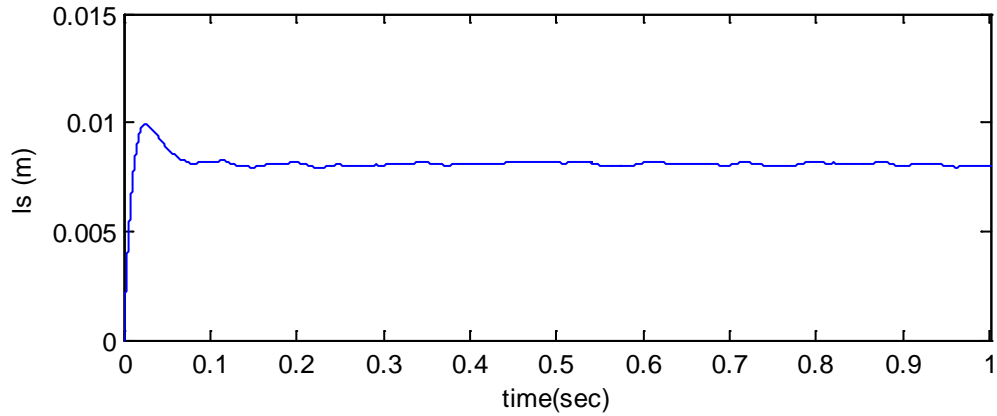


Fig. 8-15 Wire extension simulation result with pulsed laser

As the welding current and droplet radius were not changed, and all the other welding parameters were also not altered, the aerodynamic drag force, the momentum force, the electromagnetic force, and the gravitational force were not changed. Before the droplet grew to the desired size, there was not laser recoil pressure force on the droplet. When the criterion was fulfilled, the laser pulse would be exerted on the droplet. Fig. 8-16 show the laser recoil pressure force when pulsed laser was adopted in the laser enhanced GMAW. As shown in Fig. 8-17, the sudden increase in the total detaching force F_t was caused by the adding the laser recoil pressure detaching force.

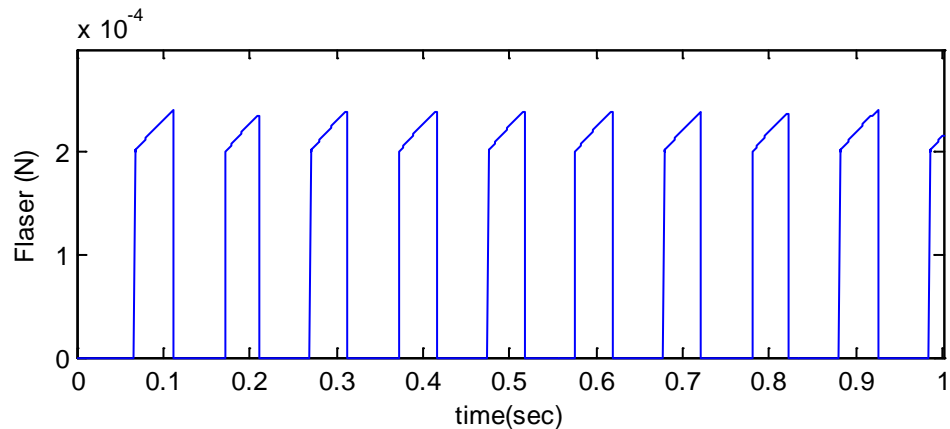


Fig. 8-16 Laser recoil pressure force simulation result with pulsed laser

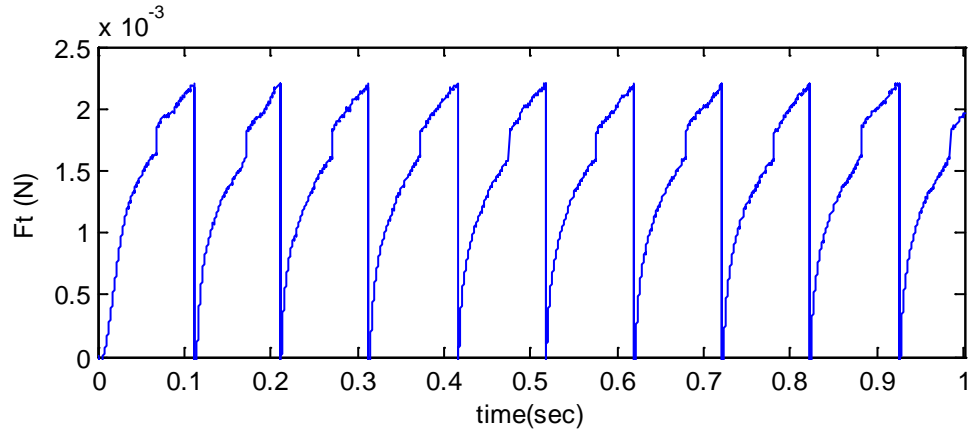


Fig. 8-17 The total detaching force simulation result with pulsed laser

From the analysis above, it is found that this nonlinear model is suitable to forecast the droplet growing process, and for the further process control. For the future closed-loop control, the input welding voltage will be replaced by the real welding voltage which will be obtained from the voltage sensor. In this case, all the states calculating will be based on the practical values. The results will be much more accurate. If this model can be combined with sensing technology, such as image processing sensing, spectrum sensing, the droplet in laser enhanced GMAW will be controlled at any desired size under any desired welding current.

8.2 Neural Network Model to Predict the Metal Transfer

In laser enhanced GMAW, the droplet size is a critical parameter that determines the process stability and produce desired appearance and quality of welds. Relatively large droplet size would lead to ripples in the welds and decrease the directionality of the welds. However, its direct measurement requires a high speed camera which may not be preferred for manufacturing applications. A soft-sensing model may thus provide an alternative to estimate the droplet size and transfer rate for the control of the laser assisted GMAW.

Soft-sensing technology has been widely used in process control and application [109-110]. Establishing a suitable model to estimate variables in a process that can't be measured or can't be measured conveniently online has become an important research subject. Methods to establish such models include mechanism modeling and regression modeling [111].

To be effective, a mechanism modeling based method requires in-depth comprehensive knowledge about the process mechanism. Such knowledge can help establish a mechanism model based on the physical relationship of the primary and auxiliary variables which may be controlled in the process. While explicit physical meaning is contained in this kind of model, the model could be complicated in most situations and has relatively large number of coefficients to be determined. In addition, this method can't be applied for processes where the process mechanism is not clear.

In industrial processes, many objects are characterized by complicated uncertainty, real-time, and high nonlinearity. Their mechanism modeling is complex and difficult. Regression models have thus been adopted by many researchers to make on-line estimation become possible [112-115]. Regression models can be established based on regression analysis of experimental data from the process. A regression model may be classified to either a linear or nonlinear model. For linear models, the least squares method [116] is widely/typically used to estimate the model coefficients/parameters. As an effective method for establishing nonlinear regression models, artificial neural network (ANN) [117] has been extensively applied due to its nonlinear mapping ability. Many process soft-sensing modeling efforts are based on ANN technology, and BP-ANN and RBF-ANN [117-119] are the most widely used ANN technologies. Although BPNN has been applied extensively, there are still some limitations, such as slow convergence speed of learning algorithm, local minimization, and over-fitting phenomenon [120]. In order to overcome these shortcomings, intelligent optimization algorithms [121-126] have been adopted to optimize the ANN. The optimization often aims to improving weights, network structure, and learning rules.

Inspired by the social behavior of animals such as bird flocking, fish schooling and swarm theory [124], particle swarm optimization (PSO) was firstly proposed as a stochastic search approach [125-126]. PSO is a kind of heuristic algorithms based on swarm intelligent, and its idea roots in artificial life and evolutionary computation theory. PSO drew much attention in decades because of the features of simple computation and rapid convergence capability, and has been applied to many scientific computation and engineering optimization problems [127-129]. As an effective training algorithm for artificial neural networks, PSO is easy to be realized, and can be used to adjust the weights of ANN conveniently [130-132]. Based on the basic PSO algorithm, improved PSO algorithms have been proposed to improve the optimization. Sub-swarms are introduced in TSCPSO algorithm to improve the global search ability of PSO, and desired results have been obtained [133-134].

In this dissertation, LS method, BPNN, PSO-BPNN and TSCPSO-BPNN models are proposed to realize real-time estimation of droplet size/diameter and transfer rate. By comparing the results from these methods, an optimal method will be chosen as the preferred estimation method for future real-time control. The experiment parameters are from the Chapter 5.

8.2.1 Least Squares Regression

In laser enhanced GMAW, as a CV mode power supply was adopted, the welding current will be mainly determined by the wire feed speed and welding voltage. Laser was only to change the droplet transfer mode, not to influence the welding parameters. As the wire extension was fixed in all these experiments, the droplet size and transfer rate will be mainly determined by the wire feed speed, welding voltage and laser power intensity. In previous discussion, the physical mechanism was preliminary discussed, but the relationship among these parameters was not clear enough to set up the real-time control algorithm. To this end, soft-sensing method was chosen as the alternative method to estimate this relationship.

Before establishing a soft-sensing model, a set of auxiliary variables need to be selected for estimating the droplet size and transfer rate after GMAW process mechanism and influential factors are analyzed. Then, the model can be obtained based on these variables. Furthermore, soft-sensing can be realized in real-time through the model based on the auxiliary variables. Fig. 8-18 shows the inputs and outputs of the Laser-enhanced GMAW process. *W.F.S* is the wire feed speed, *U* is the voltage, *L* is the laser power intensity, *DD* is the droplet diameter, and *DTR* is the droplet transfer rate. Here, the droplet diameter is used to denote the droplet size, and the value of *DTR* is the duration time of a droplet. The droplet diameter growth speed is determined by *W.F.S* and *U*, and the *L* influences the final droplet diameter when it transfers. Besides, all the three inputs correlate to *DTR*. Hence *W.F.S*, *U*, and *L* are selected as the auxiliary variables to estimate *DD* and *DTR*.

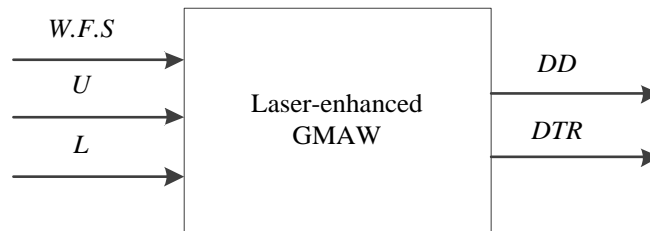


Fig. 8-18 System inputs and outputs

Table 8-2 shows auxiliary and estimation variables. In the welding process, the auxiliary variables were obtained through the monitoring system. Prior to establishing the model, the data have to be pretreated. Some wrong data need to be deleted in this step to improve the accuracy of the acquired data. More than 200 sets data were collected after experiments, and 137 sets are available for modeling. 103 sets of data are selected as training samples, other 24 set of data are used as test samples.

Because different variable has different unit, a variable may differ from other variables in several orders. It is thus necessary to normalize all the data in order to map all the data into $[0, 1]$, because modeling results may be improved if normalized data is used to establish model. Normalization can be described as follows. If data sample space of a variable is $x = (x_1, x_2, \dots, x_n)$, then normalized data is:

$$x'_i = (x_i - \min(x)) / (\max(x) - \min(x)) \quad (8-28)$$

Table 8-2 Auxiliary and estimation variables

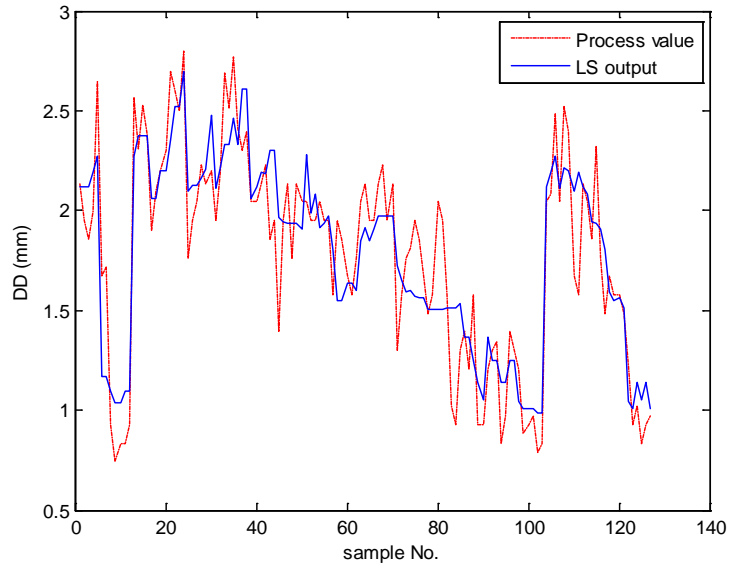
	Variable	Name	Unit	Range
1	<i>W.F.S</i>	Wire Feed Speed	Inch/min	250~400
2	<i>U</i>	Voltage	<i>V</i>	26~32
3	<i>L</i>	Laser Power Intensity	<i>W/mm²</i>	46~62
4	<i>DD</i>	Droplet Diameter	<i>mm</i>	0.7~3.1
5	<i>DTR</i>	Droplet Transfer rate	<i>ms</i>	20~440

The widely used least square method is used to construct the regression equation to estimate *DD* and *DTR* in this section. In the previous discussion, the inputs are *W.F.S*, *U* and *L*, the outputs are *DD* and *DTR*. Here, the outputs are also *DD* and *DTR*, but the inputs have to be updated. For convenience, *u*, *v* and *w* are used to denote *W.F.S*, *U* and *L* respectively.

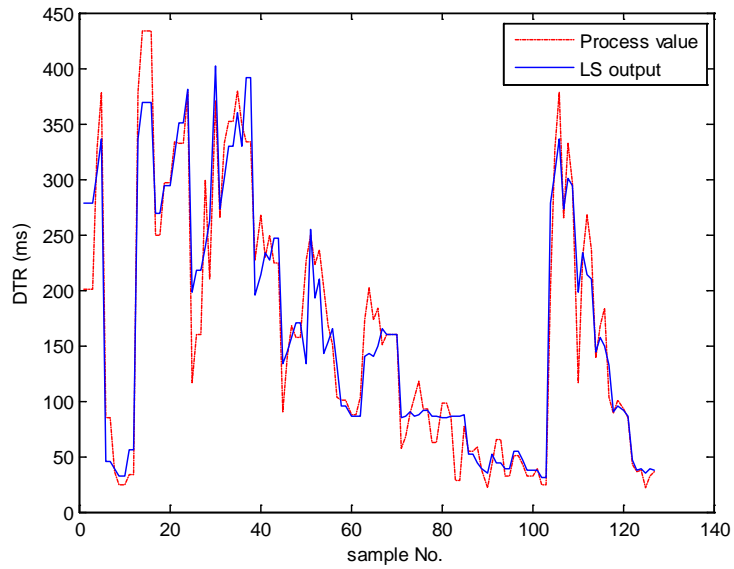
First, the inputs are selected as [*u*, *v*, *w*, *uv*, *uw*, *vw*, *u²*, *v²*, *w²*] to establish the regression equation. The simulation results are shown in Fig. 8-19. Table 8-3 shows the simulation errors.

Table 8-3 Simulation errors of LS regression with 9 parameters

	Training RMSE	Training ABE	Training RE	Testing RMSE	Testing ABE	Testing RE
<i>DD</i>	0.2331	0.1850	0.1191	0.2231	0.1662	0.1065
<i>DTR</i>	33.2066	24.3997	0.2115	30.2734	19.4012	0.1403



(a) *DD*

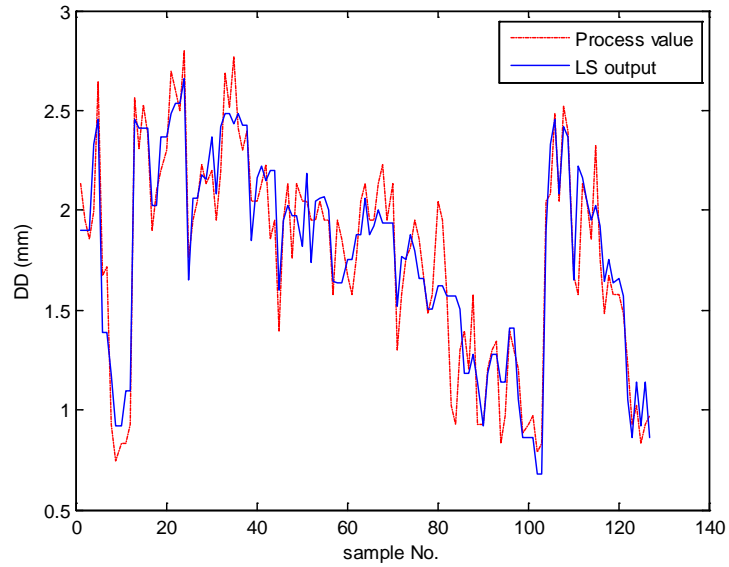


(b) *DTR*

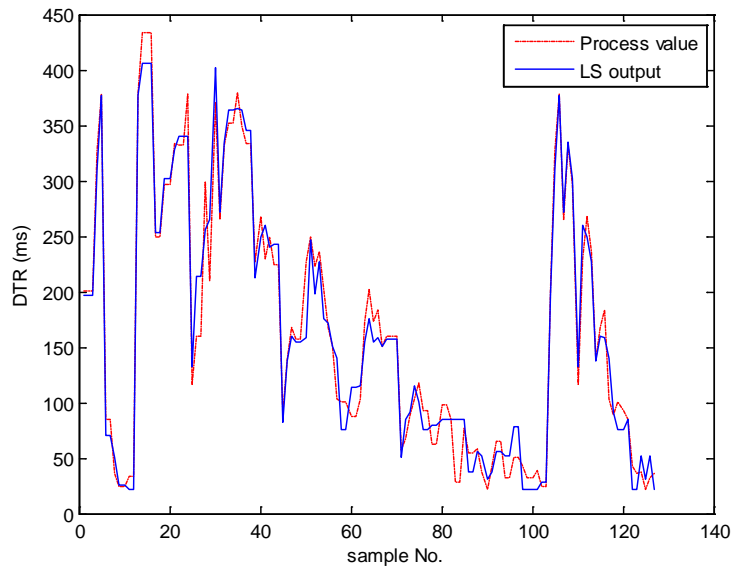
Fig. 8-19 Simulation results based on LS regression with 9 parameters: a) *DD*, b) *DTR*

When $[u, v, w, uv, uw, vw, u^2, v^2, w^2, uvw, u^3, v^3, w^3, u^2v, u^2w, v^2u, v^2w, w^2u, w^2v]$ are selected as inputs, the simulation results are shown in Fig. 8-20. Table 8-4 shows the

simulation errors, and it can be seen that the estimation is improved as the number of the parameters increases.



(a) *DD*



(b) *DTR*

Fig. 8-20 Simulation results based on LS regression with 19 parameters: a) *DD*, b) *DTR*

Table 8-4 Simulation errors of LS regression with 19 parameters

	Training RMSE	Training ABE	Training RE	Testing RMSE	Testing ABE	Testing RE
<i>DD</i>	0.1856	0.1458	0.0951	0.1822	0.1283	0.0856
<i>DTR</i>	21.0763	15.8426	0.1836	16.4199	13.2829	0.1752

8.2.2 BPNN Model Establishment

Due to its nonlinear mapping function, BPNN has been applied to establish soft-sensing models widely. BPNN model will be established to obtain the relationships between the welding parameters, *DD* and *DTR* in this section. After the model is achieved, it will be used to estimate *DD* and *DTR* of the droplet based on welding parameters in real time. In order to compare the estimation results with the LS regression, the nodes of hidden layer is selected as three, and the number of the parameters is thus sixteen which is close to nineteen used above in the LS regression.

The weights of the BPNN model are shown as follows, and the superscript of the weights denotes its layer,

$$[w_{1,1}^1, w_{1,2}^1, \dots, w_{1,n}^1, b_1^1, w_{2,1}^1, w_{2,2}^1, \dots, w_{2,n}^1, b_{12}^1, \dots, w_{m,1}^1, w_{m,2}^1, \dots, w_{m,n}^1, b_m^1, w_1^2, w_2^2, \dots, w_m^2, b^2]$$

The number of the weights for the BPNN model is

$$M = m \times (n + 1) + m + 1 \quad (8-29)$$

where n is the number of input-layer neuron nodes, and m is the number of hidden-layer neuron nodes.

$$y = \sum_{m=1}^5 w_m^2 \times f(\sum_{n=1}^3 w_{mn}^1 x_n + b_m^1) + b^2 \quad (8-30)$$

$$f(x) = 1/(1 + e^{-x}) \quad (8-31)$$

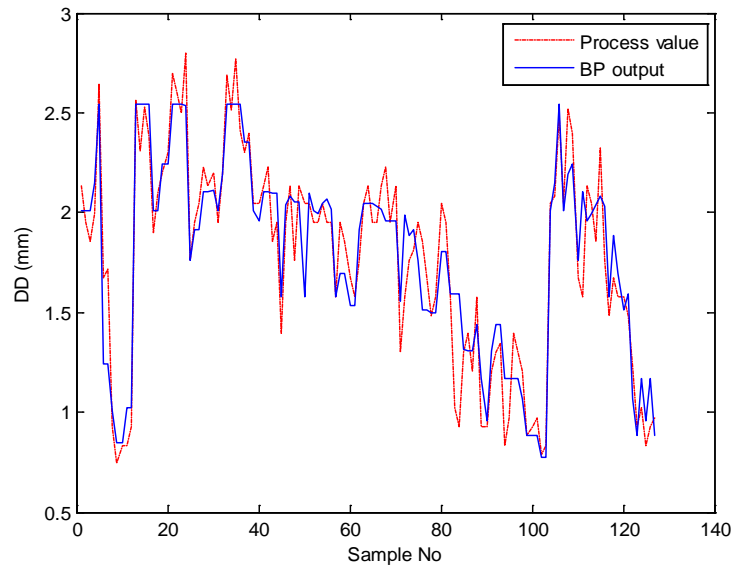
Structure of the BPNN model is 3-3-1; the number of the weights is thus 16. After the weights were obtained, Eq. (8-30) can be used to estimate DD and DTR in real-time. Here, x_1 , x_2 and x_3 denote $W.F.S$, U and L , and y denotes DD and DTR . Based on the real-time estimation of DD and DTR , the laser-enhanced GMAW process may be better analyzed to benefit its process control.

Fig. 8-21 is the model simulation results based on the BPNN model. As shown in Fig. 8-14 the data from 1 to 103 are training data, and other 24 data are test data. Table 8-5 shows the simulation errors, and it is seen that the estimation effect is no better than the LS regression method. After analyzing the experiments data, it was found that the complexity of the nonlinear relationships between the welding parameters, DD and DTR are not enough and the powerful universal nonlinear mapping ability of BPNN is not fully utilized. Hence, the estimation accuracy was not improved as compared to the LS model.

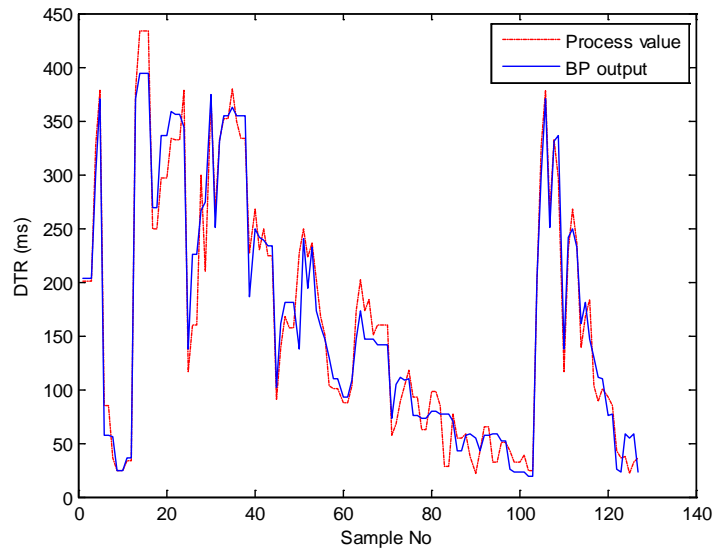
Table 8-5 Simulation errors of BPNN Model

	Training RMSE	Training ABE	Training RE	Testing RMSE	Testing ABE	Testing RE
DD	0.1764	0.1286	0.0832	0.2042	0.1716	0.1125
DTR	23.0993	17.1407	0.1811	20.5097	16.3311	0.2014

There is only one initial value in BP algorithm, and the gradient descent algorithm is applied to obtain the model. In contrast, there is a particle swarm as initial value which searches optimum based on experiential, oriented stochastic searching mode when the PSO is used to train the ANN. The probability of falling into local extremum for PSO is thus less than BP algorithm. Besides, the computation is easy and the application is more convenient in PSO algorithm. As an effective algorithm for training the ANN, PSO has been widely applied. It is thus used to improve the estimation in the next section.



(a) *DD*



(b) *DTR*

Fig. 8-21 Simulation results based on BPNN model: a) *DD*, b) *DTR*

8.2.3 PSO Based BPNN Model

In PSO, a swarm of individuals, called particles, is utilized. Assume that there are N particles searching in a D -dimensional space. All these particles are evaluated by the fitness function to be optimized. Initially, particles are assigned a group of random velocities and positions. They are updated from one generation to the next. To achieve the optimum, each particle is directed toward the personal best position, called $pbest$, found by its own so far, and the global best position, called $gbest$, found by its neighbors in the whole swarm.

In k th generation, the position of the i th particle, which represents the candidate solution, is characterized as

$$x_i^k = (x_{i1}^k, x_{i2}^k, \dots, x_{iD}^k), i = 1, 2, \dots, n \quad (8-32)$$

The position of every particle is a solution, the fitness could be got after the function was calculated through x_i , and the x_i can be evaluated based on the fitness.

The velocity of the i th particle is represented as $v_i^k = (v_{i1}^k, v_{i2}^k, \dots, v_{iD}^k), i = 1, 2, \dots, n$. Let $p_i^k = (p_{i1}^k, p_{i2}^k, \dots, p_{iD}^k)$ represents $pbest$ of i th particle, and $p_g^k = (p_{g1}^k, p_{g2}^k, \dots, p_{gD}^k)$ denotes $gbest$.

After $pbest$ and $gbest$ were obtained, the i th particle updated its velocity and position in $(k + 1)$ generation as follows:

$$v_{id}^{k+1} = wv_{id}^k + c_1r_1(p_{id}^k - x_{id}^k) + c_2r_2(p_{gd}^k - x_{id}^k) \quad (8-33)$$

$$x_{id}^{k+1} = x_{id}^k + v_{id}^{k+1} \quad (8-34)$$

where w is inertia weight. It introduces the weight of the current velocity on the next generation velocity. Inertia weight usually declines with the iteration. c_1 and c_2 , namely acceleration factors, are two positive constants. They can accelerate the searching speed of the particle, and are popularly assigned to be $c_1 = c_2 = 2$. r_1 and r_2 are random

numbers uniformly distributed in $[0,1]$. c_1r_1 and c_2r_2 provide stochastic effects of $(p_{id}^k - x_{id}^k)$ and $(p_{gd}^k - x_{id}^k)$, respectively. In the searching process, all these particles cooperate and compete with each other, and finally the optimal solution was achieved while the fitness function is optimized.

The executed steps of PSO are showed as below:

Step 1: Initialize all the particles (velocity and position) randomly.

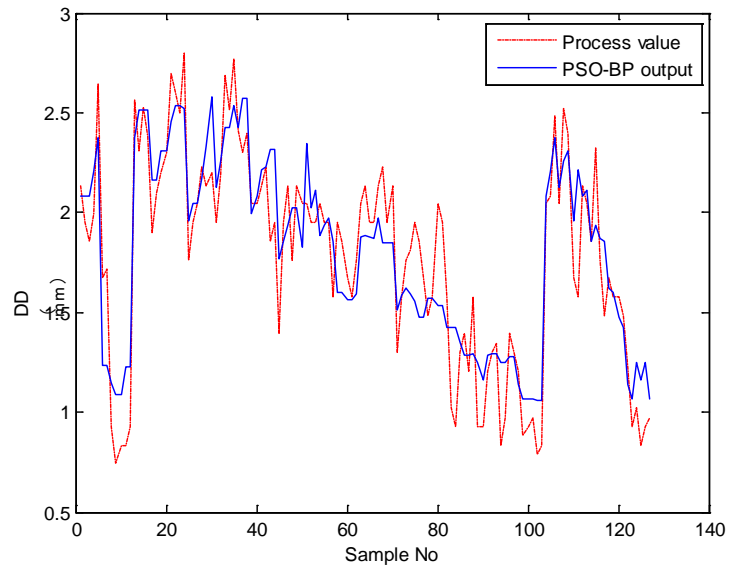
Step 2: Evaluate the fitness of each particle in the population, and derive p_{best} and g_{best} . Stop the algorithm if terminal criterions are satisfied, otherwise go to Step 3.

Step 3: Update the velocity and position of each particle according to Eq. (8-33) and (8-34), and return to Step 2.

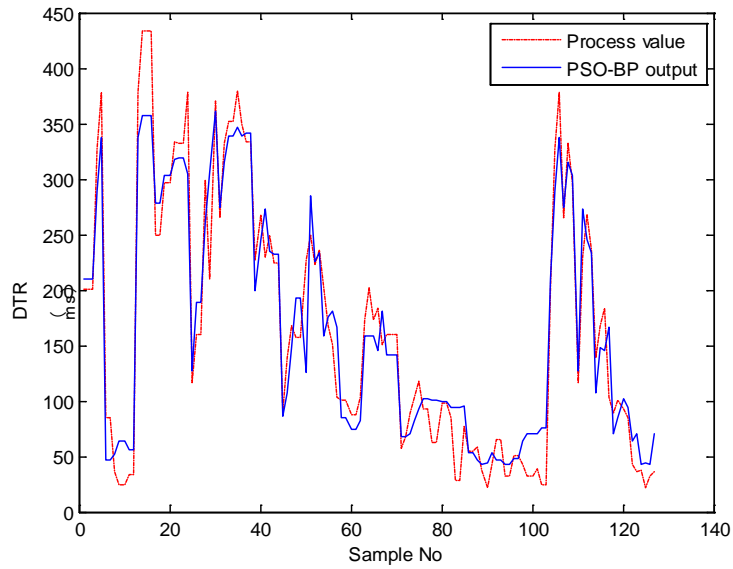
Fig. 8-22 is the PSO-BPNN model simulation results for DD and DTR . Table 8-6 shows the simulation errors, and it is seen that the estimation for DD is similar to that with the BPNN model but the estimation for DTR is worse than that with the BPNN model. This is because the hidden layer nodes are too few, and the parameters are not enough to take advantage of the searching ability of PSO. When the hidden layer nodes are 7, the PSO-BPNN model is better than BPNN model.

Table 8-6 Simulation errors of PSO-BPNN Model

	Training RMSE	Training ABE	Training RE	Testing RMSE	Testing ABE	Testing RE
DD	0.2433	0.1994	0.1357	0.2180	0.1583	0.1142
DTR	30.0621	24.0593	0.2823	24.8051	21.0559	0.2283



(a) *DD*



(b) *DTR*

Fig. 8-22 Simulation results based on PSO-BPNN model: a) *DD*, b) *DTR*

8.2.4 TSCPSO-BPNN Model

In order to avoid falling into the local extremum, PSO is similar to other stochastic optimization algorithms in enlarging the range of searching space. In the optimization process, particles fly to optimum orientation constantly. If particles fly to the local extremum, velocities of all particles maybe become zero soon, particles remain still, and it will result in local extremum convergence.

Aiming to resolving this issue, the particle swarm can be separated into three sub-swarms. Two sub-swarms called good sub-swarm fly in the direction of globally best particle (*gbest*). The other sub-swarm called bad sub-swarm flies against the direction of *gbest*. During the iterations, if the global extremum does not change after several generations and the global optimum is not found, one of good sub-swarm will be selected to change all the particles with the bad sub-swarm. The particles in the good sub-swarm may thus change the fly direction and will not remain still when meet the local extremum. The possibility for local extremum convergence is thus reduced.

Three swarm cooperative particle swarm optimization (TSCPSO) is used to train the weights of BPNN. TSCPSO improves the global search ability, and avoids local extremum of basic PSO [129-130]. Prior to designing the TSCPSO-BPNN model, a reasonable model structure, fitness function and search space need to be determined. The training process of BPNN focuses on updating link weights. The search process of TSCPSO is mainly variation of velocities and positions. The link weights of BPNN will thus correspond with the particle position.

The number of weights that need to be optimized by PSO is given by Eq. (8-29). Particle position vector of TSCPSO-BPNN is established according to the weights of ANN. The training process of ANN thus becomes searching process of optimum positions.

The particle swarm is coded as follows,

$$\text{Popul}(i) = [w_{1,1}^1, w_{1,2}^1, \dots, w_{1,n}^1, b_1^1, w_{2,1}^1, w_{2,2}^1, \dots, w_{2,n}^1, b_{12}^1, \dots, w_{m,1}^1, w_{m,2}^1, \dots, w_{m,n}^1, b_m^1, w_1^2, w_2^2, \dots, w_m^2, b^2]$$

The fitness function is the mean square error,

$$f(x) = \min(MSE) = \min ((\sum_{i=1}^N (y_i - \hat{y}_i)^2)/N) \quad (8-35)$$

Here, N is the sample number, $y_i (i = 1, 2, \dots, n)$ are the real values of the estimated variable, and $\hat{y}_i (i = 1, 2, \dots, n)$ are model output values of the estimated variable.

The algorithm steps for TSCPSO based BPNN can be described as follows:

Step1: Normalizing the input data and determining input and output sample sets of the network;

Step2: Initializing the scale and other parameters in all groups;

Step3: Initializing velocity and position of particles in three groups;

Step4: Determining the fitness function

$$f(W, B) = E(w1, b1, w2, b2) = \min ([\sum_{i=1}^N (y_i - \hat{y}_i)^2]/N) \quad (8-36)$$

y_i and \hat{y}_i are real and desired outputs of output-layer nodes. The fitness function is used to evaluate particle fitness;

Step5: Updating individual optimum value based on particle search;

Step6: Updating optimum value of subgroup and whole groups;

Step7: Calculating new velocity and position of particles;

Step8: Updating optimum position of individual particle, subgroups, and whole group;

Step9: If optimum values of whole group are not improved in ten steps, turn to step10, else turn to step11;

Step10: Changing particles between groups;

Step11: If the stop criterion is met, search will be stopped, and the optimum values are outputted. The network weights are adopted to calculate network outputs and to obtain the final fitting curve. Otherwise return to step2 to continue search.

Fig. 8-23 is the TSCPSO-BPNN model simulation results for *DD* and *DTR*. Table 8-7 shows the simulation errors. It can be seen that the estimation with TSCPSO-BPNN model is better than that with the BPNN and PSO-BPNN models due to its good generalization capability. On the other hand, the estimation with TSCPSO-BPNN model is just similar to that with the LS regression method possibly because the parameters nonlinearity is not significant.

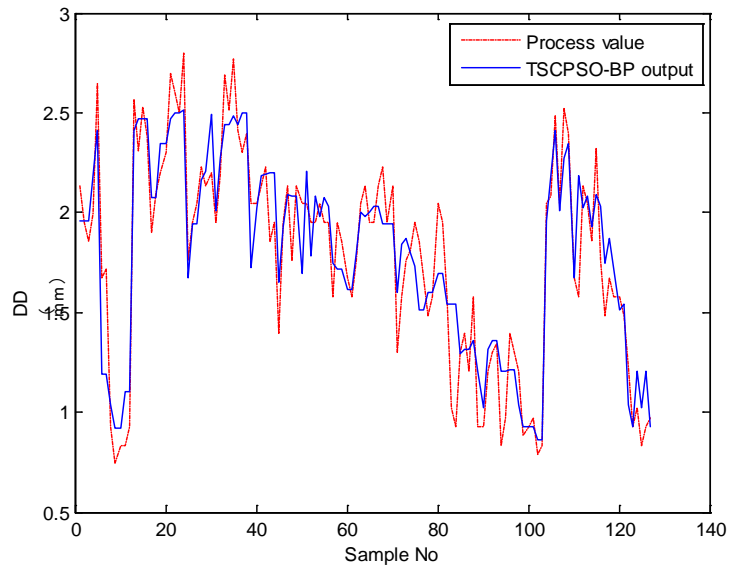
Table 8-7 Simulation errors of TSCPSO -BPNN model

	Training RMSE	Training ABE	Training RE	Testing RMSE	Testing ABE	Testing RE
<i>DD</i>	0.1962	0.1510	0.0970	0.1956	0.1476	0.0990
<i>DTR</i>	22.6193	16.5816	0.1791	19.1267	11.7923	0.1334

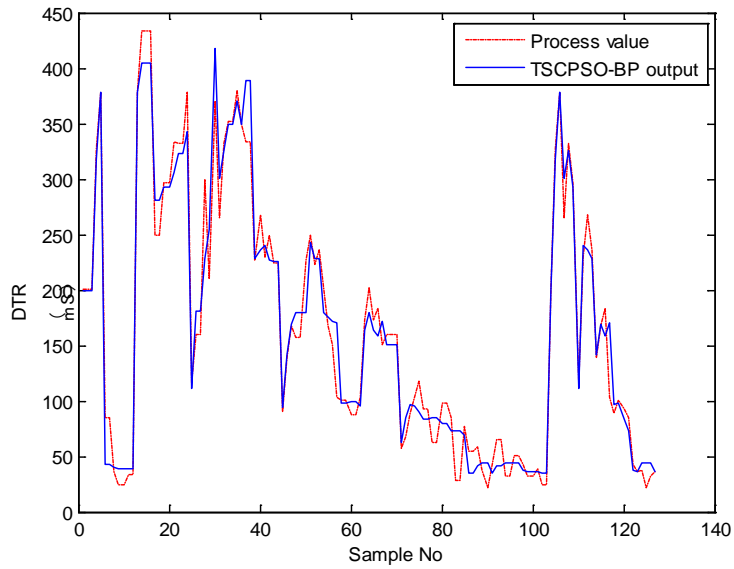
8.2.5 Comparison with LS Model

Because the relationships among the welding parameters, *DD* and *DTR* may not be nonlinear significantly, the estimation accuracy with BPNN models is no better than that with the LS model. Due to its good generalization capability, TSCPSO-BPNN model is better than the BPNN model and PSO-BPNN model. However, its estimation results are only similar to those with the LS regression method.

After analyzing the estimation results, it is found that the soft sensors using LS regression method and TSCPSO-BPNN model are capable of obtaining desired estimation. Because a LS model is much easier to be established and realized than TSCPSO-BPNN model, the LS model can be recommended as the preferred method in this paper to obtain real-time estimation for *DD* and *DTR* in laser enhanced GMAW for process control.



(a) *DD*



(b) *DTR*

Fig. 8-23 Simulation results based on TSCPSO-BPNN model: a) *DD*, b) *DTR*

8.2.6 Dimensions Reduction and Discussion

In the LS regression equation, there are nineteen parameters. Some parameters may have not contributed to the effectiveness of the model such that the dimensions of the model may be reduced. As a result, the model structure and calculation may be simplified.

Table 8-8 shows the simulation errors with models of reduced dimensions for *DD*. It can be seen that the error for model 6 is similar to that for the full model (i.e., model 1). Table 8-9 lists the variables used in the full and selected model.

Table 8-8 Simulation errors of dimensions reduction model for *DD*

	parameter	Training RMSE	Training ABE	Training RE	Testing RMSE	Testing ABE	Testing RE
Model1	19	0.1856	0.1458	0.0951	0.1822	0.1283	0.0856
Model2	18	0.1867	0.1466	0.0952	0.1806	0.1255	0.0833
Model3	17	0.1868	0.1466	0.0951	0.1797	0.1246	0.0824
Model4	16	0.1889	0.1476	0.0967	0.1833	0.1283	0.0833
Model5	14	0.1913	0.1485	0.0977	0.1876	0.1294	0.0840
Model6	13	0.1947	0.1495	0.0977	0.1906	0.1336	0.0859

Table 8-9 Corresponding variables of the models for *DD*

	Parameter	Variables
Model1	19	$[u, v, w, uv, uw, vw, u^2, v^2, w^2, uvw, u^3, v^3, w^3, u^2v, u^2w, v^2u, v^2w, w^2u, w^2v]$
Model6	13	$[u, v, w, uv, uw, vw, u^2, w^2, uvw, u^3, w^3, u^2v, v^2u]$

Based on the results from dimensions reduction, model 6 will be tested by F-test to find if these models can fit the data with fewer parameters and the results are not significantly worse. The F-test calculated results for the model is 0.8639, the corresponding critical values of the F distribution ($P= 0.05$) is 2.21. It is found that F-test for model 6 meets the

criteria. Hence, model 6 will be used to obtain estimation. Table 8-10 presents the parameters for model 6.

Table 8-10 Parameters for Model 6

	u	v	w	uv	uw	vw
Model6	- 0.179457378	- 0.256152635	0.048453356	0.005582166	1.76E-05	0.000209681

u^2	w^2	uvw	u^3	w^3	u^2v	v^2u
0.000361667	-5.98E-05	-8.54E-07	-2.97E-07	2.19E-08	-5.64E-05	-3.98E-06

The droplet size is mainly determined by the wire melting rate. Basically, the wire is melted by the anode and resistive heat which are proportional to the current and its square respectively. However, the resistive heat also depends on the length of the wire extension (L). The melting rate could be simply expressed as [1-2, 23, 25]

$$MR = aI + bLI^2 \quad (8-37)$$

where a and b are constants and I is the welding current.

In all experiments, the same welding wire was used, and wire extension was fixed. The melting rate was thus mainly determined by the welding current. As the wire feed speed and welding voltage determine the welding current, terms related with these two parameters should be contained in the model. The partial derivative with respect to the wire feed speed should be negative. Calculation shows that the dominant terms of u are u and u^3 terms. Both their coefficients are negative. Based on the resultant models, increasing the wire feed speed causes the droplet size to decrease. This is coincident with the experimental results. For the welding voltage, careful analysis of all voltage terms in the models shows that the dominant term for the welding voltage is u^2v and its coefficient is negative and that the partial derivative with respect to the welding voltage

v given by the models is negative. It is coincident with the analysis that the droplet size decreases as the welding voltage increases.

For the laser intensity, calculation shows that the partial derivative with respect to the laser intensity w given by the model is negative and it is coincident with the experimental results. Per [4], laser heat for the laser power range used in this study plays a relatively insignificant role in melting the welding wire. Hence, the laser power should be a small value term in the estimation expression. It can be found that the partial derivative with respect to the laser intensity w is much small and it is coincident with the above analysis.

8.3 Conclusions

A nonlinear model was set up for laser enhanced GMAW. Laser recoil pressure force was combined into the detachment criterion to determine the droplet detaching. The simulating results agree with the experiment ones. It indicates that this nonlinear could be used for process control.

LS regression equation, BPNN, PSO-BPNN, and TSCPSO-BPNN models have been established to estimate two major parameters in the laser enhanced GMAW: droplet size and droplet transfer rate. Results obtained by the proposed TSCPSO-BPNN model are similar with those from the much less complex LS regression and both of them can estimate the droplet size and transfer rate accurately. Model reduction has been conducted for the LS regression to improve the model confidence based on F-Test. Analysis confirmed that the resultant LS model of reduced dimension coincides with the process physics. The resultant LS model of reduced dimension can thus be proposed as a soft sensor to estimate the droplet size and droplet transfer rate in real-time for the laser enhanced GMAW.

CHAPTER 9 CONCLUSIONS AND FUTURE WORK

9.1 Conclusions

Gas Metal Arc Welding (GMAW) is widely used in the manufacturing industry, such as automotive, aerospace, and shipbuilding. Metal transfer is a very important issue, and a good understanding of this process will benefit the application of GMAW.

In this dissertation, laser enhanced GMAW was proposed and developed by adding a low power laser onto the droplet to generate an auxiliary detaching force. The metal transfer type will be changed from short-circuiting or repelled globular transfer to free flight transfer. The metal transfer in laser enhanced GMAW was systematically studied, and all the phenomena could be explained by the established physical fundamentals. Good surface formation of welds could be obtained, and full penetration could also be achieved using laser enhanced GMAW. For the future closed-loop control, control algorithm was proposed.

The main achievement and contribution of the dissertation can be summarized as follow:

- (1) An experimental system has been established and the feasibility of the novel Laser-Enhanced GMAW process was experimentally demonstrated; The laser aiming at the droplet in Laser-Enhanced GMAW can apply an auxiliary detaching force without significant additional heat;
- (2) Free flight transfers could be successfully produced at continuous currents from 90 A to 135 A with a 0.8 mm diameter steel wire without spatters;

- (3) Phenomena observed in Laser-Enhanced GMAW have been satisfactorily analyzed by applying established theories and fundamentals; Laser enhanced metal transfer process is also governed by the established physics of metal transfer, except there is a need to include the additional detaching force generated by the laser; Droplet detaching theories were reviewed and analyzed, and Dynamic Force Balance Theory (DFBM) was selected as the main theory to analyze the metal transfer phenomenon in laser enhanced GMAW; Laser recoil pressure force was recognized as the additional detaching force in laser enhanced GMAW, and its value was estimated based on established physical fundamentals.
- (4) If the metal transfer is short-circuiting transfer in conventional GMAW, Laser Enhanced GMAW may change it to drop globular transfer; if conventional and Laser Enhanced GMAW both produce drop globular, the latter reduces the diameter of the droplet; if the metal transfer is short-circuiting or drop globular transfer in conventional GMAW, Laser Enhanced GMAW may become the drop spray; the established physics of metal transfer can explain all these changes by counting the additional detach force introduced by the laser.
- (5) Laser intensity and arc voltage are major factors affecting the metal transfer in Laser Enhanced GMAW. The enhancement of the laser increases as the laser intensity increases and the droplet size could be effectively controlled by changing the laser intensity in an appropriate range. An increased arc voltage increases the current and can affect the metal transfer through an increased electromagnetic force. An increased arc voltage also increases the arc gap and possible time interval for the droplet to develop to reduce the chances for short-circuiting transfer or repelled drop globular transfer.
- (6) The dynamic balance force theory could be used to explain the detaching phenomenon in laser enhanced GMAW. The gravitational force difference due to the mass change when laser was adopted could be used to estimate the laser recoil pressure force, and the result had a reasonable accuracy.
- (7) Good formation of welds could be obtained in laser enhanced GMAW, and no spatters were generated. Full penetration could be obtained both bead on plate and

- butt joint welding, and the results were sensitive to the mean welding current and travel speed.
- (8) Controlled drop globular transfer in Laser Enhanced GMAW offers desirable metal transfer characteristics that benefit formation of quality welds. Controlled drop globular transfer extends the capability of the productive GMAW process into the range of constant current that conventionally produces undesirable drop transfer that is not most suitable for practical use. Laser enhancement provides an effective method to achieve a controlled drop globular and to empower the GMAW to use a constant current in a much increased range to meet the requirements from different applications. Droplets can be detached at a given/desired diameter in a reasonable range by applying an appropriate laser intensity under a given current (arc variable) in a reasonable range and the needed laser intensity is determined by the desired droplet diameter and the used welding current (arc variable).
- (9) A nonlinear model was set up for laser enhanced GMAW. Laser recoil pressure force was combined into the detachment criterion to determine the droplet detaching. The simulating results agree with the experiment ones. It indicates that this nonlinear could be used for process control.
- (10) LS regression equation and TSCPSO-BPNN models have been established to estimate two major parameters in the laser enhanced GMAW: droplet size and droplet transfer rate. Results obtained by the proposed TSCPSO-BPNN model are similar with those from the much less complex LS regression and both of them can estimate the droplet size and transfer rate accurately. Model reduction has been conducted for the LS regression to improve the model confidence based on F-Test. Analysis confirmed that the resultant LS model of reduced dimension coincides with the process physics. The resultant LS model of reduced dimension can thus be proposed as a soft sensor to estimate the droplet size and droplet transfer rate in real-time for the laser enhanced GMAW.

9.2 Future Work

The main objective of this research is to develop a novel laser enhanced GMAW and realize the control of metal transfer at given variables. To realize the industrial potential of laser enhanced GMAW, more work should be done to improve this novel method in several aspects which are listed as below.

- (1) Most of the experiments are conducted using CV or CC welding power supply in this research. Pulsed welding power may be utilized in the future research. With pulsed welding current waveform, the base current is used to keep the arc and the peak current is used to grow the droplet. The peak welding current is not higher than the transition one. Laser recoil pressure force will be added as an additional detaching force. In this case, the droplet could be detached at even lower mean welding current. Further if the pulsed laser power is used, it will be better. This work has been done in Chapter 6. However, the metal transfer achieved is not assured to One Pulse One Droplet (OPOD). To achieve OPOD, more work should be done.
- (2) Laser recoil pressure force is main detaching effect from the lower power laser. To better understand the mechanism of this force will benefit the utilization of this novel welding process. In this research, the laser recoil pressure is only estimated at an acceptable level, but not accurate enough. To explore the mechanism of laser recoil pressure will be the future task.
- (3) All the experiments in this research were conducted in an open-loop control system. To obtain a much more stable and consistent process, a closed-loop real time control algorithm should be established. The imaging processing technology could be adopted as the sensing technology. High speed camera could be used to record the metal transfer process, and then the image from the recorded video could be processed to obtain the droplet information, such as the droplet size, position. In this case, closed-loop control could be built to precisely monitor the laser. The laser pulse could be exerted on the droplet when the desired droplet size is fulfilled.

REFERENCES

1. O'Brien, R.L. 1991. Welding Handbook Vol. 2: Welding Processes. 8th edition, Miami, FL. American Welding Society.
2. Song, T. H.. 2001. Welding handbook: Welding methods and equipments.1 [M], Second Edition. Beijing, P R China, Chinese Welding Society.
3. Lincoln Electric. 1994. The Procedure Handbook of Arc Welding. Cleveland: Lincoln Electric. ISBN 99949-25-82-2.
4. Thomsen, J.S., 2006. Control of pulsed gas metal arc welding. International Journal of Modelling, Identification, and Control, 1(2): 115-125.
5. Wang, G., Huang, P. G., and Zhang, Y. M. 2004. Numerical analysis of metal transfer in gas metal arc welding under modified pulsed current conditions. Metallurgical and Materials Transactions B, 35(5): 857–866.
6. Praveen P., Kang M.J., Yarlagadda P.K.D.V.. 2008. Drop transfer mode prediction in pulse GMAW of aluminum using statistical model, Journal of Materials Processing Technology, 201(1): 502-506.
7. Sehun Rhee, Kannatey-Asibu, Jr. 1991. Analysis of arc pressure effect on metal transfer in gas-metal arc welding. Journal of Applied Physics, 70(9): 5068-5075.
8. Mahrle, A. and Beyer, E., 2006. Hybrid laser beam welding-classification, haracteristics, and applications. Journal of Laser Applications. 18 (3): 169-180.
9. Liu, L., Hao, X. and Song, G., 2006. A new laser-arc hybrid welding technique based on energy conservation. Materials Transactions. 47 (6): 1611-1614.

10. Bagger, C. and Olsen, F.O., 2005. Review of laser hybrid welding. *Journal of Laser Applications*. 17 (1): 2-14.
11. Casalino G.. 2007. Statistical analysis of MIG-laser CO₂ hybrid welding of Al–Mg alloy. *Journal of Materials Processing Technology*. 191 (1): 106-110.
12. Weisheit, A., Galun, R., and Mordike, B.L., 1998. CO₂ laser beam welding of magnesium-based alloys. *Welding Journal*. 77 (4): 149s-154s.
13. CAana G., Fortunato A., Ascari A., Tani G., Tomesani L. 2002. The influence of arc transfer mode in hybrid laser-mig welding. *Journal of Materials Processing Technology*. 191 (1): 111-113.
14. Liu L.M., Zhao X. 2008. Study on the weld joint of Mg alloy and steel by laser-GTA hybrid welding. *Materials Characterization*. 59(9): 1279-1284.
15. Zhou J., Thai H.L. 2008. Modeling of transport phenomena in hybrid laser-MIG keyhole welding. *International Journal of Heat and Mass Transfer*. 51(17): 125-134.
16. Cary, Howard B. and Scott C. Helzer. 2005. *Modern Welding Technology*. Upper Saddle River, New Jersey: Pearson Education. ISBN 0-13-113029-3.
17. Kalpakjian, Serope and Steven R. Schmid. 2001. *Manufacturing Engineering and Technology*. Prentice Hall. ISBN 0-201-36131-0.
18. Althouse, A. D., Turnquist, C. H., Bowditch, W. A. and Bowditch, K. E. 1984. *Modern Welding [M]*, South Holland, ILL: The Goodheart – Willcox Company, Inc..
19. Ono M., Shinbo Y., Yoshitake Ohmura A. M.. 2002. Development of laser-arc hybrid-welding, *NKK Techn.*, 86: 8 – 12.
20. Kim Y. S., Eagar T. W. 1993. Analysis of metal transfer in gas metal arc-welding, *Welding Journal*. 72(6): 269s to 278s.

21. Kim Y. S. 1989. Metal transfer in gas metal arc welding. PhD dissertation, Massachusetts Institute of Technology
22. Kim Y. S., Eagar T. W. 1993. Metal transfer in pulsed current gas metal arc-welding, *Welding Journal*. 72(7): 279s to 287s
23. Lesnewich A. 1958. Control of melting rate and metal transfer in gas-shielded metal arc welding: Part II control of metal transfer. *Welding Journal*. 37(9): 418s-425s
24. Lesnewich A. 1997. Letters to the Editor: Metal Transfer Modes Made Correct. *Welding Journal*. 76(7): 21-22.
25. Lancaster, J. F. 1984. *The Physics of Welding*. Pergamon Press, Oxford, England.
26. Song J., Hardt D.. 1994. Dynamic modeling and adaptive control of gas metal arc welding process, *Journal of Dynamic System*. 116(9): 405-413.
27. Zhang Y. M., Liguó E, Kovacevic R. 1998. Active metal transfer control by monitoring excited droplet oscillation, *Welding Journal*. 77(9): 388s-395s.
28. Zhang Y. M., Li P. J. 2001. Modified active control of metal transfer and pulsed GMAW of titanium, *Welding Journal*. 80(2): 54s-61s.
29. Lin Q., Li, X. S., Simpson W. 2001. Metal transfer measurements in gas metal arc welding, *J. Phys. D: Appl. Phys.* 34: 347-353.
30. Ponomarev, V., Scotti, A., Silvinskiy, A., Al-Erhayem, O. 2003. Atlas of MIG/MAG welding metal transfer modes. IIW Doc. XII-1771 to 1775-03. Bucharest.
31. Iordachescua D., Quintinob L. 2008. Steps toward a new classification of metal transfer in gas metal arc welding. *Journal of materials processing technology*. 202: 391-397.
32. Klas, W.. 2003. *Welding processes handbook*. [M], New York: CRC Press LLC.

33. Ed, C.. 1991. "Gas Metal Arc & Flux Cored Welding Parameters". [M], Chicago: Weldtrain.
34. Heald, P. R., Madigan, R B., Siewert, T. A and Liu, S.. 1994. Mapping the droplet transfer modes for an ER100S-1 GMAW electrode, *Welding Journal*, 73(2): 38s-44s.
35. Fan, H. G. and Kovacevic, R. 1999. Droplet formation, Detachment, and Impingement on the molten pool in Gas Metal Arc Welding, *Metallurgical and Materials Transactions B*, 30 (4): 791-801.
36. CAana G., Fortunato A., Ascari A., Tani G., Tomesani L. 2007. The influence of arc transfer mode in hybrid laser-mig welding, *Journal of Materials Processing Technology*, 191(1): 111-113.
37. Norman P., Karlsson J., Kaplan A. 2011. Mechanisms forming undercuts during laser hybrid arc welding, *Physics Procedia*, 12: 201-207.
38. Fennander, H., Kyrki, V., Fellman, A., Saleminen, A. and Kälviäinen, H. 2007. Visual measurement and tracking in laser hybrid welding, *Machine Vision and Applications*, s00138-007-0111-1.
39. Schubert, E. 2004. Process Stability of Automated Gas Metal Arc Welding of Aluminum [M]. Springer Berlin/Heidelberg, Vol299.
40. Kaielerle, S., Bongard, K., Dahmen, M., Poprawe, R., 2000. Innovative hybrid welding process in an industrial application. Proceedings of International Conference on the Applications of Lasers and Electro-Optics ICALEO 2000, Dearborn, MI, USA, 2–5 October: 91–98.
41. Process of Surface Tension
Transfer, <http://content.lincolnelectric.com/pdfs/products/literature/nx220.pdf>

42. Application of Surface Tension
Transfer, <http://content.lincolnelectric.com/pdfs/products/literature/nx310.pdf>
43. DeRuntz B.D.. 2003. Assessing the benefits of surface tension transfer welding to insuatory, Journal of Industrial Technology, 19(4): 2-8.
44. Stava E.K.. 1993. A new, low-spatter arc welding machine. Welding Journal, 72(1): 25-29.
45. Parks J.M., Stava E.K.. 1991. Apparatus and method of short circuiting arc welding. U.S. Patent, #5,003,154.
46. Stava E.K.. 1992. System and method of short circuiting arc welding. U.S. Patent, #5,148,001.
47. Stava E.K.. 2006. Short circuit arc welder and method of controlling same. US Patent, #7,109,439.
48. Hsu C.. 2006. Two stage welder and method of operating same. US Patent, #7,067,767.
49. Stava E.K.. 1993. A new, low-spatter arc welding machine. Welding Journal, 72(1): 25-29.
50. Stava E.K.. 2002. Short circuit arc welder and method of controlling same. US Patent, #6,501,049.
51. Stava E.K.. 2001. Short circuit welder. US Patent, # 6,215,100.
52. Himmelbauer K.. 2005. The CMT-Process —A revolution in welding technology, IIW Doc XII-1875-05, 20-27, IIW.
53. CMT: Cold Metal Transfer, MIG/MAG dip-transfer arc process. Brighton: Fronius USA LLC, 2007.

54. CMT: Cold Metal Transfer, MIG/MAG dip-transfer process for automated applications. Brighton: Fronius USA LLC, 2004.
55. The CMT Process –A Revolution in Materials-Joining Technology. Brighton: Fronius USA LLC, 2004.
56. Zhang H.T., Feng J.C.. 2009 The arc characteristics and metal transfer behavior of cold metal transfer and its use in joining aluminum to zinc-coated steel. *Materials Science and Engineering A*, 499: 111-113.
57. Wang J., Feng J.C.. 2008. Microstructure of Al-Mg dissimilar weld made by cold metal transfer MIG welding. *Material Science and Technology*, 24(7): 827-831.
58. Zhang H.T., Feng J.C.. 2008. Interfacial phenomena of cold metal transfer (CMT) welding of zinc coated steel and wrought aluminum. *Materials Science and Technology*, 24(11): 1346-1349.
59. Zhang H.T., Feng J.C.. 2007. Interfacial microstructure and mechanical properties of aluminum-zinc-coated steel joints made by a modified metal inert gas welding-brazing process. *Materials Characterization*, 58: 588-292.
60. Pickin C.G., Young K.. 2006. Evaluation of cold metal transfer (CMT) process for welding aluminum alloy, 11(5): 583-585.
61. Li K.H., Chen J., Zhang Y.M.. 2007. Double-electrode GMAW process and control. *Welding Journal*, 86(8): 231s-237s.
62. Wu C.S., Zhang M.X., Li K.H., Zhang Y.M.. 2007. Numerical analysis of double-electrode gas metal arc welding Process. *Computational Materials Science*, 39: 416-423.
63. Li K.H.. *Double-Electrode Gas Metal Arc Welding: Process, Modeling and Control*.

PhD Dissertation, University of Kentucky, Sept. 21, 2007.

64. Li K.H., Zhang Y.M.. 2008. Consumable Double-Electrode GMAW Part I: The Process. *Welding Journal*, 87(1): 11s-17s.
65. Li K.H., Zhang Y.M.. 2008. Consumable Double-Electrode GMAW Part II: Monitoring, Modeling, and Control. *Welding Journal*, 87(2): 44s-50s.
66. Li K.H., Zhang Y.M.. 2007. Metal transfer in double-electrode gas metal arc welding, *Journal of Manufacturing Science and Engineering-Transactions of the ASME*, 129(6): 991-999.
67. Li K.H., Zhang Y.M.. Xu P., Yang F.Q.. 2008. High strength steel welding with consumable DE-GMAW, *Welding Journal*, 88(3): 57s-64s.
68. Liu, X. P., Li, K. H., Zhang, Y. M., Johnson, Q. M.. 2007. Dual Bypass GMAW of Aluminum, *Transactions of NAMRI/SME*, 35: 335-341.
69. Shi, Y., Liu, X., Zhang, Y.M., Johnson, M. 2008. Analysis of Metal Transfer and Correlated Influences in Dual Bypass GMAW of Aluminum, *Welding Journal*, 87: 229s-236s.
70. Liu, X., Shi, Y., Johnson, M., Zhang, Y.M. 2007. Dual Bypass GMAW of Aluminum Rings. *Transaction of FABTECH International & AWS Welding Show, Chicago*: 157-158.
71. Zhang Y. M., Ligu E.. 1999. Method and system for gas metal arc welding. U.S. Patent, #6,008,470.
72. Wu Y., Kovacevic R.. 2002. Mechanically assisted droplet transfer process in gas metal arc welding. *Journal of engineering manufacturing*, 216: 555-564.
73. Yang, S. Y. Projected droplet transfer control with additional mechanical forces

- (AMF) in MIG/MAG welding process. PhD dissertation, Harbin Institute of Technology, 1998.
74. Jones, L. A., Eagar, T. W., Lang, J. H.. 1998. A dynamic model of drops detaching from a gas metal arc welding electrode, *J. Physics D: Appl. Physics*, 31(1): 107-123.
 75. Zhang Y. M., Liguó E. 2000. Numerical analysis of dynamic growth of droplet in GMAW. *Journal of Mechanical Engineering Science*, 214(10): 1247-1258.
 76. Watkins, A.D., Smartt, H.B., Johnson, J.A.. 1992. A dynamic model of droplet growth and detachment in GMAW. *International Trends in Welding Science and Technology*; Gatlinburg, Tennessee; USA; 1-5 June. pp. 993-997.
 77. Choi, J.H., Lee, J. and Yoo, C.D.. 2001. Dynamic force balance model for metal transfer analysis in arc welding. *Journal of Physics D: Applied Physics*, 34:2658–2664.
 78. Petrov, V.M., Petter, J., Petrov, M. P. and Tschudi, T.. 2007. Nano-optomechanics: from the light pressure to the Casimir force. *Materials Science and Engineering C*, 27(5): 981-984.
 79. Waszink, J.H., Piena, M. J.. 1986. Experimental investigation of drop detachment and drop velocity in GMAW. *Welding Journal*. 65(11): 289s-298s.
 80. Semak, V., Matsunawa, A.. 1997. The role of recoil pressure in energy balance during laser materials processing. *Journal of Physics D: Applied Physics*, 30(18): 2541-2552.
 81. Liu, J.H. and Hu, W.Q.. 1999. Analysis of forces on the weld pool and weld appearance during CO₂ laser welding of A3 steels. *Progress in Lasers and Optoelectronics*, 9: 141-144.

82. Naidu D.S., Moore K.L., Abdelrahman M.A., 1999. Gas metal arc welding control: Part 2 – control strategy. *Nonlinear Analysis*, (35):85–93.
83. Naidu D.S., Moore K.L., Yender R., Tyler J., 1997. Gas metal arc welding control: Part 1 – modeling and analysis. *Nonlinear Analysis, Methods and Applications*, 30(5): 3101–3111.
84. Thomsen, J.S., 2005. *Advanced Control Methods for Optimization of Arc Welding*. PhD dissertation, Aalborg University.
85. Thomsen, J.S., 2006. Control of pulsed gas metal arc welding. *International Journal of Modelling, Identification, and Control*, 1(2): 115-125.
86. Jackson, C. E., Shrubbsall, A. E. 1953. Control penetration and melting rate with welding technique, *Welding Journal*, 32(4): 172s-179s.
87. McGlone, J. C., Chadwick, D. B. 1978. The submerged arc butt welding of mild steel Part 2: The prediction of weld bead geometry from the procedure parameters, *Welding Institute Report*. 80/1978/PE.
88. Giedt, W. H., Tallerico, L, N. 1988. Prediction of electron beam depth of penetration, 1988, *Welding Journal*, 67(12): 299s-305s.
89. Metzbower, E. A. 1993. Penetration depth in laser beam welding, *Welding Journal*, 72(8): 403s-407s.
90. Kim, I. S., Basu, A., Siores, E. 1996. Mathematical models for control of weld bead penetration in the GMAW process, *International Journal of advanced Manufacturing Technology*, 12: 393-401.
91. Smartt H.B., Einerson C.J., 1993. A model for heat and mass input control in gas metal arc welding. *Welding Journal*, 72(5): 217-229.

92. Henderson D.E., Kokotovic P.V., Schiano J.L., Rhode D.S.,1993. Adaptive control of an arc welding process. *IEEE Control Systems Magazine*, 49-53.
93. Sun J.S., Wu C.S., Zhang Y.M.. 2002. Heat transfer modeling of double-side arc welding, *Acta Physics Sinica*, 51 (2): 286-290.
94. Zhang Y.M., Zhang S.B.. 1999. Method of arc welding using dual serial opposed torches. U. S. Patent, No. 5,990,446.
95. Breton E. L.. Modeling and Control of Double Sided Arc Welding Process. University of Kentucky PhD Dissertation, 2005
96. Zhang Y.M., Liu Y.C.. 2003. Modeling and control of quasi-keyhole arc welding process. *Control Engineering Practice*, Award Winning Applications-2002 IFAC World Congress, 11(12): 1401-1411.
97. Lu W., Zhang Y.M., Emmerson J.. 2007. Adaptive non-transferred plasma charge sensor and its applications, *ASME Journal of Manufacturing Science and Technology*, 129(1): 180-189.
98. Lu W., Zhang Y.M.. 2006. Robust sensing and control of the weld pool surface. *Measurement Science and Technology*, 17: 2437-2446.
99. Zhao P.C., Wu C.S., Zhang Y.M.. 2005. Modelling the transient behaviours of a fully penetrated gas-tungsten arc weld pool with surface deformation. *Proceedings of the Institution of Mechanical Engineers Part B-Journal of Engineering Manufacture*, 219 (1): 99-110.
100. Walcott B.L., Zhang Y.M., Liguó E., 2002. Robust control of pulsed gas metal arc welding. *Journal of Dynamic Systems, Measurement and Control*, 124(2):281–289.
101. Zhang Y.M., Liu Y.C.. 2007. Control of dynamic keyhole process. *Automatica*,

- 43(5): 876-884.
102. Boo K.S., Cho H.S.. 1994. A self-organizing fuzzy control of weld pool size in GMA welding processes. *Control Engineering Practice*, 2(6): 1007-1018.
103. Jou M.. 2002. A study on development of an H-infinity robust control system for arc welding. *Journal of Manufacturing Systems*, 21(2): 140-150.
104. Lu W.. Robust Sensing and control of Weld Pool Surface in Gas Tungsten Arc Welding and Its Modifications. University of Kentucky PhD Dissertation, 2004.
105. Lu Y.C.. Control of Dynamic Keyhole Welding Process. University of Kentucky PhD Dissertation, 2004.
106. Joseph M. I.. Robust Generic Model Control for Parameter Interval Systems. University of Kentucky PhD Dissertation, 2004.
107. Zhang J., Walcott B.L.. 2004. Adaptive interval model control and application. *Proceedings of the American Control Conference*, Boston, MA, June 30-July 2, 4: 3185-3190.
108. Zhang J., Walcott B.L.. 2006. Adaptive interval model control of arc welding process. *IEEE Transactions on Control Systems Technology*, 14 (6): 1127-1134.
109. McAvoy T.J.. 1992. Contemplative stance for chemical process control, *Automatica*, 28(2): 441-442.
110. Yu J.J., Zhou C.H.. 1996. Soft-sensing techniques in process control, *Control Theory and Applications*, 13(2): 137-144.
111. Richalet J., Rault A., Testud J. L., Papon J., 1978. Model predictive heuristic control: Applications to industrial processes, *Automatica*, 14(5): 413- 428.
112. Piotrowski K., Piotrowski J., Schlesinger J., 2003. Modelling of complex liquid-

- vapour equilibria in the urea synthesis process with the use of artificial neural network, *Chemical Engineering and Processing*, 42(4): 285-289.
113. Zhou Y., Hahn J., Mannan M. S., 2003. Fault detection and classification in chemical processes based on neural networks with feature extraction, *ISA Transactions*, 42(4): 651-664.
114. Liau L.C.K., Yang T.C.K., Tsai M.T., 2004. Expert system of a crude oil distillation unit for process optimization using neural networks, *Expert Systems with Applications*, 26(2): 247-255.
115. Lu C.H., Tsai C.C., 2007. Generalized predictive control using recurrent fuzzy neural networks for industrial processes, *Journal of Process Control*, 17(1): 83-92.
116. Björck Å., 1996. *Numerical Methods for Least Squares Problems*, SIAM, Philadelphia.
117. Rumelhart D. E., McClelland J. L., 1986. *Parallel distributed processing: explorations in the microstructure of cognition*, MIT Press, Cambridge, Massachusetts.
118. Moody J., Darken C. J., 1988. Learning with localized receptive fields, *Proceedings of the 1988 Connectionist Models Summer School*.
119. Moody J., Darken C. J., 1989. Fast learning in network of locally-tuned processing units, *Neural Computation*, 1: 281-294.
120. Hagan M.T., Demuth H.B., Beale M.H., 2002. *Neural Network Design*, Boston, PWS Publication Corporation.
121. Colomi A., Dorigo M., Maniezzo V., 1991. Distributed optimization by ant colonies, *Proc. of First European Conference on Artificial Life*, Paris, France,

pp.134-142.

122. Dorigo M., Stützle T., 2004. *Ant Colony Optimization*, MIT Press, Cambridge, MA, USA.
123. Kirkpatrick S., Gelatt C. D. J., Vecchi M. P., 1983. Optimization by simulated annealing, *Science*, (220): 671-680.
124. Millonas M. M., 1994. *Swarm, phase transition, and collective intelligence*, *Artificial Life III*, MA: Addison Wesley.
125. Eberhart R., Kennedy J., 1995. A new optimizer using particle swarm theory, *Proceedings of the sixth international symposium on micro machine and human science (Nagoya, Japan)*, IEEE Press, New Jersey, Piscataway, 39-43.
126. Kennedy J., Eberhart R., 1995. Particle swarm optimization, *Proceedings of the IEEE international conference on neural networks, IV*, IEEE Press, New Jersey, Piscataway, 1942-1948.
127. Kim T. H., Maruta I., Sugie T., 2008. Robust PID controller tuning based on the constrained particle swarm optimization, *Automatica*, 44(4):1104–1110.
128. Goh C. K., Tan K. C., Liu D. S., Chiam S. C., 2010. A competitive and cooperative co-evolutionary approach to multi-objective particle swarm optimization algorithm design, *European Journal of Operational Research*, 202(1): 42–54.
129. Sabat S. L., Ali L., Udgata S. K., 2011. Integrated learning particle swarm optimizer for global optimization, *Applied Soft Computing*, 11(1): 574–584.
130. Tandon V., 2001. *Closing the Gap between CAD/ CAM and Optimized CNC End Milling*, Master's thesis, Purdue School of Engineering and Technology, Indiana University Purdue University.

131. Wang S. H., Feng N. Q., Li A. G., 2003. A BP networks learning algorithm based on PSO, *Computer Applications and Software*, 20(8):74-76.
132. Chau K.W., 2007. Application of a PSO-based neural network in analysis of outcomes of construction claims, *Automation in Construction*, 16(5): 642–646.
133. Liu Z.Q., Gu X. S., Chen G. C., 2006. Three Swarms Cooperative Particle Swarm Optimization, *Journal of East China University of Science and Technology*, 32(7):754-757.
134. Wang X. W., Gu X. S., Liu Z.Q., Shang Y. Q., 2009. Soft Sensing Model of C3 Concentration of FCCU Based on PSO-BP Neural Network, *Journal of System Simulation*, 21(4):973-976.

VITA

Yi Huang was born on Jun 28, 1980 in Ningan, Heilongjiang, China.

EDUCATION:

M.S. in Materials Engineering, Harbin Institute of Technology, Harbin, China Jul, 2006

B.S. in Welding Engineering, Harbin Institute of Technology, Harbin, China Jul, 2004

PUBLICATIONS

Journal Papers

1 Yi Huang, YuMing Zhang, Nonlinear Modeling of dynamic metal transfer process in laser enhanced GMAW, Welding Journal, accepted.

2 Xuewu Wang, Yi Huang, YuMing Zhang, Droplet Transfer Model for Laser Enhanced GMAW, International Journal of Advanced Manufacturing Technology, submitted.

3 Zhenzhou Wang, Yi Huang, YuMing Zhang, Unsupervised Position Identification for the Droplet During the Pulsed Laser Enhanced GMAW Process, submitted.

4 Yi Huang, YuMing Zhang, Laser Enhanced Metal Transfer: Part II Analysis and Influence Factors, Welding Journal, 2011, 90(11): 205s-210s.

5 Yi Huang, YuMing Zhang, Laser Enhanced Metal Transfer: Part I System and observations, Welding Journal, 2011, 90(10): 183s-190s.

6 Yi Huang, YuMing Zhang, Laser Enhanced GMAW, Welding Journal, 2010, 89(1): 181s-188s

7 M.St. Wêglowski, Y. Huang, Y.M. Zhang, Relationship between wire feed speed and metal transfer in GMAW, Journal of Achievements in Materials and Manufacturing Engineering, 2008, 29(2): 191-194.

8 M.St. Wêglowski, Y. Huang, Y.M. Zhang, Effect of welding current on metal transfer in GMAW, Archives of Materials Science and Engineering, 2008, 33(1): 49-56.

9 H.T. Chen, C.Q. Wang, Cheng.Y, and Y. Huang, Y.H. Tian, Effects of solder volume on formation and redeposition of Au-containing intermetallics in Au/Ni-SnAgCu-Ni(P) solder joints, Journal of electronic materials, 2007, 36(1): 26-32.

10 H.T. Chen, C.Q. Wang, Cheng.Y, M.Y. Li, and Y. Huang, Cross-interaction of interfacial reactions in Ni (AuNiCu)-SnAg-Cu solder joints during reflow soldering and thermal aging, Journal of electronic materials, 2007, 36(1): 33-39.

11 Yi Huang, Chunqing Wang, Zhenqing Zhao. Bonding mechanism and interfacial reaction of Sn-Cu filler metal coating's soldering, ACTA METALLURGICA SINICA, 2005, 31(8): 881-885.

12 Zhenqing Zhao, Chunqing Wang, Miao Du, Yi Huang. Soldering of LD31 aluminum alloy with electro brush plated Sn-Pb, Transactions of The China Welding Institution, 2005, 26(7):67-70.

Conference Papers and Abstracts

1 Yi Huang, YuMing Zhang, Full Penetration Welding Using Laser Enhanced GMAW, Annual FABTECH International & AWS Welding Show, Chicago, IL, November 13-16, 2011

- 2 Yan Shao, YuMing Zhang, Yi Huang, Modeling and Control of Droplet Development in Laser Enhanced GMAW, Annual FABTECH International & AWS Welding Show, Chicago, IL, November 13-16, 2011
- 3 Yi Huang, YuMing Zhang, Laser Enhanced GMAW: An Energy saving and Less Contaminated Process. The 9th Global Conference on Sustainable Manufacturing, Saint Petersburg, Russia, September 28-30, 2011
- 4 Yi Huang, YuMing Zhang, Laser Enhanced GMAW: Process and Fundamentals, Annual FABTECH International & AWS Welding Show, Atlanta, GA - November 2-4, 2010
- 5 Yi Huang, YuMing Zhang, Laser Enhanced Metal Transfer, Annual FABTECH International & AWS Welding Show, Chicago, November 15-18, 2009
- 6 YuMing Zhang, Yi Huang, Control of Metal Transfer at Given Arc Variables, Proceedings of 2009 NSF Engineering Research and Innovation Conference, Honolulu, Hawaii, Jun, 2009
- 7 H.T. Chen, C.Q. Wang, C. Yan, Y. Huang, and H.Y. Liu, Investigation on interfacial reactions on AuNiCu and Ni (Cu) metallizations in SnPb, SnAg and SnAgCu solder joints, IMAPS, 2006, Taiwan IMAPS Taiwan Jun 28~Jul 1, 2006
- 8 H.T. Chen, C.Q. Wang, Cheng.Y, M.Y. Li, and Y. Huang, Effects of solder volume on redeposition of (Au,Ni)Sn₄ intermetallics in SnAgCu solder joints, ICEPT, 2006, Shanghai Date:26-29 Aug. 2006.ICEPT
- 9 H.T. Chen, C.Q. Wang, M.Y. Li, Cheng.Y, and Y. Huang, Coupling effect between two pads in Ni(Au/Ni/Cu)-SnAg-Cu sandwich solder joints during reflow and thermal aging, ICEPT, 2006, Shanghai.
- 10 Lei Wang, Chunqing Wang, Zhenqing Zhao, Yi Huang. Interfacial Characteristics of Sn_{3.5}Ag Solder on Copper after Nd:YAG Laser Surface Irradiation, 2005 International Conference on Asian Green Electronics, March 15-18,2005

Yi Huang

11/08/2011